# THE RHO-GAP GRAF1 REGULATES SKELETAL MUSCLE MATURATION AND REPAIR

Kaitlin Christine Lenhart

A dissertation submitted to the faculty at the University of North Carolina at Chapel Hill in partial fulfillment of the requirements for the degree of Doctor of Philosophy in the Department of Pathology and Laboratory Medicine in the School of Medicine.

Chapel Hill
2014

Approved by:

Joan M. Taylor

Patrick J. Brennwald

Kenneth A. Jacobson

Nobuyo Maeda

Leigh B. Thorne

Xiao Xiao

## ABSTRACT

Kaitlin Christine Lenhart: The Rho-GAP GRAF1 Regulates Skeletal Muscle Maturation and Repair
(Under the direction of Joan M. Taylor)

Skeletal muscle is a large and highly specialized tissue requiring tightly regulated processes during development and maintenance to prevent the manifestation of debilitating myopathies. The fusion of myoblasts into mature multinucleated syncitia is a critical component of muscle formation and is regulated by the tight coordination of actin- and membrane-based dynamics; however, the spatial/temporal regulation of and interrelationship between these processes is incompletely understood. We recently reported that the BAR domain-containing Rho-GAP, GRAF1, is particularly abundant in perinatal muscle undergoing fusion to form multinucleated muscle fibers and that enforced expression of GRAF1 in cultured myoblasts induced robust fusion by a process that required GAP-dependent actin remodeling and BAR domain-dependent membrane sculpting. Herein we developed a novel GRAF1-deficient mouse line to explore a role for this protein in the formation/maturation of myotubes *in vivo*. Adult GRAF1-deficient mice exhibited a significant decrease in grip strength with muscle analysis revealing a significant reduction in cross-sectional area and impaired regenerative capacity, indicating a deficiency in myoblast fusion. Indeed, a significant fusion defect was recapitulated in isolated myoblasts depleted of GRAF1. Mechanistically, we show that GRAF1 associates with endocytic recycling vesicles

and facilitates myoblast fusion, at least in part, by promoting vesicle-mediated translocation of fusogenic ferlin proteins to the plasma membrane.

Muscle plasma membrane is particular vulnerability to contraction-induced rupture and possesses specialized mechanisms for rapid membrane repair so as to preserve the syncytia. Dysferlin has been established as a critical regulator of muscle plasma membrane resealing; however, the mechanism(s) which govern dysferlin trafficking to sites of membrane damage require further investigation. We show that GRAF1 associates with and mediates deposition of dysferlin at plasma membranes of injured muscle, implicating a novel role for GRAF1 in dysferlin-mediated membrane repair. In support of this, GRAF1 depletion enhanced susceptibility to induced membrane injury in isolated myoblasts and as anticipated, exacerbated some hallmarks of muscle degeneration in the *mdx* mouse. Interestingly, GRAF1-deficient *mdx* mice exhibited unprecedented myofiber expansion and muscle growth, implicating an additional role for GRAF1 in skeletal muscle-injury response. Together, these data shed new light on the importance of GRAF1 in skeletal muscle formation and maintenance.

## ACKNOWLEDGEMENTS

I would first like to thank my advisor, Dr. Joan Taylor, who has been the most encouraging and supportive mentor. Besides being a brilliant scientist, Joan is an exceptionally dependable, honest and fair boss, and I could not have wanted for a more perfect person to help in guiding me in the initial years of my scientific career. She has always put me in a position to be successful and has been unwavering in her belief in my potential as a scientist, even when I was doubtful. But the best part about her mentorship has been her enthusiasm for our science and her willingness to discuss it (and do it!) at lengths end. I believe this mentoring has allowed me to grow exponentially as a young researcher.

I want to acknowledge my fellow lab mates, Jason, Morgan, TJ, ZK, Dean, Laura, Matt, Srilu, and several other past and present lab members, for being so generous with their time and support, and for their willingness to discuss everything from science and philosophy to baseball and the Food Network. The camaraderie we share has always made time spent in the lab a joy. I also owe many thanks Abby and Ines for their trust and patience as I learned to navigate the role of grad student mentor. They are two of the most phenomenal "kids", and surely, they have taught me more than what I could ever hope to teach them.

I want to thank my undergraduate mentor, Dr. Brian Livingston, and my old lab mates, Gio and William, from USF for taking me under their wings, showing me how much fun lab work could be, and inspiring me to apply to graduate school. Without their

encouragement and belief in my abilities as a scientist, I would have never thought it possible for me to succeed as a PhD student.

I want to thank the members of my thesis committee, Drs. Pat Brennwald, Ken Jacobson, Nobuyo Maeda, Leigh B. Thorne, and Xiao Xiao, for their scientific input and help in guiding my thesis projects. In particular, I would like to acknowledge Dr. Xiao for his generous collaborative efforts and for the sharing of his skeletal muscle expertise. Also, I'm grateful for Dr. Maeda and the Integrative Vascular Biology Program for giving me a place to share my research for the past several years. Although my research evolved into an area far removed from anything vascular-related, I was accepted into the program with open arms and have received valuable input from all members nonetheless.

I owe many thanks to Dr. Charles Jeanette and the Pathology Department for giving me and my research a home for the past 5 years. I owe a debt of gratitude to Dr. Bill Coleman for being so incredibly awesome in every way possible. His never-ending pool of wisdom, counsel and pep-talks has brightened my day on more than one occasion. I also want to thank Mrs. Dorothy Poteat, Mrs. Brenda Brock and all the invaluable ladies on the 3rd floor for taking care of everything non-science and making sure I never went off track.

I want to acknowledge all of the wonderful friends I've made since arriving to Chapel Hill because without them, I would be a lonely, sad girl. In particular, I want to first thank Laura and Jonathan, my surrogate family, for their overwhelming love and support. Thanksgiving should always be in May! I next want to thank my classmates Maria, Dinuka, Michael, Amanda and Aleeza. Finding my way through graduate school proved to be a stressful process, but being able to whine about it with others going through the same thing made it a whole lot easier! Finally I want to give a shout out to Caitlin, Lantz and Rukie.

From bar-hopping to game nights to white-water rafting, you guys have continued to bring joy, laughter and fear into my life.

I want to thank my big brother, John, for always having my back and believing in my awesomeness. I would also like to acknowledge my little sister, Mary, who knows me better than anyone, and as such, recognizes that my highly idealistic nature often leads to inaction. I want to thank her for always bringing me back down to Earth by reminding me to not just dream it, but to do it by simply imploring, "Dang it Kate, just do it already!" Finally, I'd like to thank my parents, Barney and Mary, for being the most generous people I've ever known and for working so hard to give me and my siblings the best life possible. No matter where I go in life, I am incredibly fortunate to know that they will always be with me to help guide me on my path, to catch me when I fall, and to share in my triumphs. They have never questioned my ability to accomplish anything I set my mind to, and it is because of this unconditional love and support that I am able to accomplish anything worthwhile. I owe all my success to them.

I am eternally grateful to all of these individuals for their collective and continued support. This dissertation would not have existed without them!

**TABLE OF CONTENTS**

## LIST OF TABLES

## LIST OF FIGURES

## LIST OF ABBREVIATIONS

| | |
|---|---|
| AIDS | Acquired immunodeficiency syndrome |
| BAR | Bin–amphiphysin–rvs |
| BFA | Brefeldin A |
| Bin1 | Bridging integrator 1 |
| Bin3 | Bridging integrator 3 |
| Cdc42 | Cell division cycle 42 |
| cDNA | Complementary DNA |
| CLIC/GEEC | clathrin-independent/GPI-enriched endocytosis |
| COPD | Chronic obstructive pulmonary disease |
| CSA | Cross-sectional area |
| CTX | Cardiotoxin |
| DAPI | 4',6-Diamidino-2-phenylindole |
| DGC | Dystrophin glycoprotein complex |
| DIC | Differential interference contrast |
| DM | Differentiation media |
| DMD | Duchenne muscular dystrophy |
| EBD | Evans blue dye |
| EDTA | Ethylenediaminetetraacetic acid |
| EHD1 | EPS15 homology domain-containing 1 |
| EHD2 | EPS15 homology domain-containing 2 |
| EF | Ejection fraction |
| eMHC | Embryonic myosin heavy chain |

| | |
|---|---|
| ES | Embyonic stem |
| FAK | Focal adhesion kinase |
| Fer1L5 | Ferlin-1-like 5 |
| GAP | GTPase activating protein |
| GAPDH | Glyceraldehyde 3-phosphate dehydrogenase |
| GDI | Guanosine dissociation inhibitor |
| GDP | Guanosin diphospahte |
| GEF | Guanine nucleotide exchange factor |
| GFP | Green fluorescent protein |
| GM130 | 130 kDa cis-Golgi matrix protein |
| GRAF1 | GTPase regulator associated with focal adhesion kinase-1 |
| GRAF2 | GTPase regulator associated with focal adhesion kinase-2 |
| GRMD | Golden retriever muscular dystrophy |
| GT | Gene trap |
| GTP | Guanosine triphosphate |
| GTPase | Guanosine triphosphatase |
| F-actin | Filamentous actin |
| FAK | Focal adhesion kinase |
| FS | Fractional shortening |
| HBSS | Hank’s balanced salt solution |
| HEPES | Hydroxyethyl piperazineethanesulfonic acid |
| Het | Heterozygous |
| Hom | Homozygous |

| | |
|---|---|
| IP | Immunoprecipitation |
| ISO | Isoproterenol |
| JNK | C-jun N-terminal kinase |
| kDa | Kilodalton |
| Lamp2 | Lysosomal-associated membrane protein 2 |
| LV | Left ventricle |
| LVID | Left ventricle internal diameter |
| Mbc | Myoblast city |
| MHC | Myosin heavy chain |
| MIP | Maximum intensity projection |
| MRF | Myogenic regulator factor |
| MRTF-A | Myocardin-related transcription factor-A |
| NCAM | Neural Cell Adhesion Molecule |
| NIS | Non-immune serum |
| NRCM | Primary neonatal rat cardiomyocytes |
| NTC | Non-target control |
| PBS | Phosphate-buffered saline |
| PCR | Polymerase chain reaction |
| PH | Pleckstrin homology |
| PS | Phosphatidyl serine |
| PM | Plasma membrane |
| Rab5 | Ras-related protein Rab-5A |
| Rac1 | Ras-related C3 botulinum toxin substrate 1 |

| | |
|---|---|
| RhoA | Ras homolog gene family, member A |
| RIPA | Modified radioimmune precipitation assay |
| RT-PCR | Reverse transcriptase polymerase chain reaction |
| sCK | Serum creatine kinase |
| SDS-PAGE | Sodium dodecyl sulfate-polyacrylamide gel electrophoresis |
| s.e.m. | Standard error of mean |
| SH3 | Src homology 3 |
| siRNA | Short interfering RNA |
| SM | Serum media |
| SNP | Single nucleotide polymorphism |
| SRF | Serum response factor |
| srGAP2 | SLIT-ROBO Rho GTPase-activating protein 2 |
| TBS | Tris-buffered saline |
| Thy-1 | Thymocyte differentiation antigen 1 |
| WGA | Wheat germ agglutinin |
| WT | Wildtype |

# CHAPTER 1

# BACKGROUND AND SIGNIFICANCE

## SKELETAL MUSCLE DISEASES: A BRIEF OVERVIEW

Skeletal muscle diseases, or myopathies, can be acquired or congenital, and encompass a wide array of disorders with varying effects on the body—muscle wasting and weakness being the most common symptoms. Acquired myopathies are often inflammatory and include dermatomyositis, polymyositis, and inclusion body myositis. Congenital myopathies, on the other hand, are more pathologically diverse and encompass the class of muscular dystrophies, mitochondrial myopathies, and other various non-categorized myopathies. The reason individuals afflicted with congenital myopathies present with such diverse symptoms is due to either inherited or *de novo* mutations which occur in an array of genes that play varying roles in the structural maintenance and/or repair of muscle.

Muscular dystrophies, for instance, often result from mutations in striated muscle plasma membrane (PM), or sarcolemma, -associated proteins which aid in the attachment of muscle fibers to the extracellular matrix (ECM). When any of these components are misexpressed, the myofibers become vulnerable to damage. For a comprehensive review of muscular dystrophy-linked proteins, see the works of Davies and Nowak, and Rahimov and Kunkel [1, 2]. Dystrophin, for example, is an integral member of the transmembrane dystrophin glycoprotein complex (DGC), a multi-protein complex which anchors the

sarcolemma to both the actin cytoskeleton and the ECM, thereby creating a structural scaffold which reinforces PM integrity. In instances of dystrophin depletion, the DGC becomes destabilized resulting in a fragile sarcolemma that is increasingly vulnerable to contraction-induced injury [3, 4]. In patients with Duchenne muscular dystrophy (DMD) or Becker muscular dystrophy, mutations in the dystrophin gene result in absent or defective protein, respectively. This aberrant expression augments membrane fragility and subsequent muscle fiber degeneration which becomes progressively more severe as the muscle loses the ability to regenerate.

Muscular dystrophies can also result from defects in sarcolemmal repair mechanisms such as what occurs in patients with dysferlinopathies. Dysferlinopathies result from mutations in the dysferlin gene and are characterized by progressive muscle wasting and are diagnosed as either Limb-girdle muscular dystrophy type 2B or Miyoshi muscular dystrophy [5, 6]. Following PM injury, all cell types must utilize a rapid and proficient mechanism to reseal or "patch" their membranes; skeletal muscle, being a highly strained tissue, depends heavily upon this repair process. Indeed, it has been demonstrated that dysferlin mediates $Ca^{2+}$-dependent membrane resealing of adult myofibers following injury, implicating an important role for this protein in sarcolemmal repair [7], (a more complete description of dysferlin-mediated membrane repair follows below). In summary, by understanding the diverse mechanisms which lead to muscular defects, we will be better able to appreciate proper muscle function as well as improve upon current therapeutics for treating muscular diseases.

## SKELETAL MUSCLE MATURATION DURING DEVELOPMENT AND ADULT MYOGENESIS

Skeletal muscle maturation is a finely tuned multi-step process that is initiated by the specification of mesodermal precursors into proliferating myoblasts which undergo cell cycle withdrawal, differentiation and fusion to form multinucleated muscle fibers. In developing vertebrates, muscle progenitor cells are initially specified from precursors derived from the dermomyotome, a region of the maturing somite which forms from a tissue compartment known as the paraxial mesoderm [8]. The transcription factor, Pax3, has been shown to be important for organizing dermomyotome formation as depletion of this protein induces malformed musculature in the developing mouse [9]. Further work done in gene-ablated mice have demonstrated that the subsequent specification of myoblasts is regulated through the activation of "early" myogenic regulatory factors (MRFs), which include myf-5 and myoD [10]. Moreover, Pax3 has been implicated in determining myogenic cell fate through MyoD [11]. These myoblasts can proliferate to self-renew, or be induced to exit the cell cycle and turn on the "late" MRFs, myogenin and MRF4, to induce muscle differentiation [12-15]. The upregulation of muscle-specific genes such as tropomyosin, myosin heavy chain and skeletal-α-actin then facilitate terminal differentiation and subsequent fusion to form the mature, contractile muscle syncytia (Figure 1.1).

Adult skeletal muscle tissue maintains a high capacity for regeneration, a mechanism which mimics developmental myogenesis in many aspects. This regenerative power is due to a population of resident muscle progenitor cells (termed satellite cells) which intercalate between the basal lamina and the muscle fiber sarcolemma [16]. For a comprehensive description of satellite cell biology and their pivotal role in muscle regeneration, see the excellent review by Relaix and Zammit [17]. Satellite cells are specified during

developmental myogenesis and are demarcated by expression of the transcription factor Pax7. Pax7, along with Pax3, are expressed within the somites, but become downregulated once MRFs activate. However, a proportion of $Pax3^{+}/Pax7^{+}$ cells will retain Pax7 and never express MRFs; these are the cells which will make up the satellite cell niche in the adult muscle (Figure 1.1). Following muscle injury, satellite cells will proliferate to self-renew, or they will differentiate and fuse with each other to form nascent myofibers or fuse with injured myofibers to repair the established muscle syncytia. Although debates remain regarding what dictates satellite cell fate, Kuang *et. al*. postulate that activated satellite cells undergo asymmetric division into two unequal daughter cells, with the fate of the daughter cell being determined by its locale. Specifically, the daughter that remains in contact with the basal lamina adopts a self-renewal fate and the daughter that loses basal lamina contact attains a differentiated fate. This method of asymmetric cell fate segregation would also facilitate the fusion of the differentiating daughter, as it is directly pushed into the mature myofiber upon cell division [18]. The discovery that satellite cells adopt multiple fates is significant in regards to therapeutic intervention for muscular diseases such as DMD, where satellite cell exhaustion has been shown to contribute to impaired muscle regeneration [19, 20].

## THE RHO FAMILY OF GTPASES AND THEIR TRANSCRIPTIONAL CONTROL DURING MYOGENESIS

The Rho family of GTPases comprises a group of small molecular weight (~21 kDa) signaling guanosine nucleotide-binding proteins (G proteins) that play important and well-documented roles in various aspects of intracellular actin dynamics. The best described Rho GTPases include Rac1, cdc42 and RhoA. Rac1 regulates the formation of membrane ruffles

and lamellopodia, while cdc42 controls filopodia formation at the cell periphery [21, 22]. RhoA, on the other hand, regulates contractile actin:myosin filaments to stimulate stress fiber and focal adhesion assembly [23]. Moreover, it is currently known that Rho GTPases coordinate an additional array of diverse cellular functions, including cell polarity, microtubule dynamics, vesicular trafficking, cell cycling and genetic regulation which may or may not be regulated through cytoskeletal reorganization. For extensive reviews on cellular Rho GTPase signaling, see the excellent works of Burridge and Wennerberg, Etienne-Manneville and Hall, Fukata *et. al.*, Ridley, and Raftopoulou and Hall [24-28].

Rho GTPases behave as molecular switches by possessing two interconvertible states: the inactive guanosine diphosphate (GDP)-bound state and the active guanosine triphosphate (GTP)-bound state. The binding of GDP and GTP is tightly regulated by three classes of catalytically active proteins, which include guanine nucleotide exchange factors (GEFs), guanine dissociation inhibitors (GDIs), and GTPase-activating proteins (GAPs), each of which having specific affinities towards one or more Rho GTPases. In order to propagate cell signaling, GEFs activate GTPase activity by catalyzing the release of GDP to allow for subsequent GTP binding. Once in the active GTP-bound state, the Rho GTPase is able to bind its effector protein to mediate a downstream biological response. To shut down signaling, GDIs downregulate GTPase activity by either promoting GDP binding or sequestering the GTPase in the cytosol away from downstream effectors. Alternatively, GAPs typically serve to downregulate the activity of GTPases by promoting the hydrolysis of bound GTP to GDP. Since small Rho GTPases exhibit slow intrinsic rates of GTP hydrolysis, GAPs play a critical role in the fine tuning of these molecules between active and inactive states.

In addition to regulating actin dynamics during muscle maturation (which is described in the following section), the Rho GTPases have also been shown to coordinate the transcriptional activity of skeletal muscle cells during myogenesis. For instance, studies performed in cultured murine myoblasts have demonstrated that Rac1 and cdc42 inhibit myogenesis through activation the C-jun N-terminal kinase (JNK) pathway which prevents withdrawal of myoblasts from the cell cycle [29, 30]. Alternatively, Rac1, cdc42 and RhoA have been shown to promote myogenesis through the activation of the serum response factor (SRF) and p38 pathways [29, 31, 32].

Furthermore, it has been shown that the activity of RhoA must be tightly regulated to allow for proper skeletal muscle formation. Interestingly, while some studies have shown RhoA to be a potent activator of skeletal muscle differentiation, others have shown that RhoA actually inhibits differentiation. Although this discrepancy may be due to variances in experimental design, such as timing of RhoA perturbation, it implicates the tight regulation of RhoA activity during myogenesis. For instance, while active RhoA is required for establishing myogenic cell fate and coordinating SRF-dependent transcription of myogenic factors [31-34], RhoA activity must be downregulated to promote the subsequent differentiation of muscle [29, 35, 36]. Indeed, this discrepancy was settled by Iwasaki *et. al.* who demonstrated stage-specific roles for RhoA and its effector, myocardin-related transcription factor-A (MRTF-A), during differentiation of cultured C2C12 myoblasts [37]. Specifically, RhoA activity was found to be upregulated in proliferating myoblasts; however, a subsequent downregulation of RhoA activity was required for cell cycle withdrawal, differentiation, and myoblast fusion. Moreover, it was demonstrated that the upregulation of RhoA during myoblast specification/proliferation induces MRTF-A activation, which in turn

enhanced the expression of the transcriptional inhibitor Id3 [37]. It is thought that Id3 may then bind to MRFs, such as myoD, to form transcriptionally inactive complexes which will inhibit myogenesis [38]. Once RhoA activity is diminished, data supports the idea that Id3 becomes re-repressed and terminal differentiation of myoblasts ensues.

## MECHANISMS UNDERLYING MUSCLE FUSION

Myoblast fusion contributes to developmental myogenesis and the regeneration of mature muscle as described previously. Briefly, during initial muscle development, myoblasts fuse with one another and then to nascent multi-nucleated myofibers to form the mature skeletal muscle syncytia. Once the syncytia is subject to injury, satellite cells are specified to myoblasts which then fuse in a similar fashion similar to developmental myogenesis, as well as to sites of muscle fiber damage. The cellular mechanisms which control myoblast fusion are not completely understood; however, it has been shown that dynamic and coordinated changes in actin polymerization and vesicle trafficking drive skeletal muscle formation.

### *Actin dynamics in myoblast fusion*

The actin cytoskeleton in pre-fused and fusing myoblasts is highly dynamic and undergoes dramatic changes to facilitate proper myoblast-myoblast fusion. Most of the current studies of myoblast fusion have been carried out in *Drosophila melanogaster*. In this fly model, it has been demonstrated by live-cell imaging that adhesion-dependent F-actin foci accumulate at pre-fusion sites which undergo dissolution just prior to myoblast fusion [39]. Genetic mutations in actin remodeling regulators of the Kette-SCAR/WAVE-Arp2/3

pathway have been shown to block fusion as enlarged F-actin foci fail to dissolve in these models [39]. Importantly, this same phenotype was also observed in mouse C2C12 myoblasts [40], demonstrating an important and conserved functional role for the actin cytoskeleton in myoblast fusion. Moreover, the Chernomordik laboratory and others have demonstrated that local depolymerization of the actin cortex at the site of cell-cell contact enhances viral fusogen-initiated syncytium formation by promoting the expansion of so-called fusion pores [41, 42]. Fusion pores form between two cells at early stages of cell fusion, and expand during later stages to form bridges which promote lipid mixing and cytoplasmic coalescence to drive fusion. In addition to actin disassembly, fusion pore formation and expansion is also driven by intracellular membrane shaping proteins (described below).

Signaling molecules, particularly those which effect Rho GTPase activity, have also been extensively implicated in cytoskeletal reorganization during myoblast fusion. Integrins, for instance, are heterodimeric transmembrane proteins that bind ECM proteins and indirectly interact with the actin cytoskeleton through focal adhesion complexes [43, 44]. As focal adhesions accumulate at pre-fusion sites, it is postulated that integrins become activated and signal through the Rho GTPase Rac1 to coordinate cytoskeletal rearrangements prior to fusion. Indeed, Rac1 activation has been shown to facilitate myoblast fusion by coordinating actin dynamics in various model systems [45-47]; however, Rac1 is also poised to antagonize RhoA activity at these sites [48], a process known to facilitate C2C12 myoblast fusion [35]. Cadherins, which are calcium-dependent membrane glycoproteins, are also important for reorganizing the cytoskeleton of myoblasts. M-cadherin, for instance, plays an important role in the adhesion of myoblasts prior to fusion. *In vitro* studies in C2C12 myoblasts have

demonstrated that M-cadherin-dependent adhesion activates Rac1 and is required for myoblast fusion [49]. However, if RhoA is activated, M-cadherin is degraded and fusion becomes blocked [35]. Thus, cadherin-dependent adhesion could act in concert with integrin signaling to reorganize actin and facilitate myoblast fusion.

While established data has demonstrated an important role for various Rac1-specific GEFs in myoblast fusion, such as *Drosophila* myoblast city (Mbc) and the corresponding mammalian ortholog Dock180 [50, 51], the specific signaling molecules which directly affect RhoA activity is mostly undefined. Our recent data demonstrated that the Rho-specific GAP, GRAF1, translocates to pre-fusion complexes and contributes to the down regulation of RhoA and localized actin depolymerization which is imperative for facilitating skeletal muscle differentiation and fusion [52], (a more complete description of GRAF1-dependent myogenesis follows below).

*Membrane dynamics and vesicle trafficking in myoblast fusion*

In this final stage of cell-cell fusion, nascent fusion pores of a few nanometers in diameter undergo an active expansion to yield a lumen of 10-15 μm in size. It has been shown that expansion of such pores that contain strongly bent plasma membrane rims requires persistent energy input and it has been postulated that curvature generating proteins that relax the bending energy of the rim are likely required to make expansion energetically favorable [53]. Indeed, overexpression of the lipid membrane sensing/sculpting BAR (Bin–amphiphysin–rvs) domains of GRAF1 of FCHo2 has been shown to promote viral fusogen-initiated syncytium formation [54].

Localized F-actin dissolution is believed to facilitate trafficking of intracellular vesicles to fusion sites in order to propagate fusogenic signals. In support of this, vesicle accumulation and alignment at the PMs of two apposed *Drosophila* myoblasts was captured by electron microscopy prior to fusion pore formation [55]. While this alignment of vesicles has been shown to be necessary for PM coalescence [55], the nature of these vesicles and their role in fusion is still largely unknown. Recent studies from the McNally laboratory have indicated that endocytic recycling vesicles are involved in myoblast fusion and that the ferlin family members dysferlin, myoferlin and Fer1L5 are fusogenic cargo that associates with these structures.

The ferlins make up a family of striated muscle-specific C2 domain-containing proteins that are involved in various aspects of vesicle trafficking during myoblast fusion. Dysferlin, the first family member discovered, is a membrane-associated protein that was initially found to be involved in sarcolemmal resealing of skeletal muscle fibers following injury [7]. Moreover, dysferlin has recently been implicated in intracellular vesicular trafficking; a process also important for membrane resealing [56], (dysferlin-mediated membrane resealing and repair is described in the following section). Myoferlin is expressed predominantly within myoblasts at sites of myoblast-myoblast or myoblast-myocyte fusion and has been shown to mediate endocytic recycling by returning internalized vesicles back to the plasma membrane [57]. Myoferlin-null mice exhibit smaller muscle fibers and a dystrophic phenotype due to myoblast-myotube fusion defect [57]. Fer1L5, the most recently characterized ferlin, is expressed in small multinucleated myotubes and directly binds to the endocytic recycling proteins EPS15 homology domain-containing 1 and 2 (EHD1 and EHD2). Moreover, in the absence of EHD2, Fer1L5 cannot be recruited to the

cell membrane and myoblast fusion is inhibited [58]. These data demonstrate that ferlin-dependent endocytic processes may play an important role in properly localizing integral proteins to sites of fusion in order to regulate normal muscle growth and repair. Moreover, in addition to mediating GAP-dependent actin dynamics, GRAF1 has been previously implicated in regulating clathrin-independent endocytosis, and as such, likely plays a role during ferlin-mediated endocytic recycling. In Chapter 2, I demonstrate that GRAF1 associates with EHD1-containing endocytic recycling vesicles and promotes myoblast fusion by vesicle-mediated translocation of myoferlin and Fer1L5 to pre-fusion complexes at the cell periphery.

## DYSFERLIN-MEDIATED SARCOLEMMAL INJURY REPAIR

Membrane rupture occurs frequently in mechanically active tissues, particularly in the skeletal muscle which can exhibit signs of membrane damage even under basal conditions. The transient nature of sarcolemmal injuries under normal conditions indicates that muscle cells contain intrinsic mechanisms for rapid membrane repair. Dysferlin was the first striated muscle-specific protein identified that permitted rapid sarcolemmal resealing following mechanically-induced injury. This role for dysferlin was initially demonstrated in isolated myofibers and primary muscle cells from dysferlin-null mice that were subject to laser-induced injury or microinjury, respectively [7, 59]. Investigators found that dysferlin-depleted cells exhibited delayed membrane patching and a more severe injury as assessed by uptake of a membrane impermeable fluorescent dye. Moreover, lipid vesicles were shown to accumulate at sites of sarcolemmal injury in dysferlin-deficient cells as well as biopsies from humans with dysferlin mutations [7, 60], indicating that dysferlin is important for mediating

fusion of vesicles to the PM. Indeed, the presence of dysferlin in both repair vesicles and PMs has been shown to promote docking and fusion of a "patch" to reseal the injured membrane [7, 61]. Although dysferlin has been established as an integral component of sarcolemmal injury repair, further work is required to identify additional components which aid dysferlin recruitment to sites of membrane damage. In Chapter 3, I show that GRAF1 associates with dysferlin at injured PMs and that depletion of GRAF1 prohibits sarcolemmal localization of dysferlin and impairs injury-induced membrane resealing.

## THE RHO-GAP GRAF1 AND ITS ROLE IN NON-MUSCLE CELLS

GAPs, as previously described above, are signaling molecules which act to finely tune Rho GTPase activity. GRAF1 (GTPase regulator associated with focal adhesion kinase-1) is a Rho-specific GAP that, like several other GAPs, contains additional functional domains which not only influences GTPase specificity, but also allows for coupling of GTPase regulation with other cellular processes mediated by the domains. The functional domains of GRAF1 include an N-terminal lipid binding/bending BAR domain, a phosphatidyl serine-binding plekstrin homology (PH) domain, a proline/serine rich domain which harbors multiple phosphorylation sites, and a C-terminal protein-interaction Src homology 3 (SH3) domain through which GRAF1 interacts with focal adhesion kinase (FAK) [62-65].

GRAF1 was first identified by the Parsons' laboratory as a binding partner for FAK that exhibited GAP activity preferentially for RhoA and cdc42 *in vitro* [62]. *In vivo* studies from this group have demonstrated that GRAF1 colocalizes with cortical actin structures and stress fibers, and that ectopic expression of this protein in fibroblasts induces GAP-dependent

clearance of Rho-mediated stress fibers, but could not inhibit cdc42-mediated filopodial extensions, indicating that GRAF1 behaves as a Rho-specific GAP *in vivo* [62, 63]. Further evidence indicates that mitogen-activated protein (MAP) kinase catalyzes the phosphorylation of GRAF1 on serine 510 within the serine/proline rich domain [64]. It has been postulated that such a modification so near to the protein-interacting SH3 domain may induce a conformational change, as indicated by a GRAF1 band shift following Western blot analysis, which could influence interactions with FAK or other binding partners at this site.

BAR domains have been shown to be potent inducers of lipid membrane sensing/sculpting and are often present in proteins involved in various aspects of membrane dynamics, including tubulation, endocytic vesicle budding, secretory vesicle fission, fusion pore expansion and autophagy [66]. Indeed, previous studies have shown that BAR domain of GRAF1, in conjunction with its phosphatidyl serine-binding PH domain, promotes GRAF1 localization to and induction of tubular membranes, in order to drive clathrin-independent/ GPI-enriched endocytosis (CLIC/GEEC) in cultured fibroblasts and HeLa cells [67]. Interestingly, overexpressed dominant-negative cdc42 associates with GRAF1-positive endocytic membranes [67], implicating a role for GRAF1 in coordinating Rho GTPase signaling and membrane remodeling to facilitate endocytosis. What's more, recent studies have shown that the BAR-PH domain of GRAF1 can actually form a direct interaction with its GAP domain to inhibit catalytic activity [68]. In this autoinhibited state, the BAR-PH domain maintains membrane bending properties as it was shown to induces lipid tubules in HeLa cells [68], indicating that GRAF1 can autoregulate GAP activity while simultaneously altering membrane properties. Taken together, this data demonstrates how GRAF1 can couple actin- and membrane-based dynamics by virtue of its multi-domain structure.

GRAF1 REGULATION OF SKELETAL MUSCLE DIFFERENTIATION

As previously mentioned, coordinated changes in actin polymerization and vesicle trafficking drive skeletal myogenesis, making GRAF1 a likely regulator of this process. We and others have previously shown that GRAF1 is highly expressed in terminally differentiated tissues such as the heart and brain [52, 62, 63]. Additionally, our analysis indicated that GRAF1 expression is transiently and markedly upregulated in the developing musculature of neonatal rats, but is downregulated within the adult muscle. *In vitro* studies in C2C12 skeletal myoblasts demonstrated that GRAF1 expression is upregulated in myoblasts induced to differentiate, concomitant with a reduction in RhoA activity (Figure 1.1). siRNA-mediated GRAF1 depletion of myoblasts induced attenuation of skeletal muscle differentiation marker expression and a significant increase in RhoA activity. Interestingly, treatment of GRAF1-depleted cells with Y27632, an inhibitor of the RhoA/ROCK pathway, completely restored myoblast differentiation [52]. This data taken together indicates that GRAF1 promotes skeletal muscle differentiation in a cell autonomous fashion by limiting the activity of RhoA.

Since it is postulated that RhoA activity may be necessary to keep myoblast cells in a proliferative state, we also wanted to determine whether ectopically expressing GRAF1 in C2C12s could sufficiently promote their differentiation by inactivating RhoA. As anticipated, ectopic expression of GRAF1 in C2C12 myoblasts resulted in a concomitant upregulation of skeletal muscle differentiation markers. To determine whether this process is dependent on the ability of GRAF1 to downregulate RhoA, we overexpressed a catalytically-inactive GAP domain-containing GRAF1 variant (GAPm) and found that the protein did not

induce differentiation. [52]

Moreover, *Xenopus laevis* embryos depleted of GRAF1 using morpholino antisense technology exhibited decreased expression of skeletal muscle differentiation markers and increased RhoA activity, indicating that the Rho-GAP activity of GRAF1 acts to downregulate RhoA activity during muscle development *in vivo*. Interestingly, the somitic structure of the GRAF1 morphants remained unaltered until stage 32, where we found evidence of somite tearing and myofiber splitting, which became more pronounced overtime, suggesting that GRAF1 depletion leads to progressive somite degeneration. Moreover, GRAF1 morphants exhibit a striking swimming defect and died prior to metamorphosis [52]. Collectively, this data demonstrates that GRAF1-dependent differentiation is required for proper skeletal muscle formation as well as preservation of sarcolemma integrity. Further studies utilizing an *in vivo* model to demonstrate the functional role of GRAF1 in mammalian skeletal muscle would ultimately confirm our previous findings and provide a more relevant system for studying the potential role of GRAF1 in myogenesis and sarcolemmal maintenance.

## GRAF1 REGULATION OF MYOBLAST FUSION BY GAP- AND BAR-DEPENDENT MECHANISMS

After having established that GRAF1 is both necessary and sufficient to induce skeletal muscle differentiation, we next wanted to determine whether GRAF1 is important for promoting differentiation-dependent myoblast fusion. Indeed, ectopic expression of GRAF1 in pre-differentiated C2C12 myoblasts by way of a Cre recombinase-inducible construct promoted marked myoblast fusion, while expression of the GAPm variant blocked fusion, indicating the importance of GRAF1-dependent downregulation of RhoA activity

prior to myoblast fusion. Moreover, we also observed that GRAF1 translocates to polarized tips of myoblasts (presumed pre-fusion sites) where it promotes GAP-dependent actin dissolution to likely aid in vesicle trafficking during myoblast fusion. Interestingly, expression of a GRAF1 variant containing a mutated BAR domain resulted in the same loss of fusion, indicating that GRAF1 may also modulates membrane dynamics at these pre-fusion sites [52].

## MOUSE MODELS UTILIZED HEREIN

The Taylor lab has previously demonstrated skeletal muscle-specific expression of GRAF1 *in vitro* and its striking *in vivo* upregulation during the perinatal window of mammalian development [52]. This temporal upregulation of GRAF1 coincides with initial myogenic events, and therefore demonstrates correlative evidence for the involvement of GRAF1 in mammalian muscle formation. To date, there are no reported loss-of-function mouse models for GRAF1. Therefore, in order to determine a role for GRAF1 in this process, I have utilized a novel gene trap mouse model to examine depletion of this protein *in vivo*. Our lab obtained a mouse line from the Texas A&M Institute for Genomic Medicine's Gene Trap Resource, which was generated for us from a GRAF1 gene-trapped embryonic stem cell clone in their gene trap repository. A gene trap is a DNA cassette that is designed to function when inserted into an intron of a target gene. The insertion produces incorrect splicing such that all exons downstream of the insertion site are not expressed. The GRAF1 gene trap mice have an insertion within intron 1 of the endogenous GRAF1 gene, resulting in a truncated and non-functional protein product (Figure 1.2). In Chapter 2, I demonstrate the

ability of this gene trap to globally deplete GRAF1 mRNA and protein products in the mouse, and describe the consequential affects on muscle formation therein.

Although GRAF1 is basally expressed at low levels in adult muscle, I demonstrate in Chapter 2 that GRAF1 is upregulated in injured and nascent myofibers following cardiotoxin-induced muscle injury. Furthermore, GRAF1 gene trap mice exhibit impaired muscle regeneration following injury, implicating an important role for GRAF1 in muscle maintenance. In order to test this possibility, I generated dystrophin/GRAF1 double-deficient mice by breeding our GRAF1 gene trap mice with dystrophic *mdx* mice (refer to Figure 3.6 for details of genetic cross) and analyzed the effects of GRAF1 deficiency on disease progression. The *mdx* mouse is an established and extensively utilized genetic-based model for DMD that lacks functional dystrophin protein and undergoes repeated cycles of muscle degeneration and regeneration [69, 70]. Importantly, unlike human DMD patients, *mdx* mice exhibit a much milder dystrophic phenotype, making them an excellent model in which to assess disease exacerbation/improvement following genetic or therapeutic interventions [71]. In Chapter 3, I show that dystrophin deficiency unmasks a role for GRAF1 in maintaining sarcolemmal integrity as well as an unexpected role in muscle growth, and propose the likely mechanisms for how GRAF1 regulates these processes in instances of severe muscular damage.

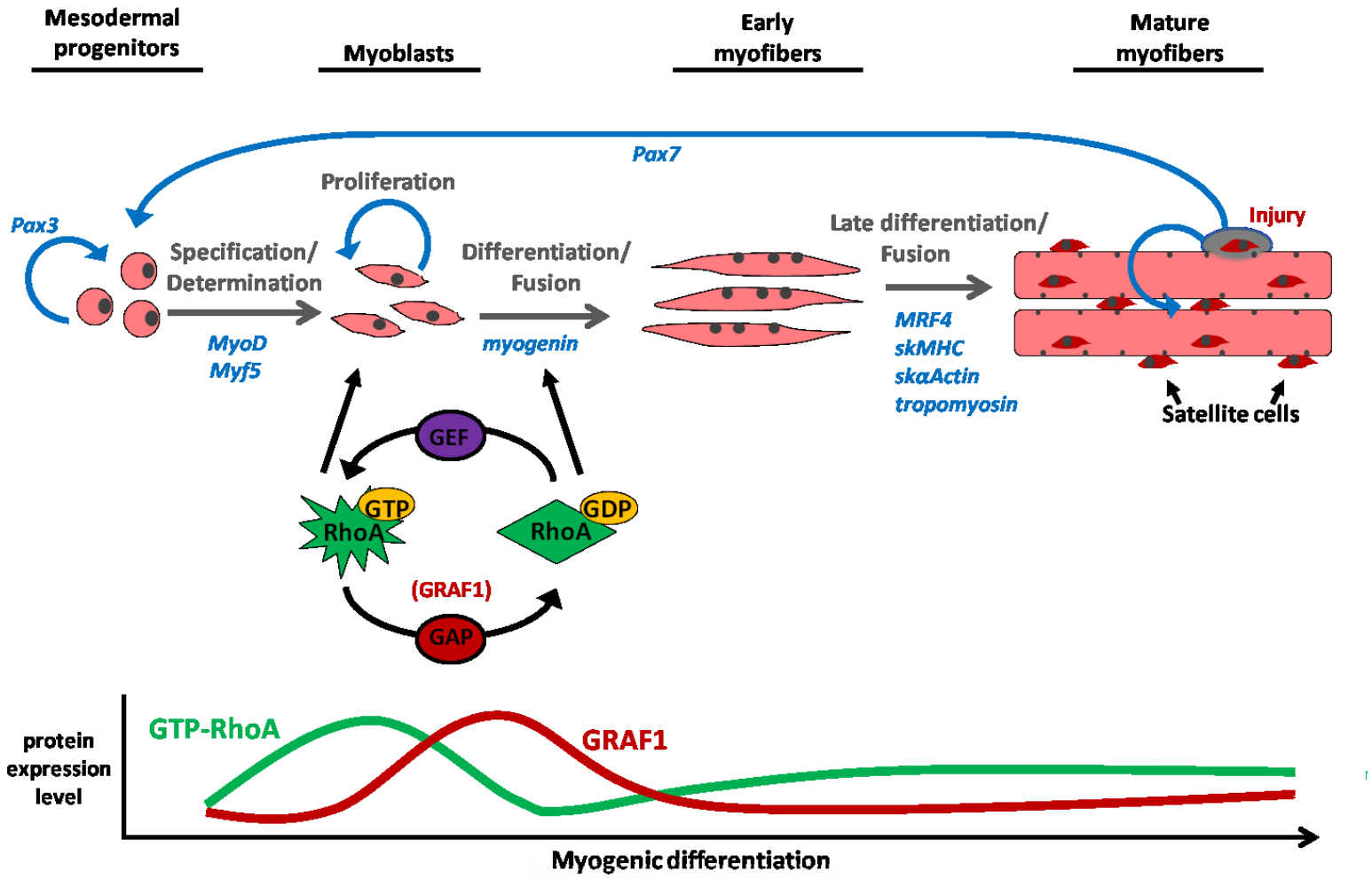
Mesodermal progenitors
Myoblasts
Early myofibers
Mature myofibers
Pax7
Proliferation
Pax3
Specification/ Determination
Differentiation/ Fusion
Late differentiation/ Fusion
Injury
MyoD
Myf5
myogenin
MRF4
skMHC
skαActin
tropomyosin
Satellite cells
GEF
GTP
RhoA
GDP
RhoA
(GRAF1)
GAP
protein expression level
GTP-RhoA
GRAF1
Myogenic differentiation

**Figure 1.1: Skeletal myogenesis is controlled GRAF1-dependent downregulation of RhoA.** Once myoblasts are specified towards a myogenic lineage, they can proliferate to self-renew or be induced to exit the cell cycle and turn on factors which facilitate progressive differentiation and myocyte fusion to form mature multinucleated myofibers. Moreover, adult skeletal muscle maintains a high capacity for regeneration, which mimics this myogenic process in many aspects. Adult muscle is intercalated with numerous muscle progenitors called satellite cells which are the major source of regeneration in this tissue. When muscle becomes injured, satellite cells will proliferate, differentiate and fuse either with each other to form nascent myofibers, or they will fuse to the injured myofiber to repair the muscle syncytium. Interestingly, it has been shown that the activity of RhoA is tightly regulated during muscle maturation, in that there needs to be an initial upregulation of active or GTP-bound RhoA to commit the progenitors to a myogenic lineage, followed by a subsequent downregulation of RhoA to facilitate progressive myogenic differentiation. This transition of RhoA from and active to inactive state relies on GTPase activating proteins, or GAPs, to hydrolyze the bound GTP to GDP. Our lab has identified Rho-specific GAP, termed GRAF1, which promotes skeletal muscle differentiation and fusion by down-regulating RhoA activity.

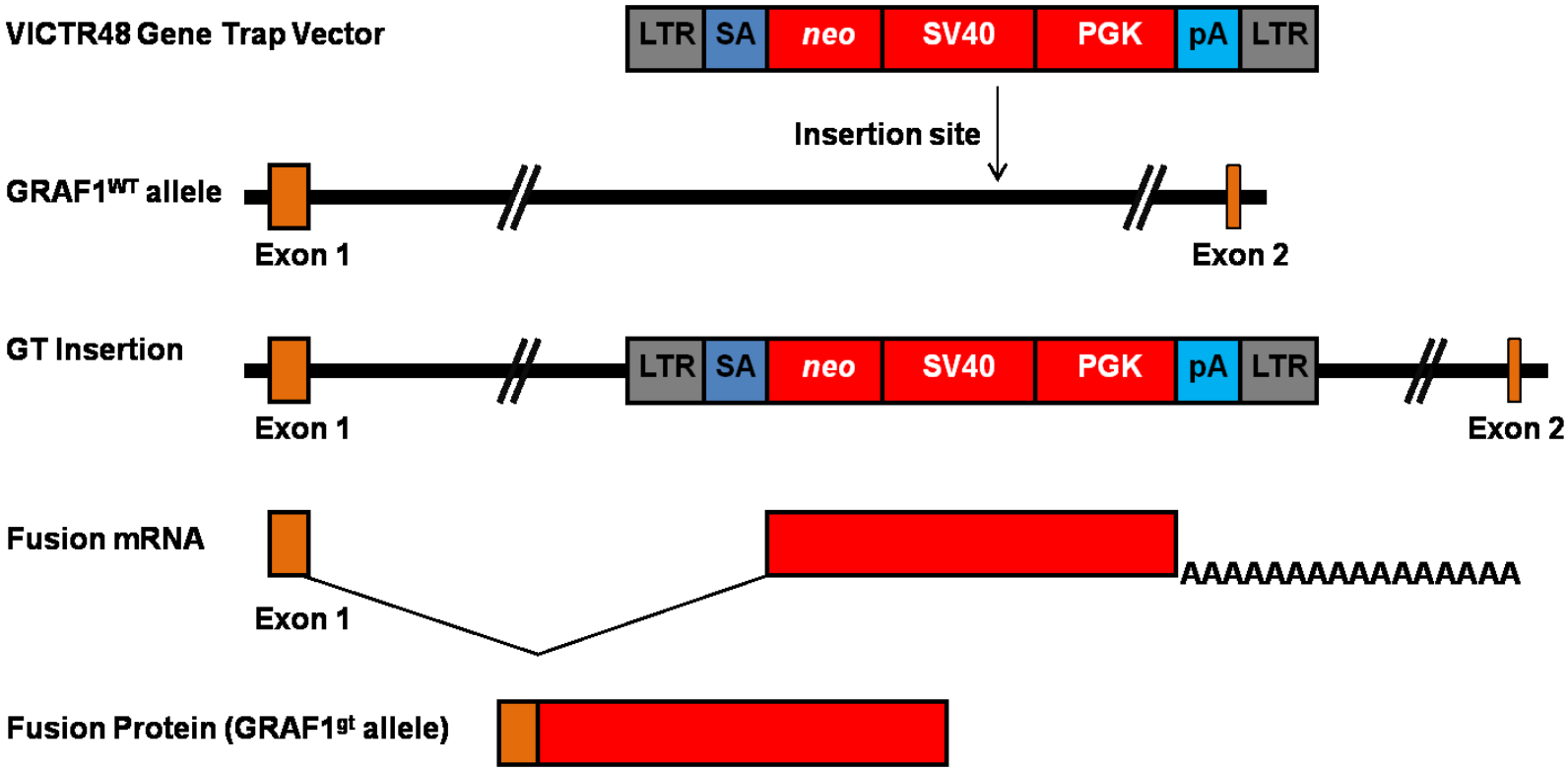
VICTR48 Gene Trap Vector
LTR
SA
neo
SV40
PGK
pA
LTR
Insertion site
GRAF1WT allele
Exon 1
Exon 2
GT Insertion
LTR
SA
neo
SV40
PGK
pA
LTR
Exon 1
Exon 2
Fusion mRNA
AAAAAAAAAAAAAAA
Exon 1
Fusion Protein (GRAF1gt allele)

**Figure 1.2: Generation of GRAF1 gene trap mice.** GRAF1 gene trap (GT) mice generated and obtained from the Texas A&M Institute for Genomic Medicine harbor the gene trapping vector VICTR48 within the first intron of *Graf1* allele. Following pre-mRNA splicing, the fusion mRNA is translated into a biologically inactive truncated protein.

# CHAPTER 2

## GRAF1 PROMOTES FERLIN-DEPENDENT MYOBLAST FUSION[1]

### INTRODUCTION

Myogenesis occurs through the fusion of singly nucleated myoblasts into multinucleated myotubes and this process is essential for proper skeletal muscle formation and injury repair. It is becoming clear that dynamic and coordinated changes in actin polymerization and vesicle trafficking are required for skeletal muscle formation. For example, formation and subsequent dissolution of an F-actin focus at the distal ends of fusion competent myoblasts is essential for myoblast-myoblast fusion [72], [55, 73, 74]. The dissolution of actin is thought to be important for promoting intercellular lipid bilayer fusion and perhaps for the recruitment of unilamellar vesicles that deposit essential fusogenic proteins and phospholipids [75], but the molecular machinery that orchestrate coordinated changes in vesicular trafficking and actin dynamics remain elusive.

Myoferlin and its family members (dysferlin and Fer1L5) are large membrane anchored proteins that contains six to seven calcium response domains (so-called C2 domains) and their structures closely resemble that of synaptotagmins, proteins that facilitate fusion of membrane-bound vesicles to the plasma membrane during exocytic neurotransmitter release [76]. Dysferlin-deficiency is causal for Limb girdle muscular dystrophy 2B, and studies in muscle fibers lacking dysferlin revealed defects in membrane

resealing following mechanical or laser-induced membrane rupture [7, 77]. The finding that dysferlin-null muscle retained accumulation of vesicles near membrane damage sites indicates that dysferlin likely mediates the final step of fusion necessary for plasma membrane repair [78]. Myoferlin and Fer1L5 which are transiently expressed during myogenesis and are known to facilitate myoblast fusion during the development of nascent muscle fibers likely function in a similar fashion. Ferlins are only transiently expressed on muscle plasma membranes and their active recruitment to the sarcolemma is tightly regulated by endocytic recycling mediated by the Eps15 homology domain (EHD)-containing proteins 1 and 2 [78-80]. While several muscular dystrophies are associated with abnormal plasma membrane localization of dysferlin, indicating the significance of this regulatory process [81, 82], [83, 84], the precise mechanisms that govern ferlin recruitment during myoblast fusion or to sites of injury are still poorly understood.

We recently identified a striated muscle enriched protein termed GRAF1 that is poised to co-regulate actin- and lipid-dynamics by virtue of its multi-domain structure that includes a N-terminal lipid binding/bending BAR domain, a phosphatidyl serine (PS)-binding PH domain, a central Rho-GAP domain, and a C-terminal protein-interaction SH3 domain that interacts with focal adhesion kinase (FAK) [85-87]. We reported that depletion of GRAF1 from developing tadpoles induced a highly penetrable dystrophic phenotype that that led to immobility [88]. Moreover, we showed that ectopic expression of GRAF1 in cultured myoblasts induced robust fusion by a process that required both GAP-dependent actin remodeling and BAR domain-dependent membrane binding or sculpting. However, since myoblast fusion does not occur in developing tadpoles, questions remained as to whether (or to what extent) GRAF1 was necessary for myoblast fusion *in vivo*. We

developed a novel line of GRAF1-deficient mice and our studies detailed herein reveal that while viable, these mice exhibit limited myogenesis. Moreover, our mechanistic studies reveal that GRAF1 and its related family member, GRAF2, regulate myoblast fusion by promoting endocytic recycling-dependent membrane recruitment of the fusogenic ferlin proteins to the plasma membrane.

## RESULTS

### *Generation of GRAF1-deficient mice*

To explore a role for GRAF1 in promoting myoblast fusion *in vivo*, we generated a GRAF1-deficient mouse line using ES cells that contained an inhibitory gene trap within the first intron of *Graf1* (Figure 2.1a). Crosses between GRAF1$^{+/gt}$ mice yielded offspring in the appropriate Mendelian ratios as assessed by validated PCR genotyping (Figure 2.1b; Table 2.1). GRAF1 was strongly but not completely depleted in all tissues evaluated indicating that our model results in a hypomorphic allele. Importantly, GRAF1 mRNA levels and protein were virtually undetectable in all skeletal muscle types evaluated (gastrocnemius, quadriceps femoralis, triceps, and diaphragm) supporting the value of this model to further investigate a role for GRAF1 in the development and maintenance of these tissues (Figure 2.1c). As previously reported, GRAF1 is also highly expressed in the brain and while a significant reduction in message and protein was observed therein, some residual expression did remain. The tissue-specific differences in residual GRAF1 mRNA levels in the GRAF1$^{gt/gt}$ mice were likely due to the differential expression or activity of splicing factors [89].

*GRAF1 is necessary to promote proper muscle growth* in vivo

No overt phenotypes were observed in GRAF1$^{+/gt}$ or GRAF1$^{gt/gt}$ mice for up to 1 year, though a modest reduction in body weight was observed in young adult homozygous mutant mice (27.2 +/-1.0 g versus 24.3 +/- 1.6 g; $p$=0.13 at 4 months of age). To determine if GRAF1 is necessary for efficient muscle growth, we quantified the cross sectional area (CSA) of different muscle types. As shown in figure 2.2, the distribution of fiber size showed a relative lack of large myofibers and more small fibers in GRAF1$^{gt/gt}$ diaphragm and gastrocnemius muscles compared to littermate controls. Concomitantly, mean fiber size of both muscles types were significantly smaller in GRAF1$^{gt/gt}$ mice than in littermate controls. Since myofiber CSA is known to correlate with force production, we next measured the grip force of GRAF1$^{+/+}$ and GRAF1$^{gt/gt}$ mice using a digital strain gauge [90]. Confirming an important role for GRAF1 in muscle formation, we found that GRAF1$^{gt/gt}$ mice exhibited a significant reduction in grip strength compared to GRAF1$^{+/+}$ mice (137.9 +/- 6.2N versus 151.2 +/- 6.8 N respectively; $p$<0.05). No significant difference in levels of differentiation markers were observed in P1 or P10 muscles, indicating that the muscle development defect was likely due to impaired muscle fusion, not differentiation (Figure 2.3a).

Besides its importance in formation of large muscle fibers during development, myoblast fusion plays a key role in the regeneration of injured muscle. To determine if GRAF1 might also function in this setting, we treated WT mice with cardiotoxin and evaluated GRAF1 expression 3, 14, and 28 days later (Figure 2.4a). We found that while GRAF1 was expressed in very low levels in un-injured adult muscle, GRAF1 was transiently increased at early stages of muscle regeneration particularly within the smaller nascent myotubes that were most abundant 3 days following injury. To explore a functional role for

GRAF1 in mediating fusion during muscle regeneration we quantified nuclear accretion and growth in regenerating WT and GRAF1$^{gt/gt}$ muscles 14 and 28 days post-injury. As shown in figure 2.4b, a significant reduction in the average number of nuclei was observed in regenerating GRAF$^{gt/gt}$ myofibers compared to GRAF1$^{+/+}$ littermates. Moreover, after 14 days, the GRAF1$^{gt/gt}$ mice exhibited a significant reduction in the number of regenerating myofibers with two or more nuclear foci (*in vivo* fusion index) (Figure 2.4c,d; Figure 2.5a). This reduction in nuclear foci persisted to 28 days post-injury and a concomitant significant reduction in the CSA of the regenerating myofibers was observed at this time point (Figure 2.4d,e; Figure 2.5c,d). Collectively, these data indicate that GRAF1 is required for optimal fusion and growth of myofibers during development and following injury.

To confirm and extend these findings, we next compared the fusion capabilities of myoblast cultures isolated from the hindlimb muscles of P2 GRAF1$^{gt/gt}$ and GRAF1$^{+/+}$ littermates. Cells were plated at high density and subjected to differentiation media (DM) to induce myotube formation. While no significant difference was observed in the differentiation index (i.e. tropomyosin positive nuclei/total nuclei) or differentiation marker expression (Figure 2.3b), a significant decrease in the fusion index (i.e. the percentage of nuclei present in multinucleated cells) was observed in GRAF$^{gt/gt}$ compared to GRAF1$^{+/+}$ cultures (Figure 2.6a-c). As well, while the cell density (nuclei/area) was not different in these cultures, the number of nuclei in multinucleated cells was lower in tropomyosin-positive GRAF$^{gt/gt}$ cells and a concomitant significant reduction in myotube length was observed (Figure 2.6d-f). Collectively, these studies indicate that GRAF1 is necessary for appropriate myoblast fusion.

*GRAF1 associates with endocytic recycling vesicles and regulates Golgi to plasma membrane vesicle trafficking*

We next utilized a well-established multipotent mesenchymal progenitor cell line (C2C12) to deconstruct the mechanisms whereby GRAF1 promotes myoblast fusion. C2C12 cells undergo asynchronous but spontaneous differentiation into multinucleated skeletal muscle myotubes when cultured under high confluence in DM [91, 92]. We previously showed that GRAF1 is recruited to discrete actin-devoid complexes at the tips of pre-fused differentiated C2C12 myoblasts [88] and our subsequent finding that Rho-GAP activity was necessary for GRAF1-dependent induction of myoblast fusion led us to speculate that GRAF1-dependent cytoskeletal remodeling was necessary for membrane merging (see figure 2.7a for example of GRAF1 locale in actin devoid region at the juncture of two cells undergoing end-to-end alignment/fusion). While GRAF1's BAR domain was also necessary for GRAF1-dependent myoblast fusion, the precise mechanism was not clear [88]. Interestingly, using differential interference contrast (DIC) microscopy to further analyze GRAF1-containing complexes in differentiated C2C12 cells, we found that endogenous GRAF1 is localized to sub-membranous vesicles at these sites (Figure 2.7b). Moreover, we found that GRAF1 co-localized with a subset of Rab5 labeled endosomes within these pre-fusion complexes but did not co-localize with Lamp2 (a marker for degrading lysosomes), indicating that GRAF1 may be a component and/or regulator of recycling endosomes. In support of this possibility, we found significant intracellular co-localization of GRAF1 with the GPI-anchored membrane protein, Thy-1, which is known to recycle from the endosomes through the Golgi apparatus and back to the plasma membrane (Figure 2.7c and [93]).

3-D reconstruction of confocal Z-stacks revealed that GRAF1 enriched regions protruded from the cell surface, and that these protrusions are localized to the precise point of

contact between fusing myoblasts (Figure 2.8a; Figure 2.9; Figure 2.10). These findings are consistent with the postulate that GRAF1-laden vesicles are recruited to the plasma membranes of fusing cells and that this process may facilitate cell to cell adhesion/fusion. In support of a role for GRAF1 in promoting vesicle to plasma membrane trafficking, we found that ectopic expression of GRAF1 in myoblasts led to pronounced cell elongation and significant surface area expansion, which necessitates addition to the plasma membrane (Figure 2.8b). This phenotype was fully attenuated by treatment with Brefeldin A (BFA), a drug that inhibits the translocation of secretory and endocytic recycling vesicles from the Golgi to the cell membrane, indicating that GRAF1 promotes plasma membrane expansion by enhancing vesicle recruitment (Figure 2.8b). To explore a role for this process in the capacity of GRAF1 to promote myoblast fusion, we utilized our Cre-inducible GRAF1 cDNA variant (termed $GRAF1^{loxp}$) that contains a GFP reporter gene (Figure 2.11 and [88]). $GRAF^{loxp}$ transfected C2C12 cells were transferred to DM prior to treatment with either LacZ (control) or Cre adenovirus to induce GRAF1 expression. Eighteen hours later, subsets of LacZ or Cre-infected cells were then treated with BFA and nuclear accretion was assessed 24 hr later. As shown in figure 2.8c, GRAF1 expressing cells (in the Cre-treated cultures) exhibited a significant increase in myotube fusion when compared with Lac-Z treated cells that contained the $GRAF^{loxp}$ construct, consistent with our previous findings that GRAF1 promotes cell fusion in pre-differentiated myoblasts [88]. Importantly, BFA treatment significantly reversed the pro-fusogenic capacity of GRAF1, indicating that GRAF1 promotes fusion of differentiated myoblasts in a vesicle trafficking-dependent manner.

*GRAF1 promotes plasma membrane recruitment of the fusogenic proteins EHD1, myoferlin, and Fer1L5*

The endocytic recycling proteins EHD1 and EHD2 were recently shown to facilitate myoblast fusion by inducing the release of vesicles from the endocytic recycling compartment and promoting subsequent 'exocytic' vesicle merging to the plasma membrane [78-80]. As shown in figure 2.12a, GRAF1 and EHD1 exhibited remarkable co-localization in pre-fusion complexes, while little overlap was observed between GRAF1 and EHD2. This finding is noteworthy, because recent studies indicate that EHD2 is primarily localized to caveolae and unlike depletion of EHD1, depletion of EHD2 does not block endocytic recycling in fibroblasts [94]. As EHD1 was previously reported to bind avidly to the fusogenic proteins, myoferlin and its family member, Fer1L5, and to promote their transport to the plasma membrane [78, 79], we next sought to determine if GRAF1 co-associated with these proteins. Indeed, we observed significant co-localization between GRAF1 and myoferlin as well as GRAF1 and Fer1L5 in pre-fusion complexes in isolated myoblasts and in intact muscle (Figure 2.12a,b). Moreover, myoferlin and GRAF1 exhibited a strong interaction as assessed by co-immunoprecipitation (Figure 2.12c). We next explored our hypothesis that GRAF1 might facilitate the recruitment of these proteins to discrete plasma membrane complexes. Since pre-fusion complexes are more readily observed in C2C12 cells than in primary myoblast cultures (because the latter fuse very rapidly in culture), we treated C2C12 cells with GRAF1 siRNAs (which resulted in a partial reduction of GRAF1 protein; Fig. 7d) and analyzed the localization of Fer1L5, myoferlin and EHD1 in cells following exposure to DM. As shown in figure 2.12e, Fer1L5 was no longer localized to foci at the plasma membrane in GRAF1-deficient cells. Additionally, we observed a significant but incomplete reduction of myoferlin and EHD1 localization to these sub-plasma membrane

structures accompanied by an increase in perinuclear vesicular staining (Figure 2.12e,f). Taken together, these data indicate that GRAF1 regulates the intracellular trafficking of the fusogenic ferlin proteins to promote membrane coalescence.

*Redundancy of GRAF proteins in myoblast fusion*

Studies detailed above indicate that loss of GRAF1 renders myoblast fusion less efficient but does not prevent myotube formation. Thus we next queried whether other members of the GRAF family might serve a redundant role in this process. In mammals, GRAF1 has two closely related family members, GRAF2 and GRAF3. We recently reported that GRAF3 was not expressed in muscle fibers, but instead was strictly restricted to visceral and vascular smooth muscle cells [95]. On the other hand all three GRAF2 isoforms [96] were expressed in peri-natal muscles, in a temporal fashion that mirrored expression of GRAF1, indicating the possibility that GRAF2 might exhibit functional redundancy and potentially compensate for the loss of GRAF1 during myotube formation (Figure 2.13a). In support of this possibility, GRAF2 expression was markedly induced upon subjecting C2C12 cells to differentiating conditions (Figure 2.13b). Moreover, GRAF2 accumulated into similar peri-nuclear and pre-fusion complexes (Figure 2.13b, bottom) where it co-localized with myoferlin. To further explore a role for GRAF2 in muscle fusion, we depleted GRAF2 from primary $GRAF1^{+/+}$ and $GRAF1^{gt/gt}$ myocytes using validated siRNAs (Figure 2.13c). We next subjected these cultures to DM for 48 hr and quantified nuclear accretion in tropomyosin positive myoblasts. As shown in figure 2.13d, GRAF2 depletion led to a significant reduction in myoblast-myoblast (bi-nucleated) and myoblast-myotube fusion (≥3 nuclei). Notably, the lack in fusion in GRAF2-depleted $GRAF1^{+/+}$ cells was even more

pronounced than was observed in myoblasts cultured from GRAF1$^{gt/gt}$ littermates. However, depletion of GRAF2 from the GRAF$^{gt/gt}$ cultures did not result in an additive fusion defect, indicating that the two family members exhibit redundant overlapping functions. In support of this notion, the recruitment of EHD1 to the tips of GRAF2 depleted C2C12 cells was markedly reduced in comparison to either control or GRAF1-depleted cells (Figure 2.13e,f).

## DISCUSSION

A clear understanding of the molecular mechanisms that govern myogenesis is important for the future development of therapies directed towards ameliorating muscle wasting that occurs with aging and is exacerbated in muscular dystrophies. We previously showed that the Rho-GTPase-activating protein, GRAF1, was transiently up-regulated during myogenesis, and that forced expression of GRAF1 in pre-differentiated myoblasts promoted robust muscle fusion by a process that required GTPase-activating protein-dependent actin remodeling and BAR-dependent membrane binding or sculpting. Through the use of our novel GRAF1 depleted mice, we now show that GRAF1 is essential for efficient myofiber growth *in vivo*. Post-natal GRAF1$^{gt/gt}$ muscles exhibited a significant and persistent reduction in cross-sectional area and adult muscles had an impaired capacity to regenerate following injury, suggestive of a lack of efficient myoblast fusion. Indeed, we found that myoblasts isolated from GRAF1 depleted mice exhibited impaired myoblast to myoblast and myoblast to myotube fusion. Our mechanistic studies reveal that GRAF1 and its related family member, GRAF2, facilitate myoblast fusion by promoting endocytic recycling-dependent membrane recruitment of the fusogenic ferlin proteins to the plasma membrane.

It has become clear that myoblast fusion occurs in a multi-step fashion in which actin cytoskeletal dynamics and membrane remodeling play key roles, but questions remain regarding the spatial/temporal regulation of and interrelationship between these processes. Over the past several years, studies have revealed that prior to fusion, differentiated myoblasts assume a bipolar elongated shape that is induced by the interaction of nonmuscle myosin 2A with actin at the plasma membrane and that these so-called F-actin foci mark the future site of myoblast fusion [72, 97]. However, subsequent dissolution of the actin focus is essential for cell-cell fusion as evidenced by the findings in *Drosophila* that mutations in known actin-remodeling genes such as *kette*, *mbc*, and *SCAR/WAVE* all lead to defective fusion accompanied by enlarged F-actin foci that fail to dissolve [55, 73]. The small GTPase RhoA has been shown to initiate actin polymerization [98, 99] and we previously showed that recruitment of the Rho-GAP GRAF1 from the perinuclear region (its sub-cellular locale in proliferating myoblasts) to the tips of pre-fused bipolar differentiated myoblasts is essential for limiting Rho-dependent actin polymerization at these sites [88]. One of the potential functions of localized actin de-polymerization is to facilitate trafficking of intracellular vesicles to the fusion site. Elegant electron microscopy studies in Drosophila myoblasts have shown that vesicles accumulate at juxtaposed inner membranes of fusing cells and that this alignment of vesicles is essential for subsequent membrane merging [55]. While the exact nature of these vesicles is not clear, studies from the McNally laboratory and others indicate that endocytic recycling vesicles (regulated by EHD1 and EHD2) are involved and that myoferlin and Fer1L5 are critical fusogenic cargo carried by these vesicles [78, 79]. Indeed, expression of a mutant EHD2 that inhibits endocytic vesicle trafficking led to cytoplasmic sequestration of ferlins and inhibited myoblast fusion.

Ferlins have been proposed to be important for mediating plasma membrane 'capturing' of intracellular vesicles, though the precise means by which the subsequent merging of plasma membranes of two cells is not clear [100]. Our findings that GRAF1 associates with myoferlin and is co-recruited to the plasma membrane with EHD1-containing endocytic vesicles indicates that GRAF1 is part of this fusogenic complex. Because GRAF1 functions to accelerate actin de-polymerization, and is necessary and sufficient for mediating the recruitment of endocytic recycling vesicles to the plasma membrane, we favor a model in which GRAF1 associates with vesicles through its BAR domain and that vesicle-associated GRAF1 facilitates clearing of sub-plasmalemmal actin to aid in vesicle capture. In support of this hypothesis, GRAF1 contains a PS-binding PH domain and PS is known to be exposed on the inner leaflets of injured membranes and the outer leaflets of exocytic vesicles (Gerke et al., 2002). Notably, our 3-D reconstructions of pre-fusion/fusion complexes reveal that the GRAF1-laden vesicles are located to regions of the cell membrane that protrude outward from the cell body. It is likely that GRAF1 facilitates this outward membrane curvature via interactions of its BAR domain with the inner neck of the membrane protrusion as has been shown for its F-BAR containing Rho-GAP relative, srGAP2 [101]. Interestingly, GRAF1 protrusions appear at the point of cell-cell contact of pre-fused cells indicating that these complexes might function to promote adhesion of two apposed myoblasts. At this stage, these protrusive complexes could promote enhanced hydrophobic attractions between the interiors of the two bilayers, and facilitate lipid transfer from one membrane to another [102, 103]. Buckled membranes also exhibit curvature-induced stress and thus can accelerate the fusion process by reducing the energy barrier membranes need to overcome at intermediate stages of fusion [76]. While our data strongly support a model whereby GRAF1 facilitates

membrane merging by promoting the recruitment of ferlin-containing vesicles, numerous cell-surface receptors have been implicated in promoting the initial stages of myoblast fusion including M-cadherin and NCAM that mediate cell recognition and integrins that mediate cell-cell adhesion and it is formally possible that GRAF1-dependent recruitment of these receptors is involved[104].

Besides specifying the position of cell-cell fusion and promoting membrane contact, GRAF1 may also play an important role in the late stages of syncytium formation which involves fusion pore expansion to allow complete coalescence of cytoplasms. In this final stage of cell-cell fusion, initial pores of a few nanometers in diameter undergo an active expansion to yield a lumen of 10-15 μm (i.e. the diameter of a typical myoblast). The Chernomordik laboratory and others have shown that expansion of such pores that contain strongly bent plasma membrane rims requires persistent energy input and they have postulated that curvature generating proteins that relax the bending energy of the rim are likely required to make expansion energetically favorable [53]. BAR domain-containing proteins are likely candidates as these domains form elongated homodimers characterized by a shallow curvature formed by the anti-parallel interaction of two α-helical coils that facilitate membrane deformation [105]. Previous studies showed that the GRAF1 BAR domain is capable of inducing tubulation of spherical lipids and can promote clathrin-independent endocytosis in fibroblasts and HeLa cells [106, 107]. Interestingly, the curvature of the membrane at the fusion pore rim and the curvature of endocytic vesicles are similar, and using an elegant model system to study the efficiency of late stages of cell-cell fusion initiated by influenza and baculoviruses, Richard et al. showed that the GRAF1 BAR domain promoted syncytium formation [108]. In support of a putative role for GRAF1 in

mediating this process during skeletal muscle cell fusion, we found that GRAF1 protein accumulates within the narrow neck that joins two fusing myoblasts (see figure 2.7a for example). Whether GRAF1 serves to stabilize the fusion pore and/or to promote endocytosis-dependent internalization of excess plasma membrane from fusing cells [75] are interesting questions for future studies.

While the loss of GRAF1 clearly makes myoblast fusion less efficient, muscle development was not completely blocked in GRAF1$^{gt/gt}$ mice. This finding indicates that other proteins are able to compensate for the loss of GRAF1. One attractive candidate is GRAF2, a closely related family member that is widely expressed [109]. We showed that like GRAF1, mammalian GRAF2 is also highly up-regulated during skeletal muscle maturation, and that GRAF2 depletion significantly attenuated myoblast-myoblast and myoblast-myotube fusion in WT primary muscle cell cultures. Moreover, GRAF2 was localized to similar pre-fusion complexes, and its depletion resulted in a marked reduction of EHD1 and myoferlin accumulation to these sites. These data taken together with the lack of an additive effect of GRAF1 and GRAF2 depletion on myotube formation indicates that these family members have functionally overlapping roles during muscle development. However, while GRAF1 and GRAF2 exhibit an identical BAR-PH-GAP-SH3 domain structure, they do have a variable serine/proline region which we previously showed is a hot-spot for phosphorylation [87], thus it is possible that these proteins are differentially regulated by kinase signaling pathways. While we did not see evidence of GRAF2 overexpression in isolated GRAF1$^{gt/gt}$ myoblasts when compared to GRAF1$^{+/+}$ cells, we have not ruled out the possibility that transient up-regulation occurs in developing GRAF$^{gt/gt}$ muscles. Other classes of BAR domain containing proteins may also be important for

promoting GRAF-independent muscle fusion. For example, two members of the Bridging integrator (Bin) family, Bin1 and Bin3 have been shown to regulate differentiation and fusion of skeletal myoblasts [110-112]. Interestingly, while Bin3 is an N-BAR only containing protein, recent studies indicate that it, like GRAF1, also regulates actin dynamics. Simionescu-Bankston et al. recently showed that Bin3 associates with and promotes the activation of the Rho-related GTPases Cdc42 and Rac1 in myoblasts [112]. Notably, activation of these GTPases is often associated with an inhibition of RhoA; however the effect of Bin3 on RhoA activity was not directly tested in this model. It will be of interest to determine whether the Bin proteins also exhibit some functional overlap with the GRAF proteins or are co-regulated through putative BAR domain heterodimerization as has been observed in other BAR family members.

In summary, we provide the first evidence that GRAF1 is necessary for efficient muscle formation *in vivo*. The phenotype of the GRAF1$^{gt/gt}$ mice resembles myoferlin-null mice [57] and our mechanistic studies reveal that GRAF1 co-associates with myoferlin and EHD1-containing endocytic recycling vesicles and regulates the recruitment of these fusogenic vesicles to the plasma membrane. This study furthers our understanding of the inter-relationship between cytoskeletal and membrane dynamics during myotube formation.

## MATERIALS AND METHODS

### *Generation of GRAF1 gene trap mice*

GRAF1 gene trap mice were generated and obtained from the Texas A&M Institute for Genomic Medicine (College Station, TX) using the OmniBank ES cell clone OST135790 which harbors the gene trapping vector VICTR48 within the first intron of *Graf1* (*Arhgap26*,

accession #: NM_175164). To generate a stable mutant mouse line, 129SvEv-derived ES cells were microinjected into host C57BL/6J mice for germline transmission of the *GRAF1* mutation. All experimental mice were maintained on a mixed 129/SvEv-C57BL/6J genetic background. Mice were genotyped utilizing the following primers: forward Primer A (5-AGCACTGTGAACACCATTCTG-3'), forward Primer C (5'-AAATGGCGTTACTTAAGCTAGCTTGC-3'), and reverse Primer B (*5'*-AAAGGACATCTGACACTACCAAA-3'). Animals were treated in accordance with the approved protocol of the University of North Carolina (Chapel Hill, NC) Institutional Animal Care and Use Committee, which is in compliance with the standards outlined in the guide for the Care and Use of Laboratory Animals.

*Primary antibodies and cDNA constructs*

Commercial anibodies were purchased from Sigma (laminin, tropomyosin (CH1) and monoclonal γ-tubulin); Abcam (EHD2, Lamp2 and Thy-1); BD Biosciences (GM130 and Rab5); Epitomics (EHD1); Cell Signaling (Myc-tag, 9B11); GAPDH (Imgenex); Novus Biologicals (myoferlin); and Developmental Studies Hybridoma Back, Univ. of Iowa (MHC, NA4). The GRAF2 (PS-GAP) antibody was a generous gift from Dr. Wen-Cheng Xiong (Georgia Regents University, GA) [109]. Derivation of the polyclonal Fer1L5 and GRAF1 antibodies was previously described [78, 88]. A hamster monoclonal GRAF1 antibody was designed in house using the identical peptide immunogen by standard methodology. The $GRAF1^{loxP}$ cDNA construct was described [88, 113]. Briefly, Myc-tagged GRAF1 was subcloned into a Cre recombinase-inducible construct, downstream of a beta-actin promoter and a GFP reporter followed by a transcriptional 'stop' site flanked as a unit by loxP sites.

As such, the GRAF1$^{loxP}$ construct allows for Cre-dependent expression of GRAF1 in a time-dependent manner. The Ad5CMV Cre recombinase adenovirus was purchased from the University of Iowa Gene Transfer Vector Core (Iowa City, IA), and the Ad5CMV LacZ adenovirus was purchased the University of North Carolina Viral Core (Chapel Hill, NC).

*Semi-quantitative RT-PCR analysis*

Total RNA was isolated from homogenized whole mouse tissues or primary mouse myoblast cultures using RNeasy Mini Kit (Qiagen) according to manufacturer's instructions. Complimentary DNA (cDNA) was obtained from 1 μg of RNA isolate using the iScript cDNA Synthesis Kit (Bio-Rad,), and PCR amplifications of 30 cycles were performed using 2.5% of total synthesized cDNA and TaKaRa Ex Taq Polymerase (Millipore) according to manufacturer's instructions using the following primers *graf1* forward 5'-TGGAAGGGTACCTGTACGTG-3' and *graf1* reverse 5'-ATCCCGTTGGTAGGTACAGT-3', $T_a$=60°C; *graf2* forward 5'-TAACAGTCATATGAAGATTTTTCGAACCTCGCCTG-3' and *graf2* reverse 5'-CTGATGGATCCTTATGCCCGAGCCTTTCGATTGAT-3', $T_a$=56°C [114]; *skeletal alpha actin* forward 5'-CAGAGCAAGCGAGGTATCC-3' and *skeletal alpha actin* reverse 5'-GTCCCCAGAATCCAACACG-3', $T_a$=50°C; and *gapdh* forward 5'-ATGGGTGTGAACCACGAGAA-3' and *gapdh* reverse 5'-GGCATGGACTGTGGTCATGA-3', $T_a$=43°C. RT–PCR products were analyzed by electrophoresis using 2.0% agarose gels.

*Cell culture, transfection and siRNA treatment*

Primary myoblasts were maintained in growth media (GM; Dulbecco's modified

Eagle's medium (DMEM) supplemented with 20% fetal bovine serum (FBS), 10% horse serum (HS) and penicillin/streptomycin). C2C12 mouse myoblasts obtained from ATCC (Catalog number CRL-1772) were maintained in DMEM supplemented with 10% FBS and antibiotics. C2C12 cells maintained in GM were transfected with Myc-tagged GRAF1 cDNA or GRAF1$^{loxp}$ cDNA using *Trans*IT transfection reagent (Mirus) according to manufacturer's instructions. Myoblasts were infected with Cre- or LacZ-expressing adenoviruses at 100 multiplicities of infection. For differentiation, myoblasts were plated on Lab-Tek CC2 chamber slides or plastic dishes pre-coated with rat tail collagen, Type I (10 μg/ml) and transferred to differentiation medium (DM; DMEM containing 2% HS). In some instances, myoblasts were treated with brefeldin A (Sigma) at indicated concentrations 12 hours prior to fixation. GRAF1 and GRAF2 were depleted from cultured myoblasts using short interfering RNA (siRNA) duplex oligoribonucleotides obtained from Invitrogen with the following sequences: *graf1*a sense *5'*-GCAGCUGUUGGCCUAUAAU(dT)(dT)-3' and anti-sense 5'-AUUAUAGGCCAACAGCUGC-3'; *graf1*b sense 5'-AAGUGGACCUGGUUCGGCAACAUUU-3' and anti-sense 5'-AAAUGUUGCCGAACCAGGUCCACUU-3'; and *graf2* sense 5'-CAAAGGUCCAGAGACUUCUGAGUAU-3' and anti-sense 5'-AUACUCAGAAGUCUCUGGACCUUUG-3'. Myoblasts maintained in GM or DM were transfected with 150 nM of total gene-specific siRNA (GRAF1 was knocked down using 75nM of both *graf1*a and *graf1*b, GRAF2 was knocked down using 150 nM of *graf2*, double depletion of GRAF1 and GRAF2 required 37.5 nM each of *graf1*a and *graf1*b and 75 nM of *graf2,* and 150nM of a GFP-specific siRNA was used as a non-target control (NTC) using DharmaFECT reagent 1 according to manufacturer's instructions (Thermo Scientific). In

some experiments, 50 nM of Block-IT red fluorescent oligonucleotides (Invitrogen) was concomitantly transfected with the siRNAs to assess transfection efficiency. After 8 hr, media was exchanged and cells were fixed or snap-frozen at indicated time points.

*Primary myoblast isolation*

Skeletal muscle from GRAF1$^{gt/gt}$ and GRAF1$^{+/+}$ littermates was meticulously isolated from 3-4 P2 neonatal mouse pups per genotype and placed in ice-cold PBS. Once all tissue was harvested, the PBS was exchanged for Hank's Balanced Salt Solution (HBSS; GIBCO) and tissue was transferred to a sterile 100 mm petri dish for mincing using a sterile razor blade in minimal HBSS. Tissue was digested using 0.2% Collagenase, Type II (Worthington Biochemicals) in HBSS incubated at 37°C for 40 min, briefly swirling every 10 minutes during incubation. Digested muscle was triturated 5 times using a wide-mouth pipette and filtered through a 100 µm nylon mesh cell strainer (BD Biosciences). The cell suspension was then incubated at room temperature for 1 hr followed by addition of 30 mL GM and centrifuged at 2,000 rpm for 3 min. Cells were pre-plated in GM for 45 min and the remaining suspension was gently transferred to new 100 mm dishes at 1 X $10^6$ cells/dish and incubated undisturbed for 72 hr prior to use.

*Myoblast differentiation and fusion assays*

Myoblasts were seeded at subconfluent densities on collagen-coated slides in GM and after 12 hr switched to DM for indicated time. The differentiated index, fusion index, and number of nuclei per field were quantified as described previously, with slight modifications [115]. Briefly, the differentiation index is defined as the ratio of number of nuclei in Tm-

positive cells to total number of nuclei counted, while the fusion index is defined as the ratio of number of nuclei in myotubes (≥2 nuclei) to total nuclei counted. Images were analyzed using ImageJ software (NIH) to measure the long axis of the cell.

*Immunohistochemistry and Immunocytochemistry*

Upon harvest, tissues were immediately embedded in Tissue-Tek O.C.T. compound (Sakura), snap-frozen in 2-Methylbutane cooled over dry ice, and cross-sectioned at 8 μm using a cryotome. Sections were post-fixed (or cultured myoblasts were fixed) in 4% paraformaldehyde, permeabilized, and stained using standard techniques. The GRAF2, tropomyosin, MHC, Myc-tag, and myoferlin antibodies were diluted at 1:500; The GRAF1, EHD1, EHD2, and Fer1L5 antibodies were diluted at 1:200; The Lamp2 and GM130 antibodies were diluted at 1:100; and the Rab5 antibody was diluted at 1:50. A mouse anti-hamster linker (SouthernBiotech) was used at 1:500 for conjugation to the GRAF1 hamster antibody. Cells/tissues were then incubated with Alexa Fluor secondary antibodies (Invitrogen), Alexa Fluor phalloidin (Invitrogen), Alexa Fluor wheat germ agglutinin (Invitrogen) and DAPI at 1:500 in PBS for 1 hr, washed and mounted.

*Muscle injury model and* in vivo *myofiber analysis*

Gastrocnemius and diaphragm muscles were harvested from 4 month old GRAF1$^{gt/gt}$ and GRAF1$^{+/+}$ littermates and processed as described previously. To induce muscle injury, 100 μL of 20 μM cardiotoxin (*Naja nigricollis*, Calbiochem) was injected into the gastrocnemius muscle of 4 month old littermates. Muscles were harvested 3, 14 and 28 days post-injury and processed as described. Images were acquired and analyzed using ImageJ

software to quantify myofiber cross sectional area. The *in vivo* fusion index was quantified as described previously [116]. Briefly, the *in vivo* fusion index is described as the ratio of number of myofibers with ≥2 centrally located nuclear foci to total number of regenerating myofibers.

*Fluorescence ratio analysis*

The EHD1 fluorescence ratio is defined as the ratio of the EHD1 signal within a pre-fusion complex (10 $\mu m^2$ yellow box, Figure 2.12f) to the EHD1 signal within the remainder of the cell. Integrated density values obtained using ImageJ were used in the calculation of EHD1 fluorescence ratios. Tm-positive cells which contained 1 or 2 nuclei, and exhibited an elongated phenotype with a prominent pre-fusion complex were imaged using a Zeiss 710 confocal microscope set to a 2 μm pinhole.

*Protein isolation, Western blotting and co-immunoprecipitation*

Tissue samples were snap-frozen in liquid nitrogen, sonicated in modified radioimmune precipitation assay (RIPA) buffer (50mM HEPES pH 7.2, 0.15 M NaCl, 2 mM EDTA, 0.1% Nonidet P-40, 0.05% sodium deoxycholate, 0.5% Triton X-100 plus 1mM sodium orthovanadate and 1X concentrations of both Halt Protease Inhibitor Cocktail (Thermo Scientific) and Halt Phosphatase Inhibitor Cocktail (Thermo Scientific)), and cleared by centrifugation. Cultured C2C12 mouse myoblasts were directly lysed and cleared in RIPA buffer. For immunoprecipitation studies, 1 mg of cleared lysate was incubated with 10 μg of either an anti-GRAF1 antibody (polyclonal) or the corresponding non-immune sera (NIS) overnight at 4°C. The solution was then mixed with 75 μL of a 50% slurry of Protein

A Sepharose beads (Sigma) in TBS and rotated at 4°C for 2 hr. Beads were then quickly tapped down in a refrigerated centrifuge and rinsed 3 times with ice-cold RIPA + inhibitors and once with TBS before beads were boiled in 50 μL of sample buffer. Lysates were resolved by SDS-PAGE, transferred to nitrocellulose membranes, and immunoblotted with antibodies at 1:1000 dilutions using standard techniques.

*Microscopy*

Cells and tissue sections were examined by confocal microscopy using a Zeiss CLSM 710 Spectral Confocal Laser Scanning Microscope. Confocal Z-stack images were obtained and 3D images were reconstructed using AMARIS software.

*Statistical analyses*

All statistical analyses were performed using Student's t-test. Data are expressed as mean ± s.e.m. and $p$-values $<0.05$ were considered statistically significant. Western blots were performed three separate times with representative images shown. Cellular phenotypes were scored from three independent experiments.

| Parental Genotypes | Total Offspring | Pup Genotype | | | *P*-value |
|---|---|---|---|---|---|
| | | +/+ *n* (%) | +/- *n* (%) | -/- *n* (%) | |
| +/- X +/- | 458 | 109 (23.8) | 233 (50.9) | 116 (25.3) | 0.767 |

**Table 2.1: Genotype distribution among offspring of *Graf1* heterozygous (+/−) intercross.** *n* = number of animals; *P*-value is compared to normal Mendelian distribution (25%, 50%, 25%) using a chi-squared test.

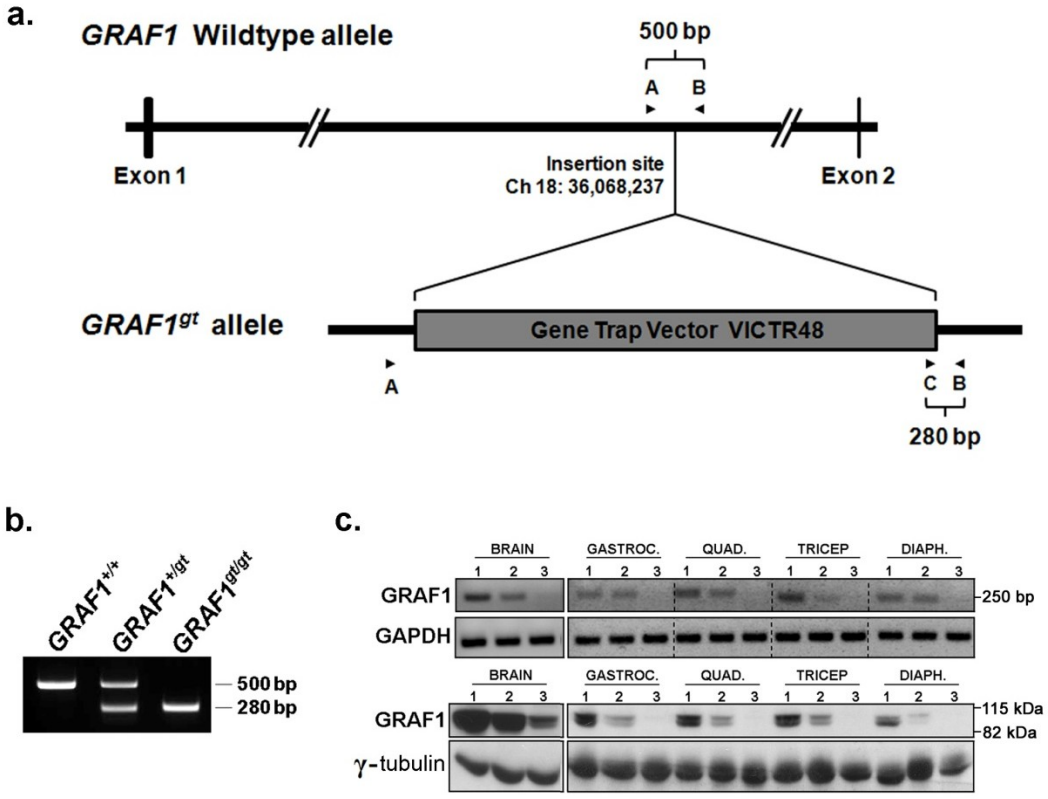
a.
GRAF1 Wildtype allele
500 bp
A
B
Exon 1
Insertion site
Ch 18: 36,068,237
Exon 2
GRAF1gt allele
Gene Trap Vector VICTR48
A
C
B
280 bp
b.
GRAF1+/+
GRAF1+/gt
GRAF1gt/gt
500 bp
280 bp
c.
BRAIN
GASTROC.
QUAD.
TRICEP
DIAPH.
1 2 3
GRAF1
GAPDH
250 bp
115 kDa
82 kDa
γ-tubulin

**Figure 2.1: Gene trap insertion at the *Graf1* locus disrupts gene expression. (a)** The gene trap vector VICTR48 integrated into the first intron of the mouse *Graf1* gene. Arrowheads indicate primer annealing sites for genotype analysis. **(b)** PCR-based genotyping of isolated tail DNA differentiate wildtype ($GRAF1^{+/+}$) and homozygous mutant ($GRAF1^{gt/gt}$) animals by fragments of 500 and 280 bp, respectively. Heterozygotes ($GRAF1^{+/gt}$) present with both fragments. **(c)** RT-PCR analysis (*top*) of GRAF1 cDNA and Western blot analysis (*bottom*) of GRAF1 protein from P7 pups confirm reduced tissue expression from (1) wildtype, to (2) heterozygous, to (3) homozygous mutant animals. GAPDH (cDNA) and γ-tubulin (protein) were used as loading controls. Gastroc.=Gastrocnemius; Quad.=Quadriceps femoris; Diaph.=Diaphragm.

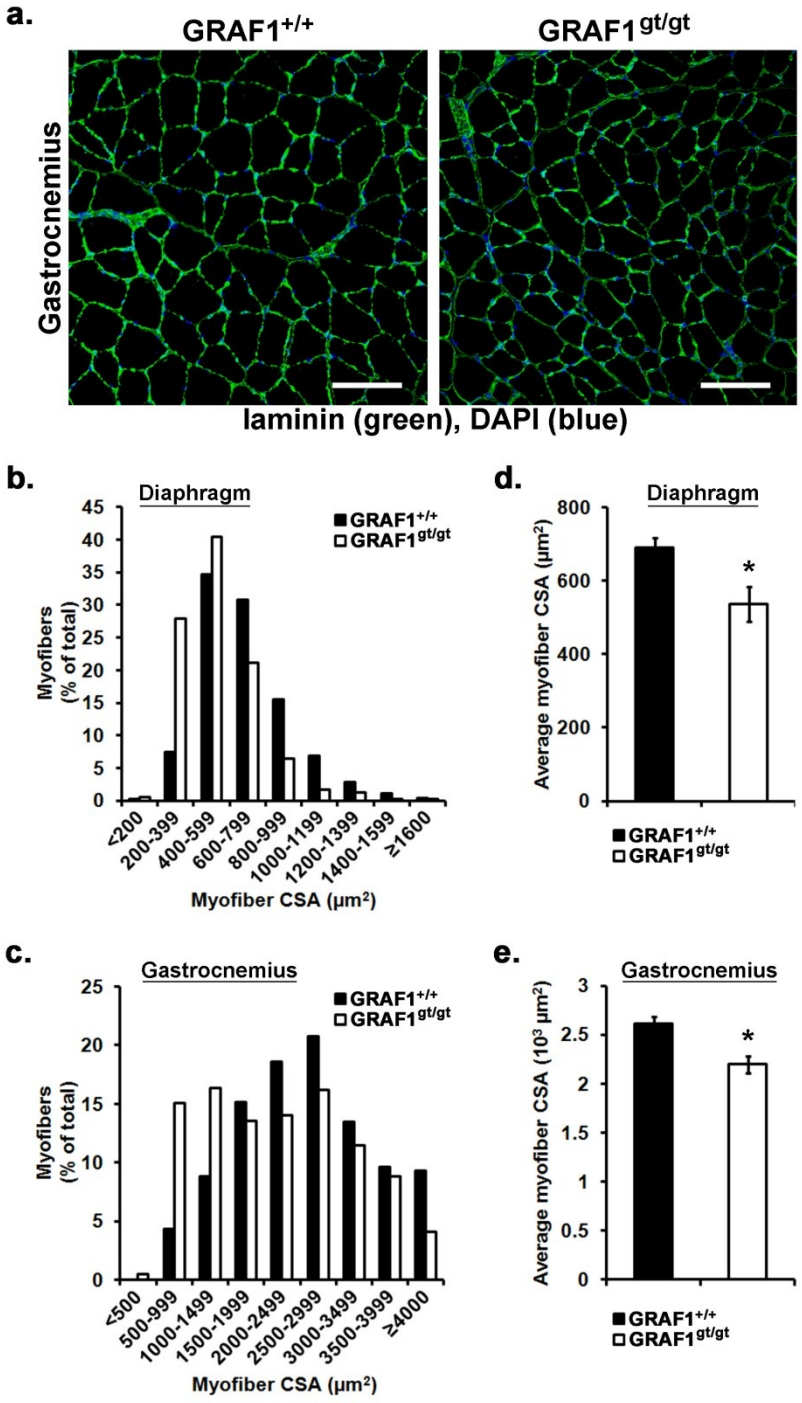
a.
GRAF1+/+
GRAF1gt/gt
Gastrocnemius
laminin (green), DAPI (blue)
b.
Diaphragm
GRAF1+/+
GRAF1gt/gt
Myofibers (% of total)
<200
200-399
400-599
600-799
800-999
1000-1199
1200-1399
1400-1599
≥1600
Myofiber CSA (μm2)
d.
Diaphragm
Average myofiber CSA (μm2)
*
GRAF1+/+
GRAF1gt/gt
c.
Gastrocnemius
GRAF1+/+
GRAF1gt/gt
Myofibers (% of total)
<500
500-999
1000-1499
1500-1999
2000-2499
2500-2999
3000-3499
3500-3999
≥4000
Myofiber CSA (μm2)
e.
Gastrocnemius
Average myofiber CSA (10³ μm²)
*
GRAF1+/+
GRAF1gt/gt

**Figure 2.2: GRAF1 regulates myofiber growth *in vivo*. (a)** Gastrocnemius muscle from 4 month old GRAF1$^{gt/gt}$ mice exhibit smaller myofibers than GRAF1$^{+/+}$ mice. Laminin (green) demarks myofiber boundaries. Nuclei are counterstained with DAPI (blue). **(b,c)** Frequency histograms demonstrating myofiber distribution by cross-sectional area (CSA) of diaphragm and gastrocnemius muscle from 4 month old GRAF1$^{+/+}$ and GRAF1$^{gt/gt}$ mice. **(d,e)** Average myofiber CSA of diaphragm and gastrocnemius muscle (**p*<0.05; *n*=350 myofibers/mouse, *N*=5 mice per genotype). Data are represented as ± s.e.m. Scale bars=100 μm.

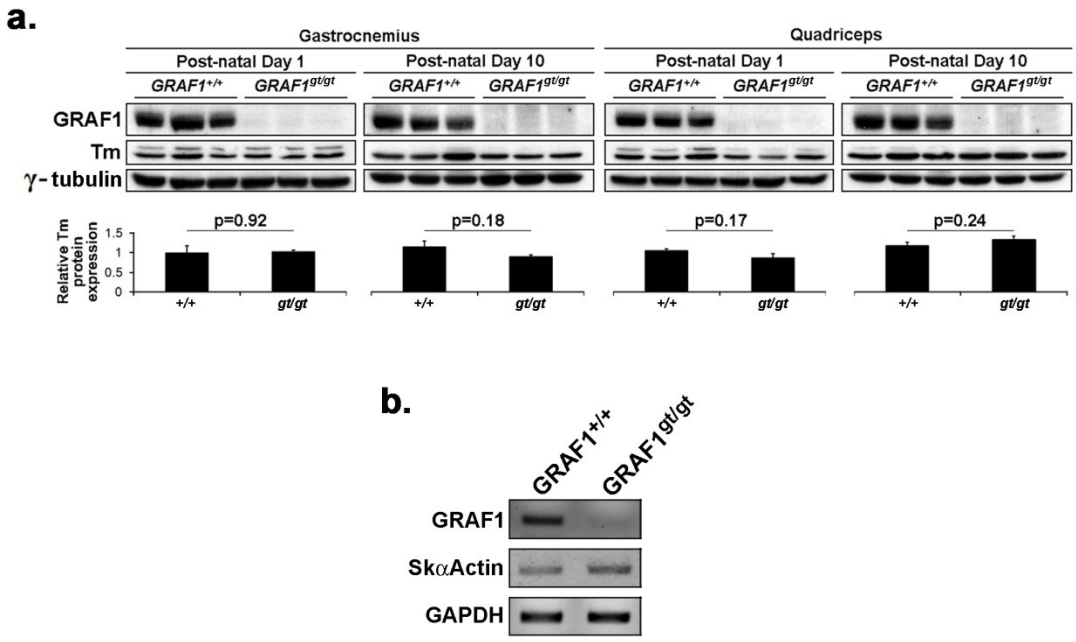
a.
Gastrocnemius
Quadriceps
Post-natal Day 1
Post-natal Day 10
GRAF1+/+
GRAF1gt/gt
GRAF1
Tm
γ-tubulin
Relative Tm protein expression
1.5
1
0.5
0
p=0.92
p=0.18
p=0.17
p=0.24
+/+
gt/gt
b.
GRAF1+/+
GRAF1gt/gt
GRAF1
SkαActin
GAPDH

**Figure 2.3: GRAF1-depletion does not alter muscle differentiation *in vivo.* (a)** Differentiation was assessed in gastrocnemius and quadriceps muscle lysates from $GRAF1^{+/+}$ and $GRAF1^{gt/gt}$ P1 and P10 pups. No significant difference was seen in the relative amount of tropomyosin (Tm) protein between genotypes compared with γ-tubulin as a loading control. Data are represented as ± s.e.m. **(b)** Differentiation was assessed in $GRAF1^{+/+}$ and $GRAF^{gt/gt}$ primary myoblasts cultured in DM for 36 hr. Reverse transcriptase-PCR analysis of skeletal α-actinin dicates comparable differentiation marker expression. GAPDH is shown as a loading control.

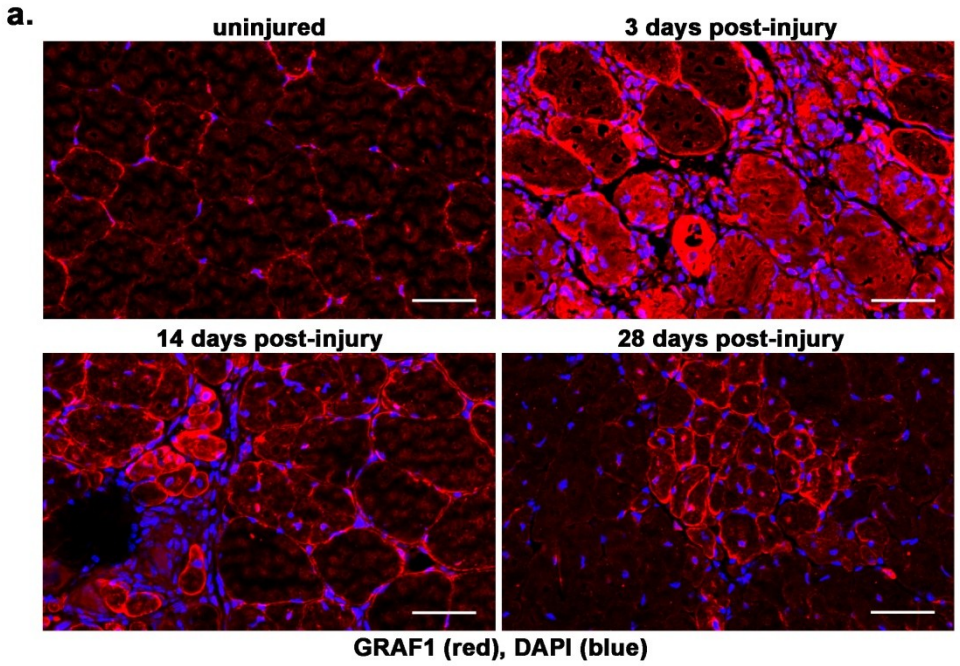
a.
uninjured
3 days post-injury
14 days post-injury
28 days post-injury
GRAF1 (red), DAPI (blue)

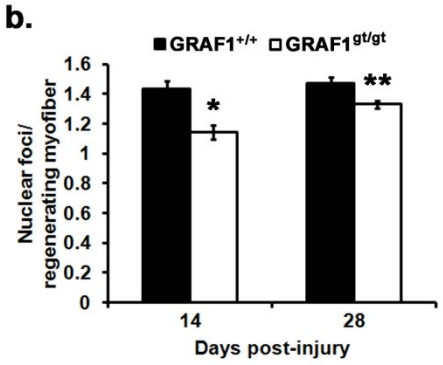
b.
GRAF1+/+ GRAF1gt/gt
Nuclear foci/ regenerating myofiber
1.6
1.4
1.2
1
0.8
0.6
0.4
0.2
0
*
**
14
28
Days post-injury

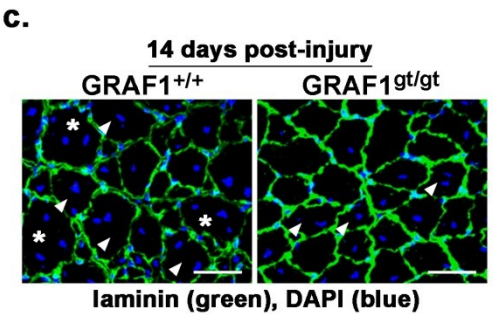
c.
14 days post-injury
GRAF1+/+
GRAF1gt/gt
laminin (green), DAPI (blue)

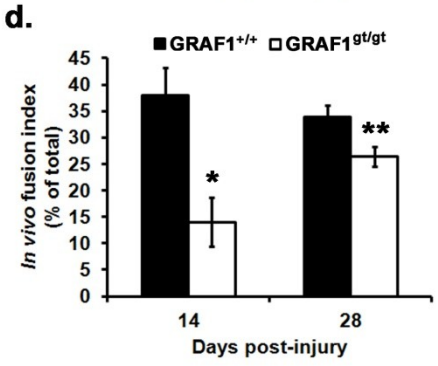
d.
GRAF1+/+ GRAF1gt/gt
In vivo fusion index (% of total)
45
40
35
30
25
20
15
10
5
0
*
**
14
28
Days post-injury

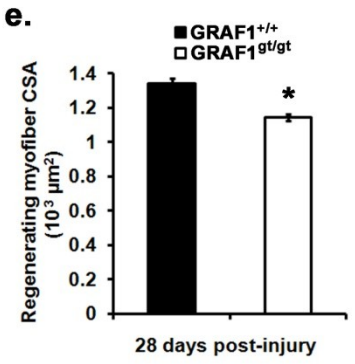
e.
GRAF1+/+
GRAF1gt/gt
Regenerating myofiber CSA (10³ µm²)
1.4
1.2
1
0.8
0.6
0.4
0.2
0
*
28 days post-injury

**Figure 2.4: GRAF1 depletion impairs muscle regeneration. (a)** Immunohistochemical analysis of GRAF1 expression (green) in uninjured adult gastrocnemius muscle and at 3, 14, and 28 days following cardiotoxin-induced injury. Wheat germ agglutinin (WGA) (red) demarks myofiber boundaries. Nuclei are counterstained with DAPI (blue). **(b)** Graphical representation of average nuclear foci per regenerating myofiber 14 and 28 days following cardiotoxin injection into the gastrocnemius muscle (*$p$<0.005, **$p$<0.05; $n$=250 and $n$=500 myofibers/mouse at 14 and 28 days-post injury, respectively; $N$=3-5 mice per genotype). **(c)** Regenerating gastrocnemius muscle from GRAF1$^{gt/gt}$ mice (14 days following cardiotoxin-induced injury) display fewer regenerating myofibers with 2 (*arrowheads*) or 3 (*asterisks*) nuclear foci in comparison to GRAF1$^{+/+}$ mice. Laminin (green) demarks myofiber boundaries. Nuclei are counterstained with DAPI (blue). Scale bars=20 μm. **(d)** Graphical depiction of the *in vivo* fusion index for regenerating myofibers 14 and 28 days-post injury (*$p$<0.005, **$p$<0.05; $n$=250 and $n$=500 myofibers/mouse at 14 and 28 days-post injury, respectively; $N$=3-5 mice per genotype). **(e)** Average CSA of regenerating myofibers 28 days post-injury (*$p$<0.05; $n$=350 myofibers/mouse, $N$=3-4 mice per genotype). Data are represented as ± s.e.m. Scale bars=100 μM, unless otherwise indicated.

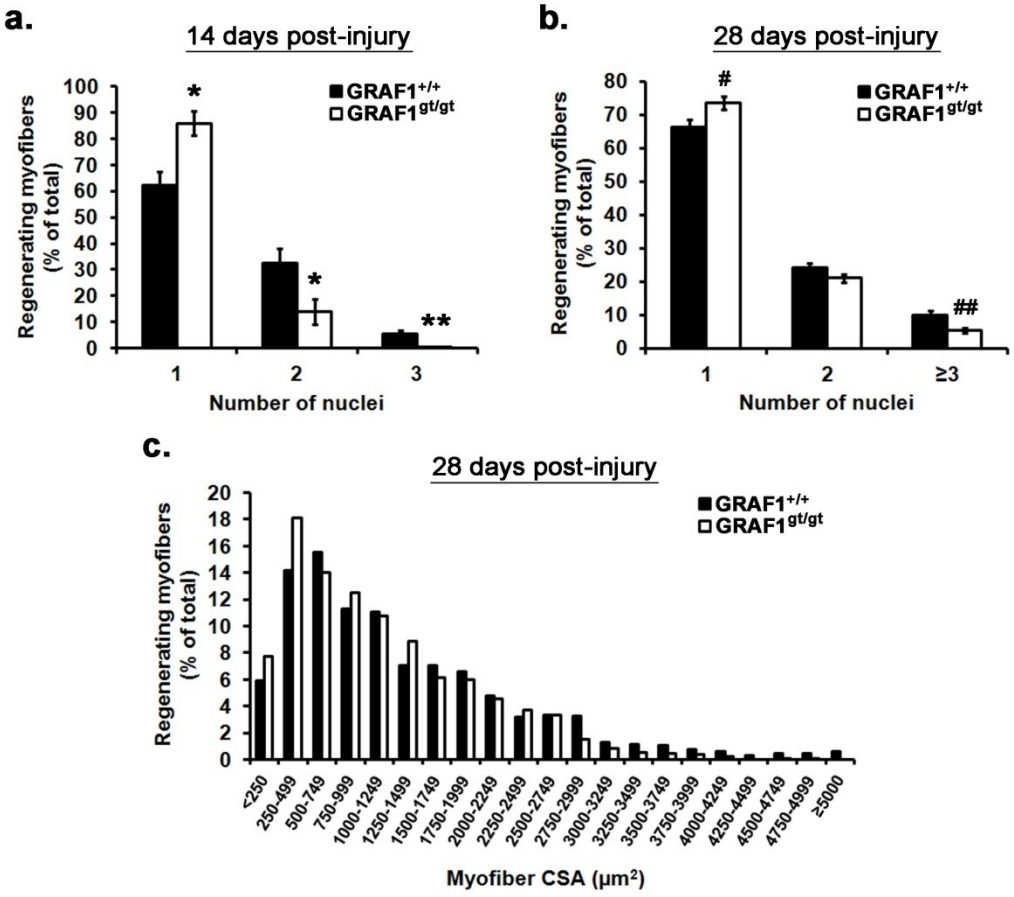
a.
14 days post-injury
Regenerating myofibers (% of total)
GRAF1+/+
GRAF1gt/gt
Number of nuclei
b.
28 days post-injury
Regenerating myofibers (% of total)
GRAF1+/+
GRAF1gt/gt
Number of nuclei
c.
28 days post-injury
Regenerating myofibers (% of total)
GRAF1+/+
GRAF1gt/gt
Myofiber CSA (μm²)

**Figure 2.5: GRAF1 depletion impairs muscle regeneration (*supplemental*). (a,b)** Quantification of nuclear foci per regenerating myofiber 14 and 28 days following cardiotoxin injection into the gastrocnemius muscle **(***$p<0.005$, **$p<1X10^{-4}$, $^{\#}p<0.05$, $^{\#\#}p<0.01$; $n=250$ and $n=500$ myofibers/mouse at 14 and 28 days-post injury, respectively; $N=3$-5 mice per genotype). Data are represented as ± s.e.m. **(c)** Frequency histogram demonstrating regenerating myofiber distribution by cross-sectional area (CSA) of gastrocnemius muscle 28 days post-injury.

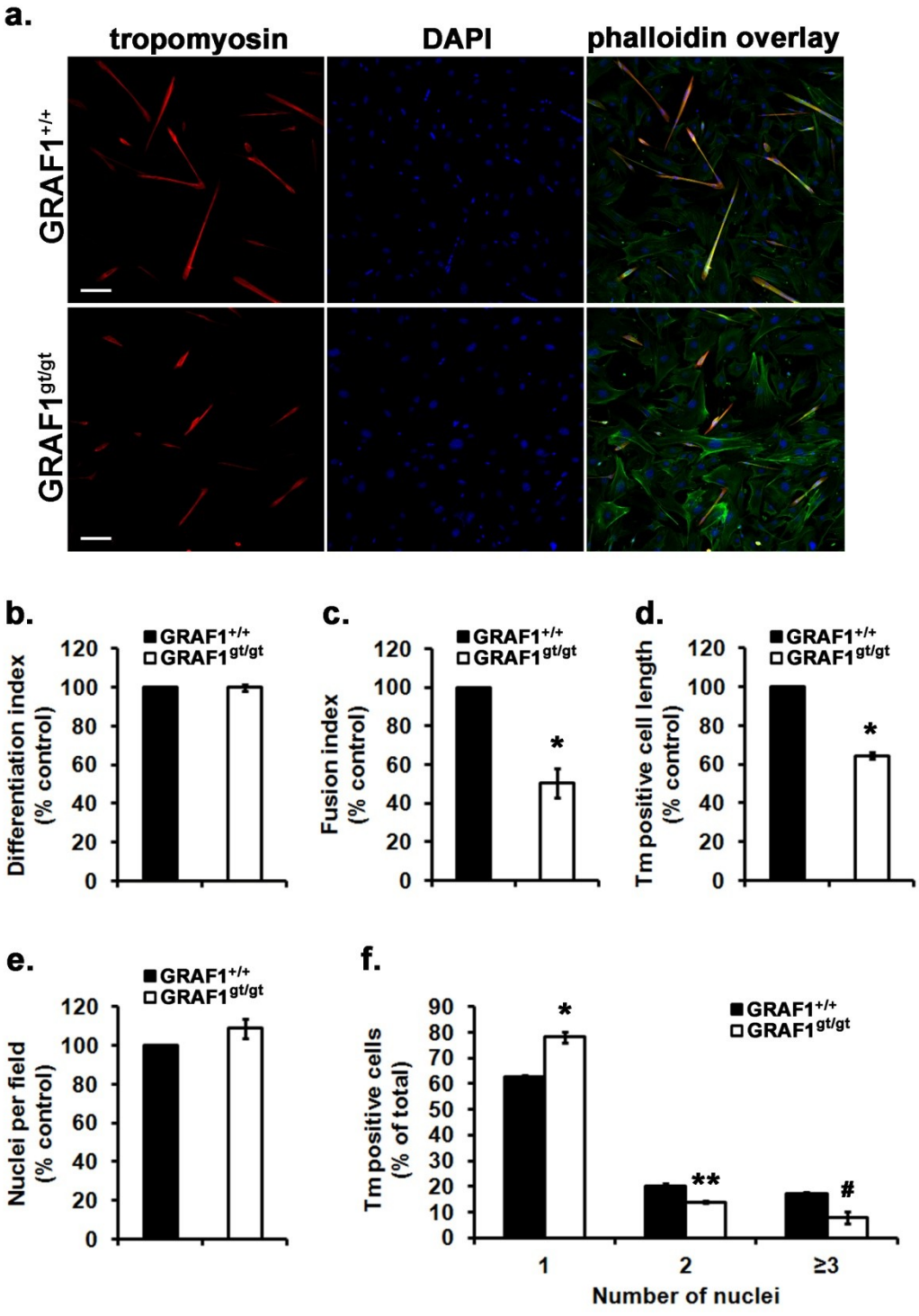
a.
tropomyosin
DAPI
phalloidin overlay
GRAF1+/+
GRAF1gt/gt
b.
Differentiation index (% control)
GRAF1+/+
GRAF1gt/gt
c.
Fusion index (% control)
d.
Tm positive cell length (% control)
e.
Nuclei per field (% control)
f.
Tm positive cells (% of total)
Number of nuclei
1
2
≥3

**Figure 2.6: GRAF1 depletion inhibits *in vitro* myotube formation. (a)** Representative images of GRAF1$^{+/+}$ and GRAF1$^{gt/gt}$ primary cultures immunostained for tropomyosin (Tm) at 72 hr in differentiation media (DM). F-actin and nuclei were counterstained with phalloidin and DAPI, respectively. **(b)** GRAF1$^{+/+}$ and GRAF1$^{gt/gt}$ cells immunostained in (3a) exhibited no significant difference in their differentiation index. **(c)** The GRAF1$^{gt/gt}$ cells exhibited a significant decrease in their fusion index (*$p$<0.005). **(d)** Tm-positive GRAF1$^{+/+}$ cells were significantly longer than GRAF1$^{gt/gt}$ cultures (*$p$<5X10$^{-4}$). The number of nuclei per field was comparable between GRAF1$^{+/+}$ and GRAF1$^{gt/gt}$ cultures. **(f)** GRAF1$^{gt/gt}$ cells exhibited reduced nuclear accretion with a significant increase in mononucleated cells (*$p$<0.005) and decrease in bi-nucleated (**$p$<0.01) and multi-nucleated ($^{\#}p$<0.05) cells in comparison to GRAF1$^{+/+}$ controls. At least 1,000 Tm-positive cells, 250 myotubes, and 10,000 nuclei were scored over 50 images per genotype for each assay. Data are represented as ± s.e.m., $N$=3 independent experiments. Scale bars=100 μm.

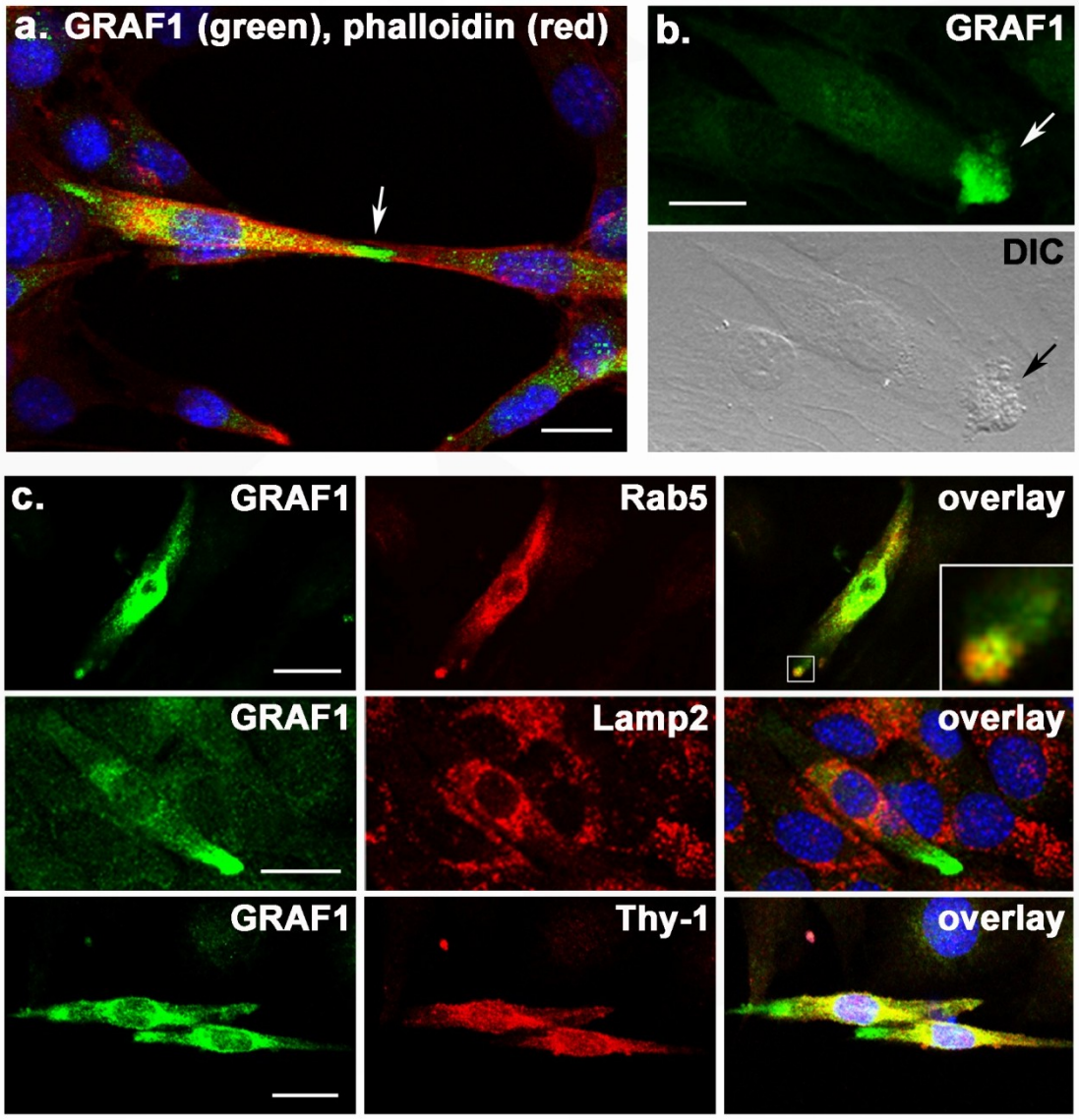
a. GRAF1 (green), phalloidin (red)
b.
GRAF1
DIC
c.
GRAF1
Rab5
overlay
GRAF1
Lamp2
overlay
GRAF1
Thy-1
overlay

**Figure 2.7: GRAF1 is present within endocytic structures in pre-fused myoblasts.**

**(a)** GRAF1 is selectively accumulated within the cytoplasmic bridge (*white arrow*) between actively fusing C2C12 myoblasts. **(b)** GRAF1 co-localizes with intracellular vesicles (*arrows*) as visualized by DIC microscopy in 48 hr differentiated C2C12 myoblasts. **(c)** Membrane-associated GRAF1 co-localizes with the early endosomal marker Rab5 (*top*), but not with Lamp2-positive lysosomes (*middle*). Peri-nuclear GRAF1 co-localizes with the endocytic recycling protein Thy-1 (*bottom*). Nuclei are counterstained with DAPI (blue). Scale bars=20 μm.

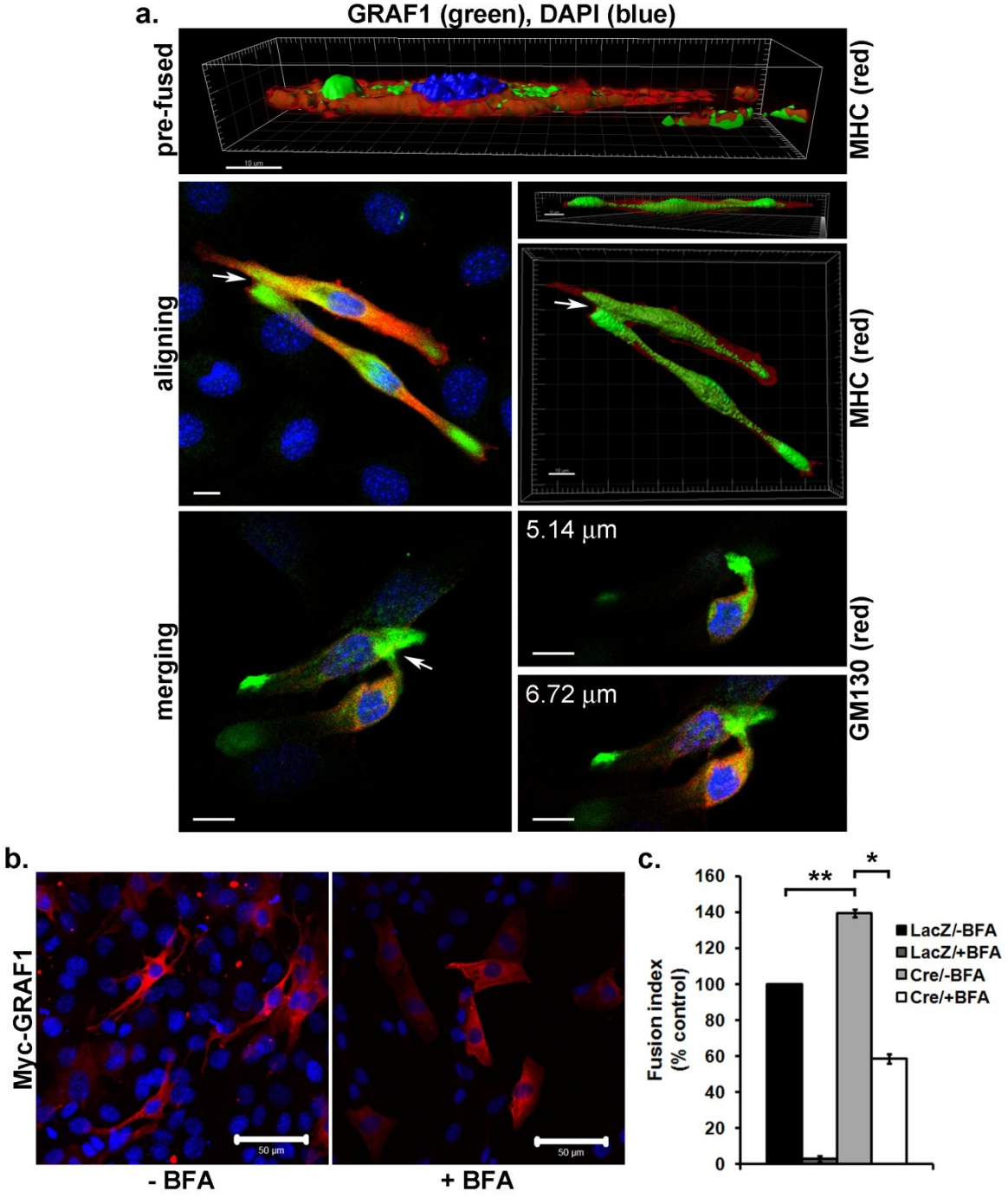
a.
GRAF1 (green), DAPI (blue)
pre-fused
MHC (red)
aligning
MHC (red)
merging
5.14 µm
6.72 µm
GM130 (red)
b.
Myc-GRAF1
- BFA
+ BFA
c.
Fusion index (% control)
160
140
120
100
80
60
40
20
0
**
*
LacZ/-BFA
LacZ/+BFA
Cre/-BFA
Cre/+BFA

**Figure 2.8: GRAF1-dependent membrane protrusions and myoblast fusion are dependent on vesicular trafficking. (a)** C2C12 cells were treated with DM for 49-72 hrs, stained for endogenous GRAF1 (and other indicated antibodies), and visualized by confocal microscopy. Confocal slice views and digital decovolution and 3-D renderings are shown. GRAF1 is localized to complexes that protrude from cells at pre-fusion complexes (*top,* also see figure 2.4 for confocal slice view) and at the points of cell-cell attachment (*middle, white arrows*) as demonstrated using image deconvolution of confocal Z-stacks. GRAF1 is localized to the precise point of contact between fusing myoblasts (*bottom, white arrow*), note high levels of GRAF1 accumulation in the protrusion of a myoblast that appears to be diving in to a GRAF1-labeled region of a myotube. See figure 2.9 for the gallery view of confocal slices of this 6.71 μm maximum intensity projection (MIP). Myosin heavy chain (MHC) demarks cell boundaries in top and middle panels. GM130 demarks Golgi bodies in bottom panel. **(b)** Representative images of C2C12 cells maintained in growth media and transfected with Myc-tagged GRAF1 for 24 hr. Twelve hr prior to fixation, cells were treated with (*left*) or without (*right*) 0.1 μg/mL brefeldin A (BFA). Myc (red) demarks GRAF1 overexpressing cells. Nuclei are counterstained with DAPI (blue). Scale bars=50 μm. **(c)** C2C12 cells were transfected with a Cre recombinase-inducible Myc-tagged GRAF1 targeting construct, induced to differentiate for 48 hr in DM, and transduced with Cre or control LacZ adenovirus for 36 hr. Twelve hr prior to fixation, cells were treated with 0.3 μg/mL BFA. Dual Myc and DAPI staining were used to quantify the fusion index (*$p<1X10^{-4}$, **$p<0.005$). Data are represented as ± s.e.m., $n$=75-100 cells/condition, $N$=3 independent experiments. Scale bars=10 μm, unless otherwise indicated.

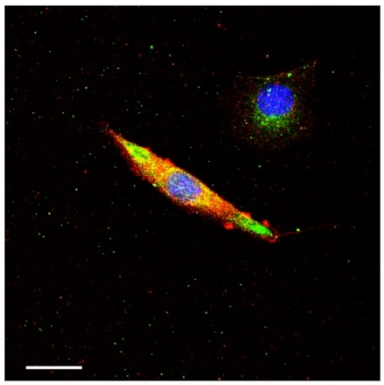

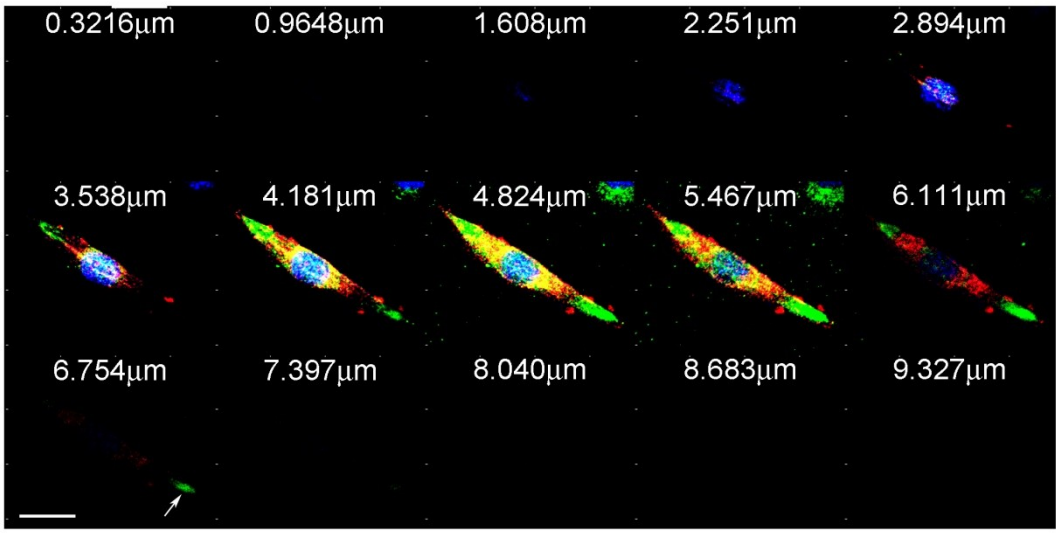
0.3216µm
0.9648µm
1.608µm
2.251µm
2.894µm
3.538µm
4.181µm
4.824µm
5.467µm
6.111µm
6.754µm
7.397µm
8.040µm
8.683µm
9.327µm

**Figure 2.9: GRAF1 expression in a pre-fused myoblasts.** Top panel is a maximum intensity projection (MIP) of an 8.05 μm section of a C2C12 myoblast differentiated for 72 hr in DM and immunostained for GRAF1 (green), myosin heavy chain (MHC) (red), and DAPI (blue). Bottom panel is a gallery view of the MIP. White arrow denotes GRAF1 accumulation at pre-fusion site. Scale bars=10 μm.

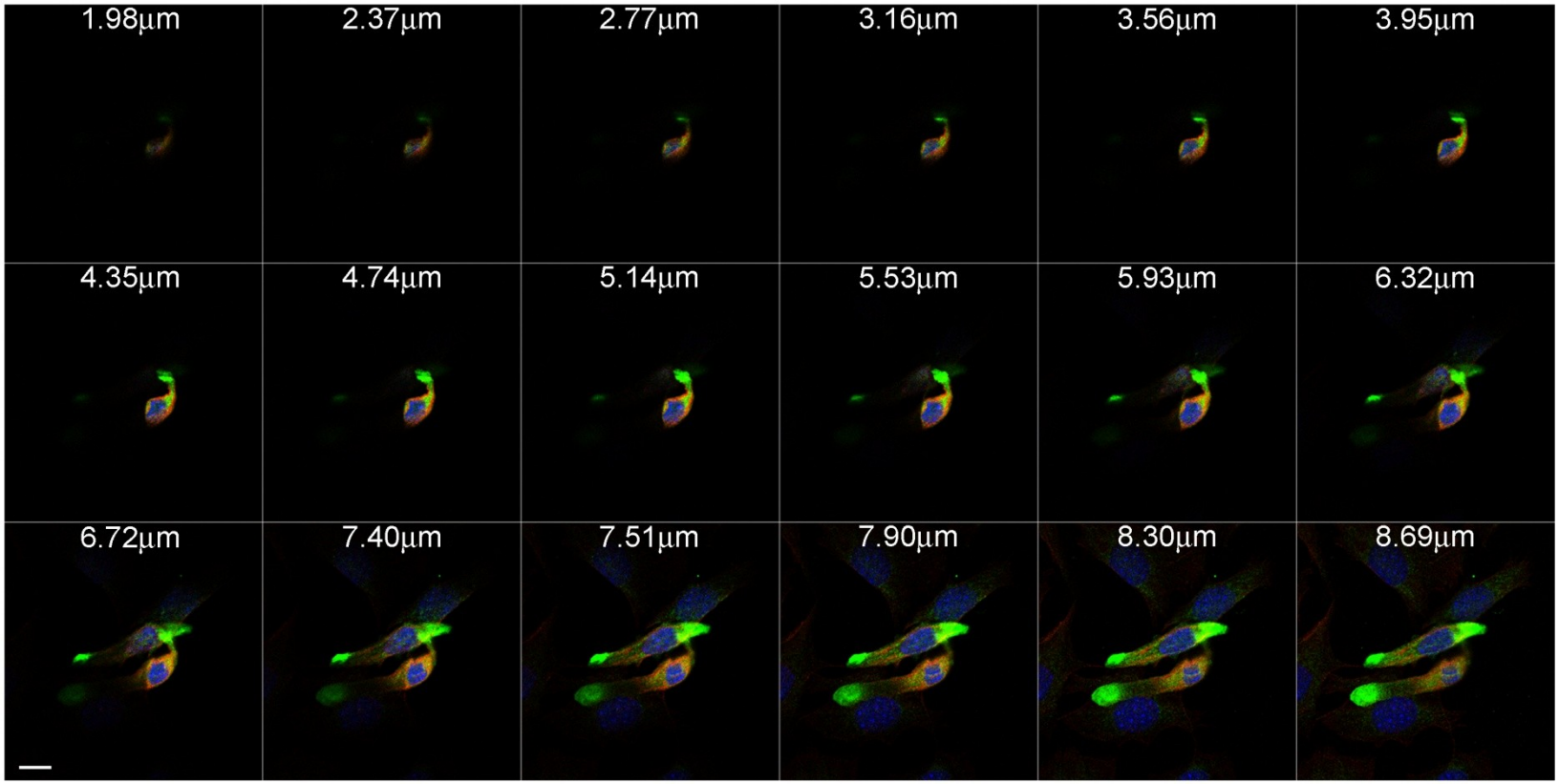
1.98µm
2.37µm
2.77µm
3.16µm
3.56µm
3.95µm
4.35µm
4.74µm
5.14µm
5.53µm
5.93µm
6.32µm
6.72µm
7.40µm
7.51µm
7.90µm
8.30µm
8.69µm

**Figure 2.10: GRAF1 expression in fusing myoblasts.** Gallery view of a 6.71 μm section of two fusing C2C12 myoblasts. GRAF1 (green), myosin heavy chain (MHC) (red), and DAPI (blue). Scale bar=10 μm.

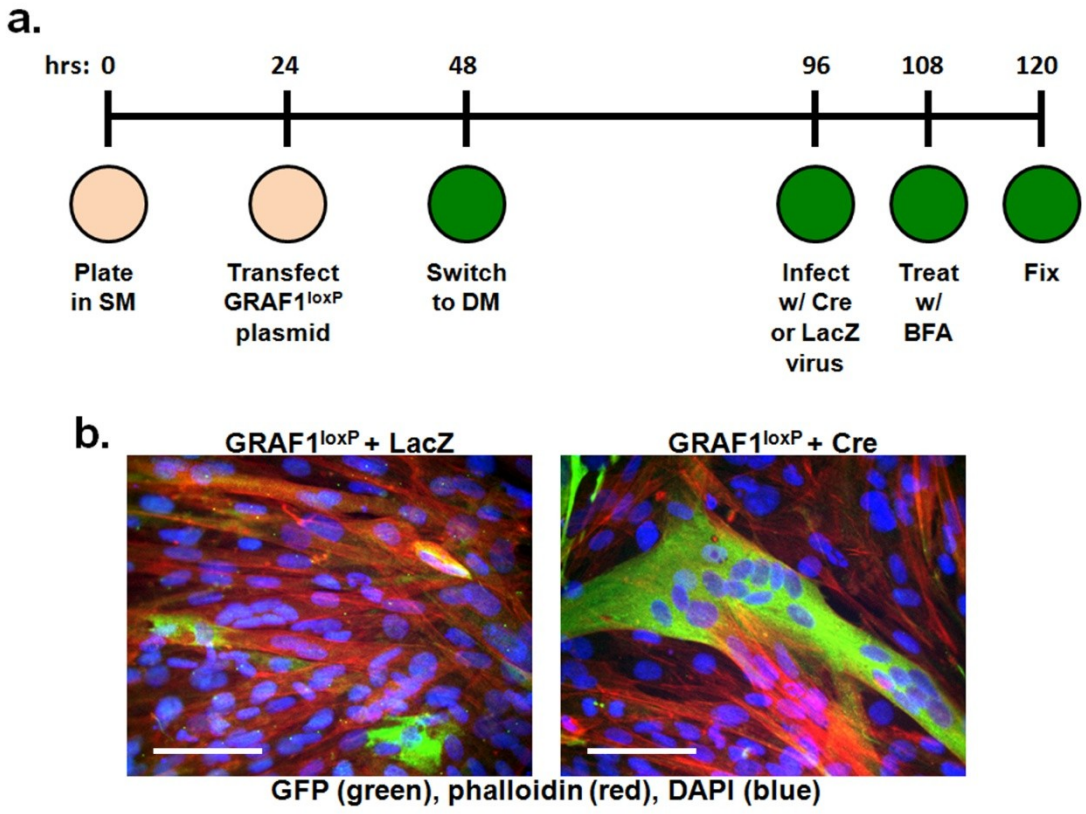
a.
hrs: 0
24
48
96
108
120
Plate in SM
Transfect GRAF1loxP plasmid
Switch to DM
Infect w/ Cre or LacZ virus
Treat w/ BFA
Fix
b.
GRAF1loxP + LacZ
GRAF1loxP + Cre
GFP (green), phalloidin (red), DAPI (blue)

**Figure 2.11: Cre recombinase-inducible GRAF1 expression. (a)** Diagram illustrates the protocol used for the treatment of C2C12 myoblasts with Brefeldin A. Refer to methods for experimental details. **(b)** 24 hr post-transfection with the GRAF1$^{loxP}$ construct, cells were exposed to DM for 48 hr then transduced with LacZ (*left*) or Cre (*right*) adenovirus for an additional 24 hr. Representative images reveal marked cell fusion in GRAF1-overexpressing cells in comparison to controls. Scale bars=50 μm.

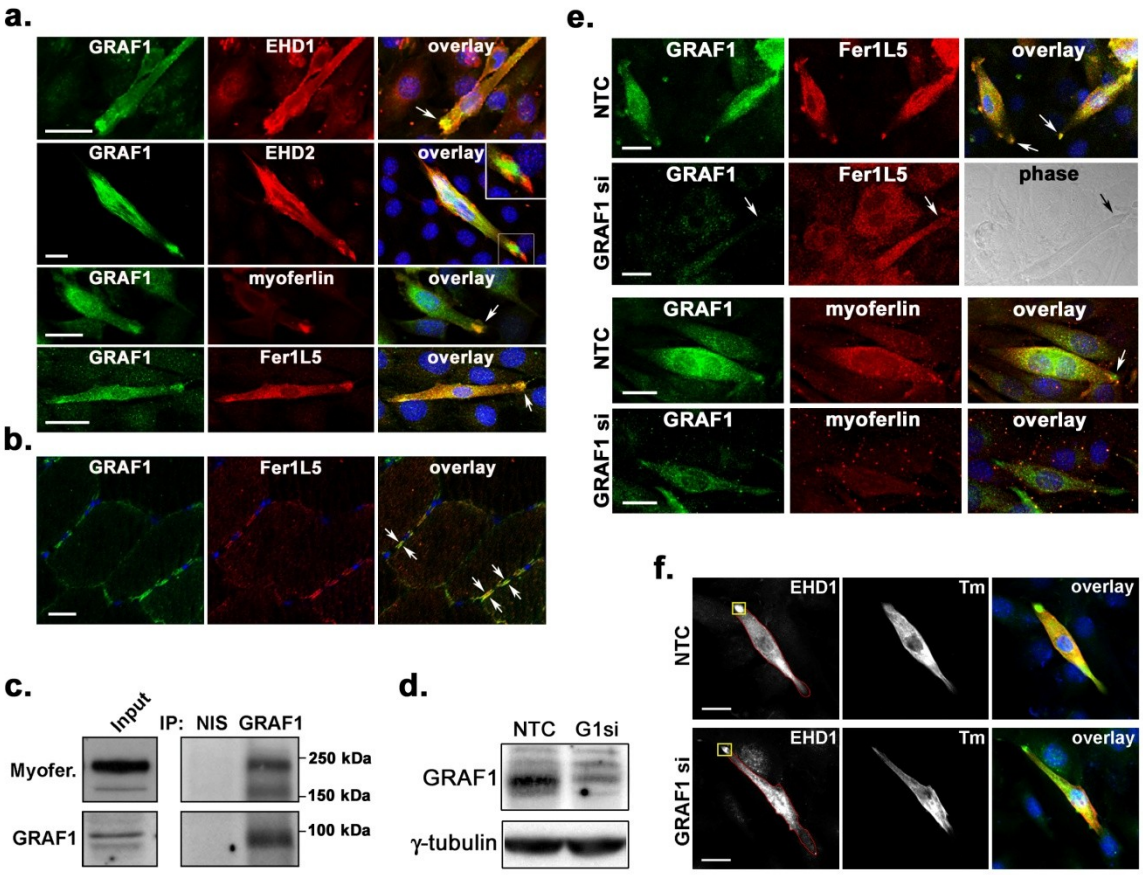
a.
GRAF1
EHD1
overlay
GRAF1
EHD2
overlay
GRAF1
myoferlin
overlay
GRAF1
Fer1L5
overlay
b.
GRAF1
Fer1L5
overlay
c.
Input
IP: NIS GRAF1
Myofer.
GRAF1
250 kDa
150 kDa
100 kDa
d.
NTC G1si
GRAF1
γ-tubulin
e.
NTC
GRAF1 si
GRAF1
Fer1L5
overlay
phase
myoferlin
f.
EHD1
Tm
overlay

**Figure 2.12: GRAF1 associates with the fusogenic ferlin proteins and promotes recruitment of the endocytic recycling machinery to pre-fusion complexes. (a)** C2C12 cells exposed to DM for 36 hr were co-immunostained with GRAF1 and EHD1 (*top*), EHD2 (*top middl*e), myoferlin (*bottom middle*) or Fer1L5 (*bottom*) antibodies. White arrows indicate co-localization of proteins at pre-fusion sites. High power inset reveals limited co-localization of GRAF1 and EHD2. **(b)** Tibialis anterior muscle cryo-sections from a 6 month old wildtype mouse were co-stained with GRAF1 and Fer1L5 antibodies (note sarcolemmal co-localization). **(c)** Anti-GRAF1 rabbit polyclonal antibody and non-immune sera (NIS) immunoprecipitations (IP) from C2C12 cells exposed to DM for 72 hr. Blots were probed with an anti-myoferlin antibody or hamster anti-GRAF1 antibody. *Input* contains 20% of cellular lysate used for IP. **(d)** C2C12 cells transfected with GRAF1-specific (G1si) or control (NTC) siRNA and exposed to DM for 36 hr were lysed and immunoblotted with GRAF1 antibody to assess knockdown efficiency. γ-tubulin is shown as a loading control. **(e)** C2C12 cells treated as in (6d) were co-stained with GRAF1 and either Fer1L5 or myoferlin antibodies. GRAF1 and ferlins co-localization at polarized tips in NTC treated cells, but both Fer1L5 and myoferlin mis-localized in GRAF1 knockdown cells. **(f)** C2C12 cells treated as in (6d) were co-stained with EHD1 and Tm antibodies to demark differentiated myoblasts. Images illustrate the method of quantifying EHD1 protein at pre-fusion complexes. ImageJ software was used to measure the intensity of EHD1 signal at a pre-fusion complex (*yellow box*) relative to the signal within the rest of the cell. Refer to figure 2.13f for quantification. Scale bars=20 μm.

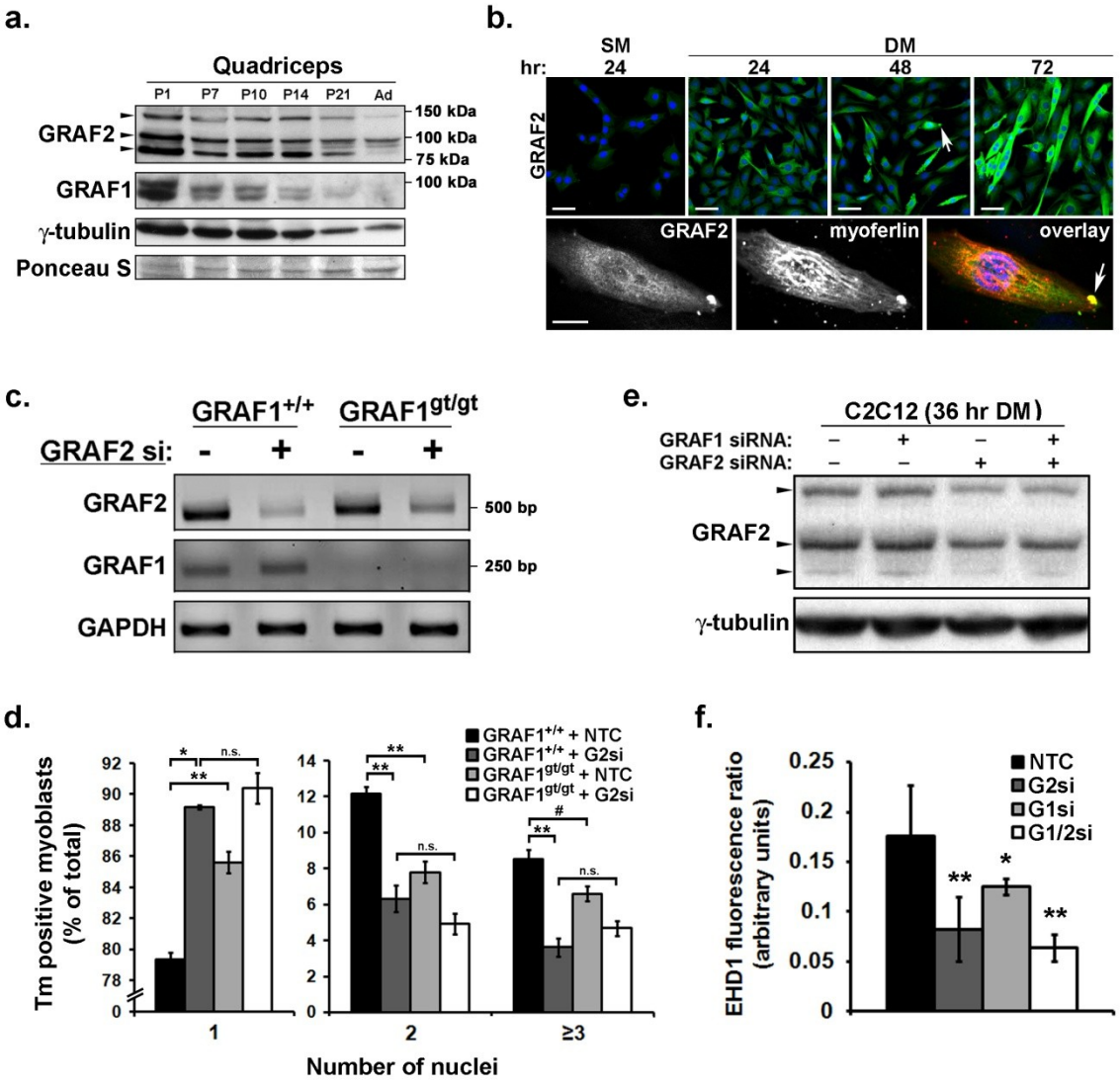
a.
Quadriceps
P1
P7
P10
P14
P21
Ad
GRAF2
GRAF1
γ-tubulin
Ponceau S
150 kDa
100 kDa
75 kDa
100 kDa
b.
SM
DM
hr:
24
24
48
72
GRAF2
GRAF2
myoferlin
overlay
c.
GRAF1+/+
GRAF1gt/gt
GRAF2 si:
-
+
-
+
GRAF2
GRAF1
GAPDH
500 bp
250 bp
e.
C2C12 (36 hr DM)
GRAF1 siRNA:
GRAF2 siRNA:
GRAF2
γ-tubulin
d.
Tm positive myoblasts (% of total)
GRAF1+/+ + NTC
GRAF1+/+ + G2si
GRAF1gt/gt + NTC
GRAF1gt/gt + G2si
n.s.
Number of nuclei
1
2
≥3
f.
EHD1 fluorescence ratio (arbitrary units)
NTC
G2si
G1si
G1/2si

**Figure 2.13: GRAF1 and GRAF2 have functionally overlapping roles in muscle fusion.** **(a)** Western blot analysis of GRAF1 and GRAF2 protein levels in postnatal (P) and adult (Ad) mouse quadriceps at the indicated time of development. γ-tubulin and Ponceau S-stained blots are shown as loading controls. **(b)** Cells exposed to GM and DM for indicated times were immunostained for GRAF2. Note increased expression during C2C12 differentiation and recruitment of GRAF2 to pre-fusion complexes (*arrows*). Scale bars=50 μm. Bottom panels are high magnification images that reveals co-localization of GRAF2 and myoferlin at the tip of a myoblast exposed to DM for 48 hr. **(c)** $GRAF1^{+/+}$ and $GRAF^{gt/gt}$ primary myoblasts transfected with GRAF2-specific or control (NTC) siRNA and exposed to DM for 36 hr were assessed for GRAF2 and GRAF1 expression by reverse transcriptase-PCR. GAPDH is shown as a loading control. **(d**) $GRAF1^{+/+}$ primary myoblasts depleted of GRAF2 by siRNA knockdown exhibited reduced nuclear accretion in comparison to NTC-treated control $GRAF1^{+/+}$ myoblasts. Moreover, depletion of GRAF2 in $GRAF1^{gt/gt}$ cells exhibited a further reduction in nuclear accretion in comparison to NTC-treated $GRAF1^{+/+}$ and $GRAF1^{gt/gt}$ myoblasts (*$p$<1X$10^{-4}$, **$p$<0.005, $^{\#}p$<0.05, n.s.=not significant; $n$=300 cells/condition, $N$=3 independent experiments). **(e)** C2C12 cells were transfected with control (NTC), GRAF1-, GRAF2-, or both GRAF1- and GRAF2-specific siRNAs and exposed to DM for 36 hr before being lysed and immunoblotted with a GRAF2 antibody to assess protein knockdown efficiency. γ-tubulin is shown as a loading control. **(f)** Quantification of the EHD1 fluorescence ratio (refer to figure 2.12f and methods for details) in C2C12 cells transfected with control (NTC), GRAF1-, GRAF2-, or both GRAF1- and GRAF2-specific siRNAs that were exposed to DM for 36 hr and immunostained for EHD1 and Tm to demark differentiated myoblasts (*$p$<0.05, **$p$<0.005; $n$=50 cells/condition, $N$=3

independent experiments). Data are represented as ± s.e.m. Scale bars=10 μm, unless otherwise indicated.

# CHAPTER 3

## GRAF1 DEFICIENCY IMPAIRS SARCOLEMMAL INJURY REPAIR AND VARIABLY INFLUENCES MUSCLE PATHOLOGY IN DYSTROPHIN-DEFICIENT MICE[2]

### INTRODUCTION

The plasma membrane (PM) functions as a physical barrier which protects the intracellular environment from the extracellular milieu, and continuous maintenance of this barrier is essential to support the proper function and vitality of all cells. The PM of striated muscle cells, or sarcolemma, is particularly susceptible to rupture as it endures significant mechanical stress and strain during muscle contraction. As such, muscle possesses a remarkable ability to maintain sarcolemmal integrity and function, and previous studies have demonstrated two prominent mechanisms responsible for such efficient maintenance: 1) sarcolemmal stabilization and 2) sarcolemmal membrane repair.

Sarcolemmal stabilization is mediated by the dystrophin glycoprotein complex (DGC) which localizes to the inner surface of the PM. The DGC functions primarily as a strong mechanical link between the intracellular cytoskeleton and the extracellular matrix (ECM) to stabilize the sarcolemma and transmit force laterally during muscle lengthening and contraction [117]. An integral component of the DGC, dystrophin, is responsible for directly linking the contractile cytoskeleton to the sarcolemma through interaction with the transmembrane protein, β-dystroglycan [117, 118]. It has long been known that patients with

Duchenne muscular dystrophy or the milder Becker muscular dystrophy exhibit a loss of or reduction in dystrophin expression, respectively [119]. This deficiency increases sarcolemmal fragility in the heart and skeletal muscle and leads to severe muscular injury in the presence of even mild stress, resulting in cardiac damage and progressive skeletal muscle degeneration and weakness [4].

Sarcolemmal injury repair is mediated by various mechanisms which become activated in response to an influx of extracellular $Ca^{2+}$ in order to rapidly reseal the PM. $Ca^{2+}$-sensing annexin proteins act as first responders to sarcolemmal insult by sequestering intracellular vesicles to form an endomembrane patch that is trafficked to the site of disruption. Dysferlin, a membrane anchored calcium-binding protein present on repair vesicles and on the plasma membrane, mediates docking and fusion of the patch to reseal the membrane breach and prevent further influx of $Ca^{2+}$. Dysferlin and its family members (myoferlin and Fer1L5) share functional similarities to synaptotagmins, proteins which are known to facilitate synaptic vesicle fusion and plasma membrane repair [76, 120]. Recent studies have shown that dysferlin is rapidly recruited to PM-repair patches in response to injury [7], and that skeletal muscle fibers lacking dysferlin exhibited defects in $Ca^{2+}$-dependent membrane resealing following mechanical or laser-induced membrane rupture [7, 77]. Indeed, dysferlin deficiency is causal for Limb-girdle muscular dystrophy 2B and Miyoshi myopathy in humans [5, 6], and dysferlin null mice have been shown to develop progressive muscular dystrophy as well. What's more, these mice also exhibit significant systolic dysfunction when stressed by conditions known to promote cardiomyocyte membrane disruption including exercise, isoproterenol (ISO) infusion, or genetic depletion of dystrophin [121, 122]. These data indicate that dysferlin plays a crucial role in repairing

sarcolemmal wounds to maintain integrity of both heart and skeletal muscle tissues. However, further work is required to identify additional components which aid dysferlin recruitment to sites of membrane damage.

We previously showed that GRAF1 (GTPase regulator associated with FAK-1) is a Rho-specific GTPase activating protein that is expressed predominantly in striated muscle and mediates actin- and membrane-based dynamics to promote myoblast fusion [52]. Interestingly, we found that depletion of GRAF1 from developing tadpoles induced a highly penetrable dystrophic phenotype that that led to immobility [88]. Moreover, we showed that GRAF1-deficient mice exhibited a reduced capacity to regenerate following cardiotoxin-induced muscle injury (see Chapter 2 for review). Taken together, this data indicates a role for GRAF1 in the maintenance/repair of skeletal muscle. We previously showed that GRAF1 associates with the ferlin family members, myoferlin and Fer1L5, and that GRAF1 is required for proper sarcolemmal recruitment of these proteins in order to promote myoblast fusion (see Chapter 2 for review). Therefore, we hypothesized that GRAF1 would also regulate the trafficking of dysferlin to sites of injured sarcolemma in order to facilitate membrane patch-repair. Our studies show that GRAF1 associates with and mediates deposition of dysferlin at plasma membranes of injured muscle. Moreover, depletion of GRAF1 enhanced susceptibility to membrane injury in isolated myoblasts and exacerbated some hallmarks of muscle degeneration in the *mdx* mouse. Interestingly, GRAF1-deficient *mdx* mice exhibited unprecedented myofiber expansion and muscle growth, implicating an alternative role for GRAF1 in skeletal muscle-injury response.

RESULTS

*GRAF1 is recruited to disrupted plasma membranes and associates with the membrane repair protein dysferlin*

Dysferlin is anchored to both intracellular vesicles and PMs and its distribution between these compartments is tightly regulated by endocytic recycling. In response to injury in normal muscle, dysferlin is rapidly recruited to PM-repair patches [7]. Notably, aggregation and reduced PM association of dysferlin are observed in several muscular dystrophies including caveolinopathies and sarcoglycanopathies, suggesting that dysferlin mis-targeting could also play a role in the pathogenesis of these diseases [81-84]. We found that GRAF1 re-distributed from Z-bands (where it colocalizes with α-actinin) to the plasmalemma in dystrophin-depleted muscle from a golden retriever dog model of Duchenne muscular dystrophy (GRMD) (where it co-localized and co-associated with dysferlin; Figure 3.1a,b). Since GRAF1 is expressed at high levels in the adult heart, we wanted to assess the effect of GRAF1 depletion on dysferlin localization. As shown in figure 3.1c, PM localization of dysferlin was reduced in GRAF1-depleted hearts, indicating that GRAF1 may be important for the trafficking of dysferlin to sites of repair, as $GRAF1^{gt/gt}$ hearts show signs of cardiac muscle degeneration (data not shown).

In strong support of a role for GRAF1 in mediating vesicle trafficking during injury repair, we found that mechanically-induced myotube membrane rupture resulted in the rapid (within 2 min) recruitment of endogenous GRAF1 from peri-nuclear compartments to the site of membrane lesion where it co-localized in sub-membranous vesicles with the membrane trafficking protein, annexin A1 (Figure 3.2). Co-staining with phalloidin indicated that these regions are nearly completely devoid of actin-based structures and we have previously shown that ectopic expression of GRAF1 induced a marked clearing of cortical F-actin [88].

Together, this data indicates the possibility that GRAF1 regulates a general repair mechanism necessary for re-sealing membranes damaged by mechanical stress

*GRAF1 is required for optimal striated muscle membrane repair* in vitro

To directly test whether GRAF1 is necessary for membrane repair, we have developed a sophisticated *in vitro* laser-injury/repair system. $GRAF1^{+/+}$ and $GRAF1^{gt/gt}$ primary myoblasts were incubated with membrane-impermeable FM 1-43 dye prior to a laser pulse on a defined area of the cell (Figure 3.3a). Time lapse images revealed efficient PM resealing following laser injury as demonstrated by a transient increase in FM 1-43 fluorescence within the wounded region in $GRAF1^{+/+}$ myoblasts (Figure 3). In contrast, when myotubes isolated from $GRAF1^{gt/gt}$ mice were subjected to an identical laser burst, a pronounced and widespread increase in FM 1-43 fluorescence and dramatic membrane blebbing were observed (Figure 3). Moreover, 21/28 of the injured GRAF1 null cells succumbed to $Ca^{2+}$ overload as assessed by hyper-contracture and release from the substratum, while all $GRAF1^{+/+}$ cells (23/23) remained well-spread and adherent. Moreover, our data in adult ventricular cardiomyocytes indicate that, similar to skeletal muscle cells, GRAF1 is rapidly recruited to sub-plasmalemmal sites following membrane permeabilization with saponin (Figure 3.4), and that pronounced re-sealing defects were found in GRAF1-depleted cardiomyocytes prior to and after saponin treatment in comparison to control cells as assessed by FM 1-43 uptake (Figure 3.4b). \

*GRAF1 depletion compromises sarcolemmal integrity under pathological conditions*

To determine whether GRAF1 (like dysferlin) was critical for maintenance of

membrane integrity, GRAF1$^{gt/gt}$ mice were subjected to cardiotoxin (CTX) into the left ventricular wall or to 3x5 mg/kg intraperitoneal (i.p.) injections of isoproterenol (ISO) over a 24 hr period. Sarcolemmal damage was evaluated in these models by standard Evans blue dye (EBD) exclusion protocols (i.p. injection immediately following injury). As shown in figure 3.5a, cardiomyocyte sarcolemmal damage was minimal in CTX-injected control mice and, when found, was restricted to the sub-epicardial zone. In stark contrast, large clusters of EBD-positive cardiomyocytes were apparent in the myocardial wall adjacent to the cardiotoxin injection site in GRAF1$^{gt/gt}$ hearts. Likewise, ISO-induced contraction led to an increase in EBD-positive myocytes in GRAF1-depleted hearts. Moreover, myocardial injury can be assessed by the presence of cardiac troponin within the blood which leaks from cardiomyocytes with injured PMs. Therefore, we measured serum cardiac troponin levels in CTX- and ISO-treated GRAF1-depleted mice, and found that they exhibited significantly higher levels versus GRAF1$^{+/+}$ control mice (Figure 3.5b,c). Taken together, these data indicate that GRAF1 is required to maintain proper cardiomyocyte integrity during muscle contraction.

Dystrophin deficiency has been shown to exacerbate cardiac and skeletal defects in dysferlin-null mice [121, 123]. Therefore, we wanted to determine if depleting GRAF1 in the context of muscular dystrophy could unmask its function in contraction-induced membrane repair. To test this hypothesis, dystrophin/GRAF1 double-deficient offspring were generated using the breeding scheme depicted in figure 3.6 (refer to figure legend for description of mouse nomenclature). Male and female offspring were age matched to 6 and 7 months, respectively, to ensure sufficient disease progression. As shown in figure 3.7a, hearts from male mdx mice present with increased interstitial fibrosis (i.e. collagen deposition as

visualized by Sirius red staining under polarized light) in comparison to GRAF1$^{+/+}$ (WT) controls. As anticipated, dystrophin/GRAF1 double-deficient (mdx/GT$^{Hom}$) mouse hearts exhibited a further increase in interstitial fibrosis in comparison to mdx mice, with small patches of fibrotic scars indicating areas of focal necrosis. The exacerbated cardiac damage in the GRAF1 deficient *mdx* heart indicates that GRAF1 is protective against contraction-induced myocyte damage under pathological conditions. Indeed, we found that female mdx/GT$^{Hom}$ hearts exhibited a significant increase in left ventricle (LV) size and mass in comparison to mdx hearts as assessed by echocardiography (Figure 3.7b,c). Moreover, mdx/GT$^{Hom}$ hearts exhibited enhanced ventricular dysfunction as assessed by ejection fraction (EF) and fractional shortening (FS). Collectively, these data indicate that GRAF1 plays a critical role in maintaining cardiomyocyte sarcolemmal integrity and in facilitating intrinsic cardiomyocyte membrane repair processes during pathological insults.

We next wanted to determine if GRAF1 plays a similar role in maintaining skeletal muscle sarcolemmal integrity. It is well documented that *mdx* mice undergo a period of acute skeletal myofiber necrosis and degeneration that begins around 3-4 weeks of age. Therefore, we harvested tibialis anterior muscle from 3 week old pups injected with EBD and assessed dye accumulation in disrupted fibers. While punctuate areas of EBD-positive muscle fibers were detected in mdx muscle (indicative of focal necrosis) [124], *mdx* mice lacking just one functional copy of GRAF1 (mdx/GT$^{Het}$) mice was sufficient to promote wide-spread EBD accumulation (Figure 3.8). It is worth mentioning that GRAF1$^{gt/gt}$ (GT) and WT muscle did not exhibit any EBD-positive muscle fibers, which implies that depletion of GRAF1 does not destabilize DGCs at the sarcolemma. This data indicates that GRAF1 likely maintains sarcolemmal integrity by repairing contraction-induced membrane damage.

*GRAF1 depletion induces myofiber expansion and muscle growth in* mdx *mice*

Skeletal muscle tissue, unlike cardiac tissue, maintains a high capacity for regeneration and our previous work has shown that GRAF1-deficient muscle exhibit delays in this process (see Chapter 2 for review). Therefore, we hypothesized that adult dystrophin/GRAF1 double-deficient mice would exhibit an exacerbated dystrophic phenotype in comparison to *mdx* mice. Interestingly, and contrary to our hypothesis, adult mdx/GT$^{Hom}$ mice exhibited a gross increase in body size due solely to marked growth of the musculature in these animals (Figure 3.9a,b). This muscle growth significantly increased the body weight of mdx/GT$^{Hom}$ mice in comparison to mdx and WT controls. As previously mentioned, GRAF1 is a negative regulator of RhoA activity, and elevated RhoA activity has been shown to be associated with muscle hypertrophy. Therefore, we next wanted to determine if this increase in mdx/GT$^{Hom}$ muscle size was the result of induced myofiber hypertrophy. As the frequency histogram in figure 3.10a demonstrates, mdx/GT$^{Hom}$ tibialis anterior muscle actually contained a larger percentage of smaller-sized myofibers than mdx muscle, which is confirmed by a significant decrease in overall myofiber size in these mice (Figure 3.10b). Although mdx/GT$^{Hom}$ mice exhibited smaller fibers than mdx and WT controls, the muscle from these mice contained significantly more myofibers per area, indicating that myofiber expansion is likely causal for the marked growth observed in these mice (Figure 3.10c). Moreover, mdx/GT$^{Hom}$ tibialis anterior muscle did not exhibit any obvious increases in fibrosis or myofiber splitting in comparison to mdx muscle (data not shown), which could contribute to increases in muscle mass and cross-sectional myofiber number, respectively. Since myofiber CSA is known to correlate with force production, we next measured the forelimb grip force of these mice and found that while mdx/GT$^{Hom}$ and

mdx/GT$^{Het}$ mice exhibited a significant reduction in grip strength compared to WT, these mice exhibited a small, though not significant, increase in grip strength compared to mdx mice. Taken together this data indicates that depletion of GRAF1 induces the expansion of smaller-sized myofibers in the context of chronic injury, which may play a protective role against muscle degeneration and loss of function. However, it's worth noting that mdx/GT$^{Hom}$ muscle exhibited fiber size variability, a hallmark of ongoing muscle degeneration/regeneration, indicating that these myofibers are not protected against injury (Figure 3.10a).

*GRAF1 depletion does not alter tibialis anterior muscle regeneration in the* mdx *mouse*

In Chapter 2, we demonstrated that regeneration of GRAF1-deficient muscle following acute CTX injury was delayed due to a defect in fusion; however, the data in figure 3.10 indicates that regeneration may actually be enhanced (i.e. increase in myofiber number and presence of myofiber size variability) under conditions of chronic injury. To test this, we quantified nuclear accreation and growth of regenerating myofibers in mdx/GT$^{Hom}$ and mdx tibialis anterior muscles from adult mice. Interestingly, mdx/GT$^{Hom}$ muscle contained a comparable percentage of regenerating fibers (as demarcated by centrally-localized nuclear foci) to mdx muscle. Moreover, these muscles exhibited no change in the average number of nuclear foci per regenerative fiber or the number of regenerating fibers with two or more nuclear foci (*in vivo* fusion index) (Figure 3.11c,d). Taken together, this data indicates that depletion of GRAF1 in the *mdx* mouse does not enhance or diminish regeneration under conditions of chronic muscle injury.

*Depletion of GRAF1 prohibits hallmarks of muscle degeneration in the* mdx *diaphragm*

Since the tibialis anterior muscle of mdx/GT$^{Hom}$ mice did not exhibit altered regeneration or other signs of increased muscle pathology (such as fibrosis) compared to mdx mice, we decided to investigate the diaphragms of these mice, as this muscle exhibits the most severe dystrophy of all muscle types in the *mdx* mouse. Interestingly, immunostaining diaphragm cross-sections for embryonic MHC (eMHC) to demark regenerating myofibers revealed that while mdx mice exhibited numerous eMHC-positive fibers, mdx/GT$^{Het}$ and mdx/GT$^{Hom}$ diaphragms exhibited minimal eMHC staining (Figure 3.12). The diaphragm, like the other muscle in the GRAF1-depleted *mdx* mice, exhibited significant growth (as quantified by diaphragm cross-sectional thickness) and myofiber expansion (Figure 3.13a,b). Interestingly, Sirius red staining demonstrated that while mdx diaphragms exhibited profound fibrosis (measured as collagen deposition; see methods for quantification details), the mdx/GT$^{Hom}$ diaphragms exhibited a significant reduction in fibrosis while mdx/GT$^{Hwt}$ diaphragms manifested an intermediate phenotype (Figure 3.13a,c). Taken together, this data indicates that established hallmarks of muscular dystrophy (i.e. presence of centrally-nucleated regenerating myofibers and increased fibrosis) were reversed in GRAF1 depleted *mdx* mice. Interestingly, although mdx/GT mice exhibited a reduction in diaphragm fibrosis compared to mdx mice, the composition of the collagen in the mdx/GT diaphragm resembled that of mdx diaphragm (Figure 3.13d; refer to methods for quantification details). Specifically, Sirius red stained mdx and mdx/GT diaphragms exhibited enhanced red birefringence in comparison to normal muscle, indicative of increased deposition of Type I collagen and other dense and highly ordered collagens in the ECM of these tissues. This data suggest that although mdx/GT muscle is less fibrotic than mdx muscle, it still requires a

strong extracellular scaffold in which to maintain muscle function.

## DISCUSSION

Previous studies have demonstrated that dysferlin null skeletal myoblasts exhibit delayed membrane patching and a more severe injury following laser-induced injury as assessed by uptake of FM 1-43 dye [7]. Our data shows that GRAF1 deficient myoblasts also undergo a similar attenuation in laser-induced membrane repair. Moreover, the association of GRAF1 with dysferlin in injured muscle indicates that GRAF1 may play an important role in dysferlin-mediated membrane repair. We propose that GRAF1 may regulate the trafficking of dysferlin to sites of sarcolemmal injury, and indeed, we have previously shown that GRAF1 is required for proper trafficking of other ferlin proteins to the PM prior to myoblast fusion (see Chapter 2 for details). However, examining these processes by way of live-cell imaging could provide useful information regarding the dynamic interaction between GRAF1 and ferlin proteins in muscle fusion and sarcolemmal repair.

ISO injury of dysferlin null hearts has been shown induced marked sarcolemmal injury as demonstrated by EBD uptake [125]. Interestingly, we also showed that GRAF1$^{gt/gt}$ hearts exhibit an increased susceptibility to sarcolemmal injury following both ISO treatment and CTX injection. Furthermore, the loss of dysferlin at the PM of cardiomyocytes in the GRAF1 deficient hearts supports the notion that GRAF1 may regulate the trafficking of dysferlin to the sarcolemma. While the exact mechanism of CTX injury is not well-understood, ISO has been shown to increase contractility of the heart which is, in part, dependent on RhoA activity. Therefore, under conditions of contraction-induced injury, altered RhoA activity in the GRAF1 deficient hearts may impart altered cytoskeletal

dynamics which my induce DGC instability or prevent proper trafficking of vesicles to sites of membrane rupture. Since GRAF1-depleted muscle does not exhibit significant membrane fragility under basal conditions, it is likely that GRAF1 does not destabilize DGCs. Immunostaining of GRAF1 deficient hearts and skeletal muscle for components of the DGC, such as dystrophin and β-dystroglycan, could be done to support this notion.

Previous studies have demonstrated that dysferlin/dystrophin double-deficient mice exhibit a more severe muscle pathology than both *mdx* or dysferlin null mice, and, importantly, the onset of the muscle pathology occurred much earlier than it did in dysferlin null mice [123]. Therefore, based on our findings that GRAF1 may be a component of dysferlin-mediated membrane repair, we hypothesized that GRAF1/dystrophin double-deficient mice would exhibit an exacerbated dystrophic phenotype similar to dysferlin/dystrophin double-deficient mice. Although we found some indication of increased muscle pathology in these mice, we also observed robust muscle growth and myofiber expansion which is not present in dysferlin/dystrophin double-deficient mice, indicating an additional role for GRAF1 under conditions of chronic pathological insult.

Although GRAF1 deficient *mdx* diaphragms exhibit a reduction in fibrosis and regenerative fibers, our preliminary data indicates that these mice exhibit elevated levels of serum creatine kinase (sCK), a marker of muscle membrane damage (data not shown). Further assessments needs to be made to determine how sCK levels of GRAF1 deficient *mdx* mice compares to that of *mdx*; however it is presumed that double-deficient mice will exhibit higher levels based on our findings that muscle from these mice at 3 weeks of age exhibit marked sarcolemmal instability. Moreover, an assessment of EBD accumulation in muscle of these adult mice should confirm the sCK analysis.

Interestingly, although GRAF1-depleted *mdx* hearts exhibited increased fibrosis, the diaphragm exhibited less in comparison to *mdx*. This discrepancy is likely due to the regenerative capacity of skeletal muscle, which is lacking in the heart. In *mdx* skeletal muscle, the increased sarcolemmal injury induces robust myogenesis in order to repair the musculature as well as form new myofibers. We show that in the absence of GRAF1, *mdx* muscle undergoes more severe sarcolemmal injury (presumably due to defects in PM injury repair), as demonstrated in 3 week old mice. Therefore, we postulate that the signal to induce myogenesis is enhanced in these mice, accounting for the significant growth of the muscle. However, due to defects in fusion in the absence of GRAF1, myofibers do not fuse as readily, and as such, may account for the increase in myofiber number. Since we see decreases in fibrosis and regenerative fibers in mdx/GT mice, it may be that the smaller fibers confer a resistance to contraction-induced damage, thereby acting to protect the muscle as opposed to exacerbating the dystrophic phenotype.

Although we show that tibialis anterior muscle from 6 month old male mdx/GT$^{Hom}$ mice maintained regenerative capacity, it would be interesting to know if the propensity of muscle regeneration is altered in aged mice. To test this, Pax7+ satellite cell expansion could be quantitated in muscle sections from aged mice subjected to a bout of acute CTX-induced muscle injury. Additionally, regeneration could be quantified by staining for markers of differentiation, such as myogenin or MHC.

In summary, we provide the first evidence that GRAF1 associates with the membrane repair protein, dysferlin, and is necessary for efficient skeletal and cardiac PM repair. The GRAF1/dystrophin double-deficient mice exhibited more severe muscle pathology than both *mdx* and GRAF1-depleted mice, while also exhibiting muscle growth which was not

consistent with dysferlin/dystrophin double-deficient mice. This data implicates an additional role for GRAF1 in skeletal muscle-injury response, which requires further investigation.

## MATERIALS AND METHODS

### *Generation of mice*

Double-deficient mice (mdx/GT$^{Het}$ and mdx/GT$^{Hom}$) and control mice (WT, GT and mdx) were generated by breeding female mdx/C57/B10 (*mdx*) mice with male GRAF1-depleted (GRAF1$^{gt/gt}$) mice (refer to page 102 for description of genotype) through two generations (Figure 3.6). The genetic background of all experimental mice is a mixture of C57/B10, 129/SvEv and C57BL/6J. F2 pups were genotyped for the *mdx* allele and the GRAF1 allele as described previously [126], (refer to page 38). Echocardiographic analysis was performed in age-matched female offspring. All other analyses were performed in age-matched male offspring. Animals were treated in accordance with the approved protocol of the University of North Carolina (Chapel Hill, NC) Institutional Animal Care and Use Committee, which is in compliance with the standards outlined in the guide for the Care and Use of Laboratory Animals.

### *Echocardiography*

Left ventricular function was assessed by 2D echocardiography in conscious 7 month old female mice using the Visualsonic Ultrasound System (Vevo 660) with a 30 MHz high-frequency transducer as described previously [127]. Echocardiographic measurements from three consecutive cycles were averaged using Visual Sonics software.

*Grip force measurements*

Muscle forelimb grip strength was analyzed using an automated strain gauge as described previously [128].

In vivo *muscle injury models*

To induce cardiac injury, $GRAF1^{+/+}$ (wildtype) and $GRAF1^{gt/gt}$ (GRAF1-depleted) mice were subject to intracardic injections of 25 μL of 20 μM cardiotoxin (CTX) (*Naja nigricollis*, Calbiochem). After 24 hr, mice were subject to intraperitoneal injection of PBS containing 5% Evans blue dye (EBD), and hearts were harvested 24 hr later. Alternatively, mice were injected with EBD and subsequent injections of isoproterenol (ISO) at 0, 16 and 23 hr timepoints, and hearts were harvested 1 hr following final injection. For both injury models, blood was collected at time of tissue harvest and serum isolated to assess troponin T levels according to manufacturer's instructions (Life Diagnostics). To induce skeletal muscle injury, 50 μL of 20 μM CTX was injected into the quadriceps and tibialis anterior muscles of 4 month and 12 month old male mice, respectively. Mice were injected with EBD after 6 days and muscle harvested 24 hr later.

*Primary cell isolation, cell culture and siRNA treatment*

Primary and C2C12 mouse skeletal myoblasts were isolated and cultured as described previously (refer to pages 40-41). Primary adult rat cardiomyocytes were isolated by the Langendorff method (see review [129]). GRAF1 was depleted from cultured myocytes using short interfering RNA (siRNA) duplex oligoribonucleotides obtained from Invitrogen with the following sequences: graf1a sense 5'-GCAGCUGUUGGCCUAUAAU(dT)(dT)-3' and

anti-sense 5'-AUUAUAGGCCAACAGCUGC-3'; and graf1b sense 5'-AAGUGGACCUGGUUCGGCAACAUUU-3' and anti-sense 5'-AAAUGUUGCCGAACCAGGUCCACUU-3'. Myocytes were transfected with 50 nM of GRAF1 siRNA (25nM of both graf1a and graf1b) or a GFP-specific siRNA as a non-target control using DharmaFECT reagent 1 according to manufacturer's instructions (Thermo Scientific). After 24 hr, media was exchanged and cells were fixed.

In vitro *injury repair assays*

For laser repair assay, $GRAF1^{+/+}$ and $GRAF1^{gt/gt}$ primary skeletal myoblasts were differentiated for 72 hr before addition of FM 1-43 (Invitrogen), a membrane-impermeable dye, for 5 min prior to laser injury. Healthy, intact myoblasts were targeted with a 10 second laser pulse, mode-locked on a 2µm (l) x 0.5µm (w) x 2µm (d) region of the plasma membrane (PM). Time-lapse images were acquired prior to and for up to 45 min following injury. The fluorescent intensity within (and remote to) the damaged site was quantified using Zeiss LSM 710 imaging software. Furthermore, to investigate GRAF1 redistribution to disrupted PMs, differentiated C2C12 myoblasts were mechanically injured with a scalpel blade 2 min prior to fixation and immunohistochemical analysis. For saponin repair assay, siRNA-treated primary cardiomyocytes were treated with FM 1-43 and permeabilized with 0.01% saponin, or left untreated as a control, for 1 min prior to fixation.

*Immunohistochemistry and immunocytochemistry*

Harvested mouse hearts and diaphragm muscles were immediately fixed in 4% paraformaldehyde, and processed for paraffin embedding using standard techniques.

Unfixed frozen dog tissues, a generous gift from Dr. Joe Kornegay, were fixed and processed as above. Alternatively, mouse tibialis anterior muscles were immediately embedded in Tissue-Tek O.C.T. compound (Sakura) and snap-frozen in 2-Methylbutane cooled over dry ice. For immunohistochemistry, tissues were cross-sectioned at 8 μm, post-fixed in 4% paraformaldehyde (frozen sections), treated for antigen retrieval using 10 mmol/L citrate buffer (pH 6.0), and stained using standard techniques. For immunostaining of cultured myocytes, cells were fixed in 4% paraformaldehyde, permeabilized using PBS containing 0.1%Triton X-100 and 0.1% sodium citrate (for cardiac myocytes) or PBS containing 0.4% Triton A-100 (for skeletal myocytes). Tissues/cells were incubated with primary antibodies at 1:200 dilutions at 4°C overnight. Commercial anibodies were purchased from Sigma (laminin, monoclonal γ-tubulin); Abcam (α-actinin); Lifespan Biosciences (annexin a1); Leica Microsystems (dysferlin); and Developmental Studies Hybridoma Back, Univ. of Iowa (eMHC, troponin T). Derivation of the GRAF1 rabbit and hamster antibodies were described previously (refer to page 38). Tissues were then incubated with Alexa Fluor secondary antibodies (Invitrogen), Alexa Fluor phalloidin (Invitrogen), Alexa Fluor wheat germ agglutinin (Invitrogen) and DAPI at 1:500 in PBS for 1 hr, washed and mounted. Flourescent images were acquired using a Zeiss LSM 710 confocal laser-scanning microscope. ImageJ software was used to quantify myofiber cross sectional area and the *in vivo* fusion index (refer to page 42 for details).

*Histological analysis*

Tissue sections processed as above were subjected to haematoxylin and eosin (H&E) staining using standard techniques or Picrosirius red staining according to manufacturer's

instructions (Polysciences), and visualized using bright field microscopy. To quantify diameter thickness, cross-sectional widths along the length of a tissue section were measured and averages calculated using ImageJ software. To quantify diaphragm fibrosis, Sirius red-stained tissues were first imaged under linear polarized light using identical gain. ImageJ was then used to quantify the integrated density of the red and green signal from each image. Collagen deposition is described as the sum of the red and green signal density per area of tissue. Collagen composition is described as the the average ratio of red to green signal density per area of tissue. Images were acquired using an Olympus BX61 microscope.

*Co-immunoprecipitation*

For immunoprecipitation studies, isolated mouse quadriceps muscle was sonicated in modified radioimmune precipitation assay (RIPA) buffer (50mM HEPES pH 7.2, 0.15 M NaCl, 2 mM EDTA, 0.1% Nonidet P-40, 0.05% sodium deoxycholate, 0.5% Triton X-100 plus 1mM sodium orthovanadate and 1X concentrations of both Halt Protease Inhibitor Cocktail (Thermo Scientific) and Halt Phosphatase Inhibitor Cocktail (Thermo Scientific)), and cleared by centrifugation. 1,000 µg of cleared lysate was incubated with 10 µg of either an anti-GRAF1 antibody (polyclonal) overnight at 4°C. The solution was then mixed with 75 µL of a 50% slurry of Protein A Sepharose beads (Sigma) in TBS and rotated at 4°C for 2 hr. Beads were then quickly tapped down in a refrigerated centrifuge and rinsed 3 times with ice-cold RIPA + inhibitors and once with TBS before beads were boiled in 50 µL of sample buffer. Eluates and a 2% lysate input were resolved by SDS-PAGE, transferred to nitrocellulose membranes, and immunoblotted with an anti-dysferlin antibody and an anti-GRAF1 antibody (monoclonal) at 1:1000 dilutions using standard techniques.

*Statistical analyses*

All statistical analyses were performed using Student's t-test. Data are represented as mean ± s.e.m. and $p$-values $<0.05$ were considered statistically significant.

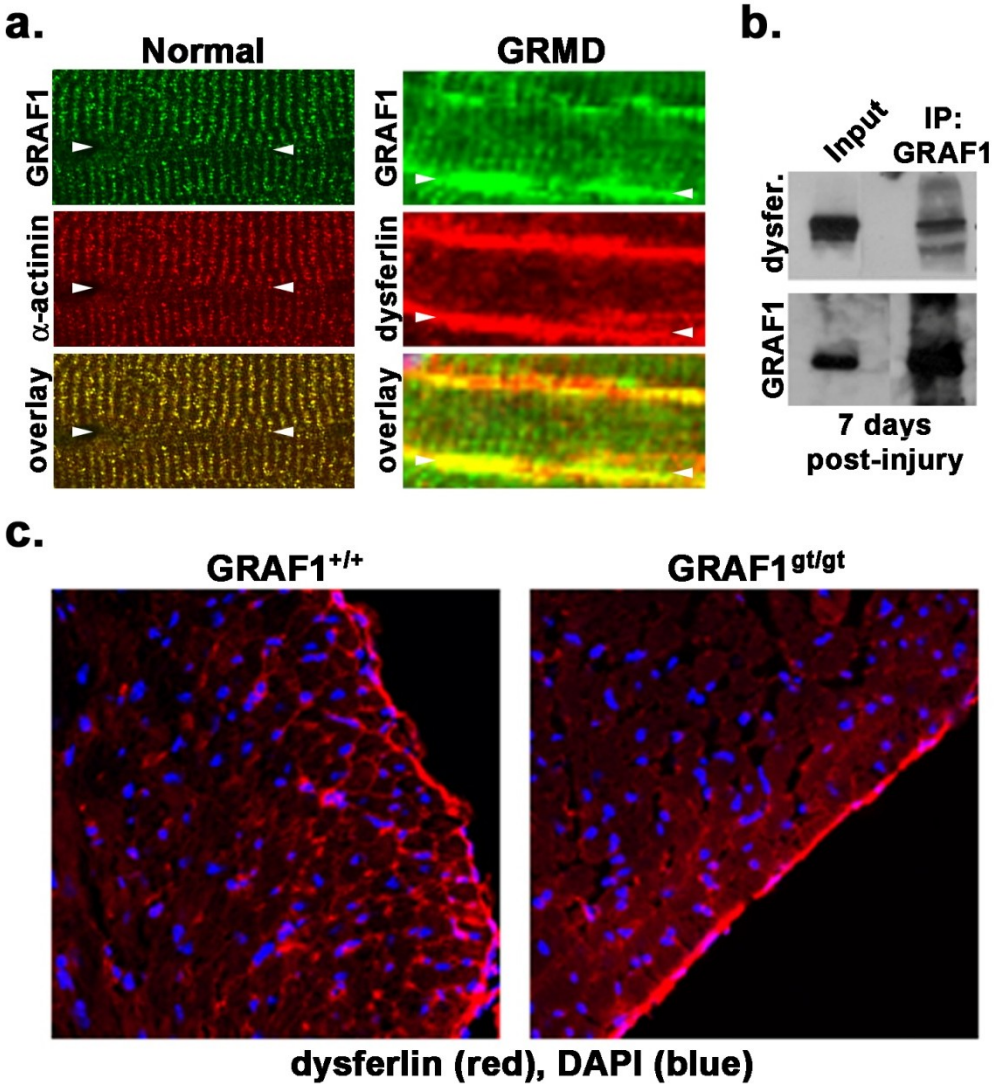
a.
Normal
GRMD
GRAF1
α-actinin
overlay
GRAF1
dysferlin
overlay
b.
Input
IP: GRAF1
dysfer.
GRAF1
7 days post-injury
c.
GRAF1+/+
GRAF1gt/gt
dysferlin (red), DAPI (blue)

**Figure 3.1: GRAF1 redistributes to the plasma membrane in injured/dystrophic muscles, complexes with dysferlin, and is necessary for dysferlin localization. (a)** Immunohistochemical analysis of GRAF1 expression (green) in normal and dystrophic (golden retriever muscular dystrophy (GRMD)) muscle. Co-staining for α-actinin and dysferlin (red) demonstrates localization of GRAF1 at Z-discs and plasmalemma in normal muscle and GRMD muscle, respectively. **(b)** Anti-GRAF1 rabbit polyclonal antibody immunoprecipitation (IP) from adult quadricep muscle 7 days following cardiotoxin-induced injury. Blots were probed with an anti-dysferlin antibody or hamster anti-GRAF1 antibody. *Input* contains 2% of cellular lysate used for IP. **(c)** Immunohistochemical analysis of dysferlin (red) in $GRAF1^{+/+}$ and $GRAF1^{gt/gt}$ adult mouse hearts indicates mis-localization in the absence of GRAF1. Nuclei are counterstained with DAPI (blue).

**a.**

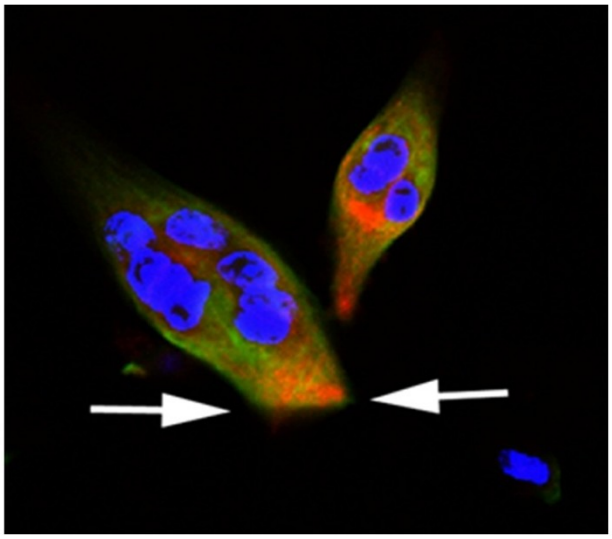

GRAF1 (red), phalloidin (green), DAPI (blue)

**b.**

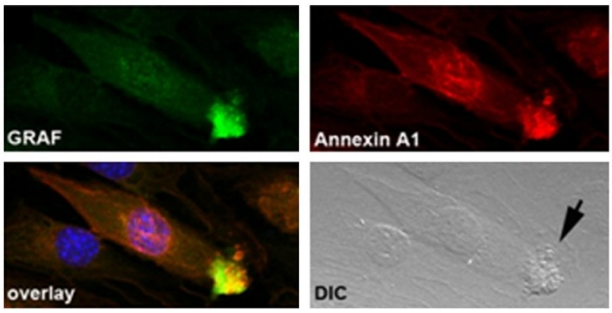

**Figure 3.2: GRAF1 is dynamically recruited to disrupted plasma membranes. (a)** A 72 hr differentiated C2C12 myoblast cut with a scalpel blade was fixed 2 min post-injury and stained for GRAF1 (red). Note accumulation of GRAF1 at the site of injury. F-actin and nuclei were counterstained with phalloidin (green) and DAPI (blue), respectively. **(b)** GRAF1 (green) co-localizes with the membrane fusion/repair protein, Annexin A1 (red), in pre-fused myoblasts (36 hr differentiation). Note GRAF1 co-localization in sub-membranous vesicles (*arrow*) as visualized by DIC microscopy.

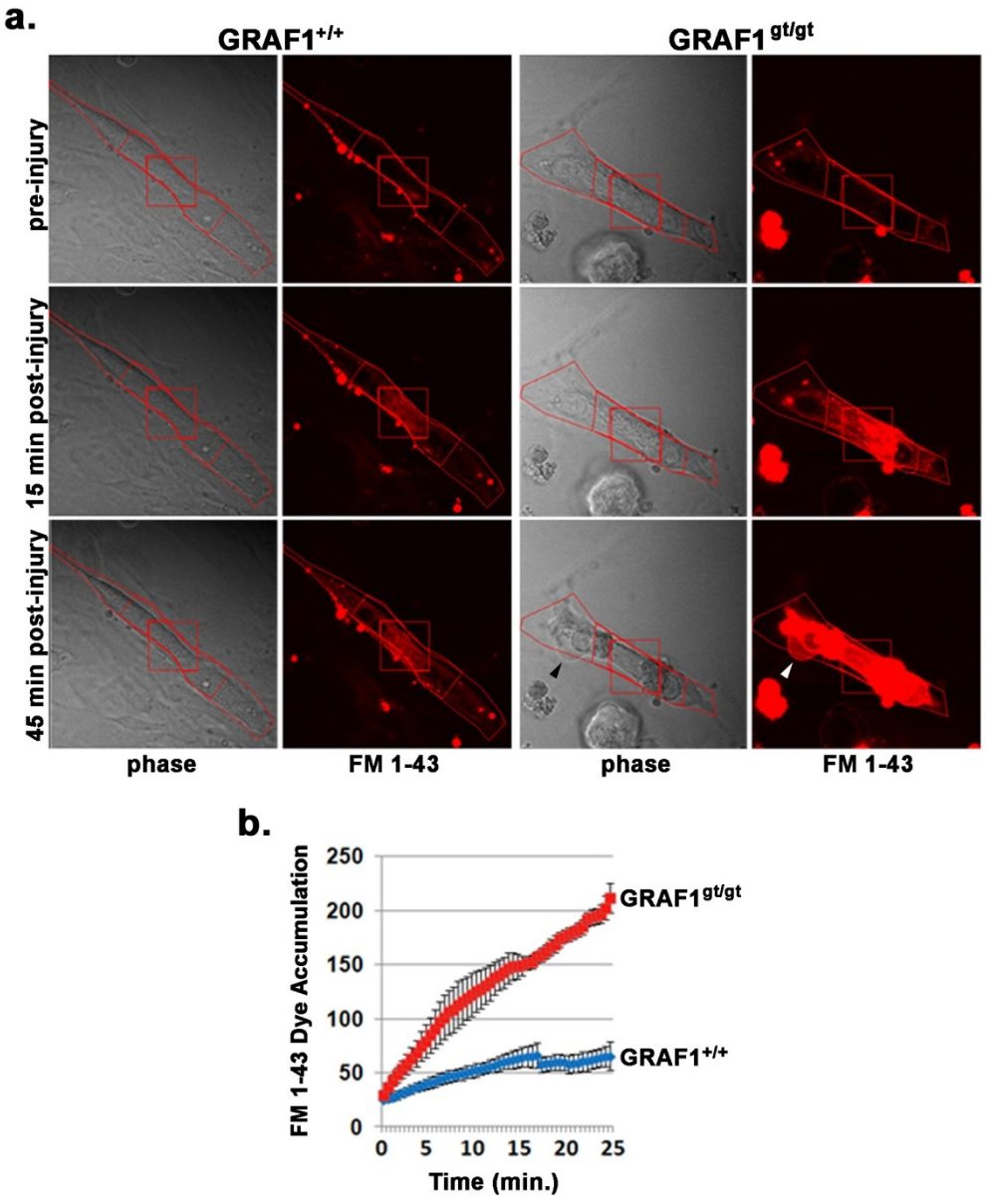
a.
GRAF1+/+
GRAF1gt/gt
pre-injury
15 min post-injury
45 min post-injury
phase
FM 1-43
phase
FM 1-43
b.
FM 1-43 Dye Accumulation
250
200
150
100
50
0
0
5
10
15
20
25
Time (min.)
GRAF1gt/gt
GRAF1+/+

**Figure 3.3: GRAF1 depletion impairs skeletal myotube membrane repair. (a)** GRAF1$^{+/+}$ and GRAF1$^{gt/gt}$ primary myotubes were treated with FM 1-43 membrane dye (red) for 5 min and imaged prior to confocal-directed laser injury (denoted by red square) (*top panels*) and 15 min (*middle panels*) and 45 min (*bottom panels*) post-injury. Note pronounced FM 1-43 accumulation and membrane blebbing (*arrowheads*) in GRAF1$^{gt/gt}$ cells. **(b)** Quantification of dynamic FM 1-43 dye accumulation up to 25 min following injury ($n$=23-28 cells per genotype; $N$=5). Data are represented as ± s.e.m.

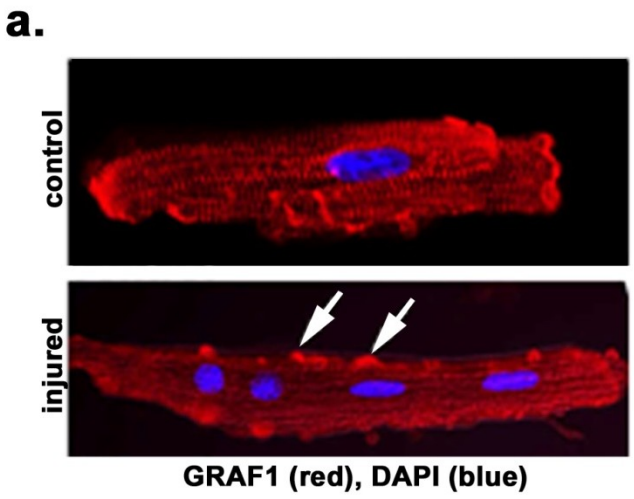
a.
control
injured
GRAF1 (red), DAPI (blue)
b.
FM 1-43 dye-labeled cardiomyocytes (% of total)
70%
60%
50%
40%
30%
20%
10%
0%
si GFP
si GRAF
IB:GRAF
IB:tubulin
si GFP
si GRAF
*
**
No treatment
Saponin treated

**Figure 3.4: GRAF1 depletion reduces the membrane repair capability of cultured cardiomyocytes. (a)** Immunohistochemical analysis of GRAF1 expression (red) in control and saponin treated (injured) cultured adult rat ventricular cardiomyocytes. Note the translocation of GRAF1 to the plasma membrane of injured cardiomyocytes (*white arrows*). Nuclei are counterstained with DAPI (blue). **(b)** Quantification of FM 1-43 dye-positive cardiomyocytes treated with or without saponin following transfection with control (GFP) or GRAF1-specific siRNAs. Note significant increase in dye accumulation in GRAF1-depleted cells following injury. Western blot demonstrates efficient GRAF1 knockdown. γ-tubulin stained blot is shown as loading control.

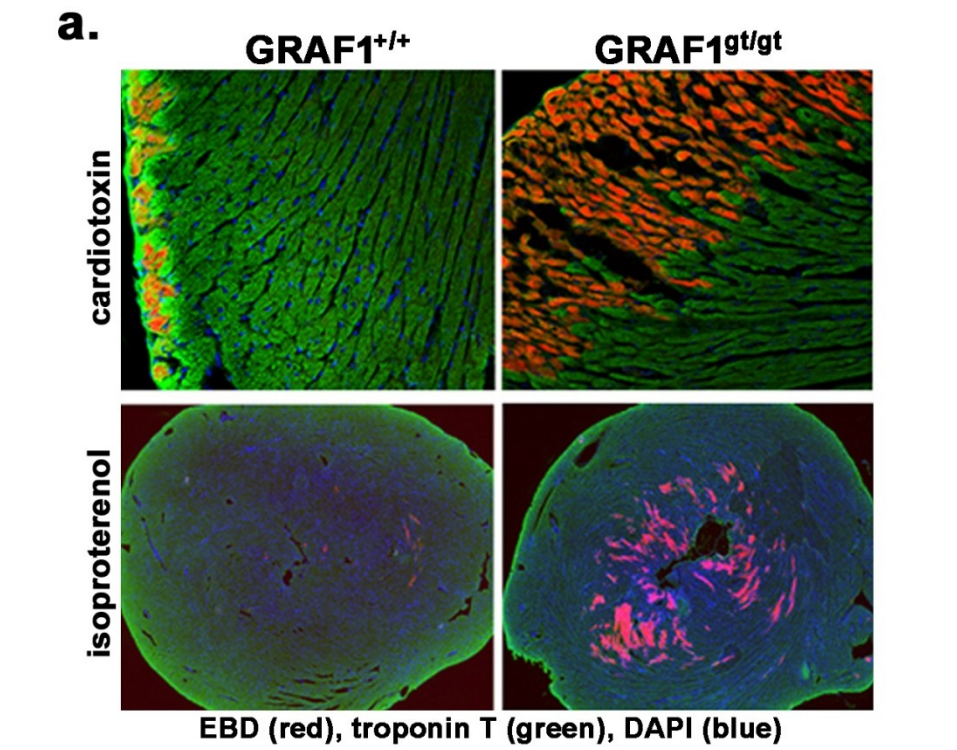
a.
GRAF1+/+
GRAF1gt/gt
cardiotoxin
isoproterenol
EBD (red), troponin T (green), DAPI (blue)
b.
% EB-positive LV area
25
20
15
10
5
0
GRAF1+/+
GRAF1gt/gt
*
*
CTX
ISO
c.
Serum troponin (ng/dL)
8
6
4
2
0
GRAF1+/+
GRAF1gt/gt
*
CTX
ISO

**Figure 3.5: GRAF1 is required for optimal cardiomyocyte membrane repair *in vivo*.**

**(a)** Representative images of Evans blue dye (EBD) (red) uptake in hearts of $GRAF1^{+/+}$ and $GRAF1^{gt/gt}$ adult mice 24 hrs after subjection to intracardiac injection of cardiotoxin (CTX) (*top panels*) or intraperitoneal injection of isoproterenol (ISO) (*bottom panels*). Cardiomyocytes and nuclei are counterstained with troponin T antibody (green) and DAPI (blue), respectively. **(b)** Graphical representation of the area of EBD uptake in the left ventricle (LV) cross section of injured hearts. **(c)** Quantification of serum troponin levels in injured mice. Note significant increases in markers of cardiomyocyte damage in $GRAF^{gt/gt}$ mice. (*N*=6-7 mice per genotype). Data are represented as ± s.e.m.

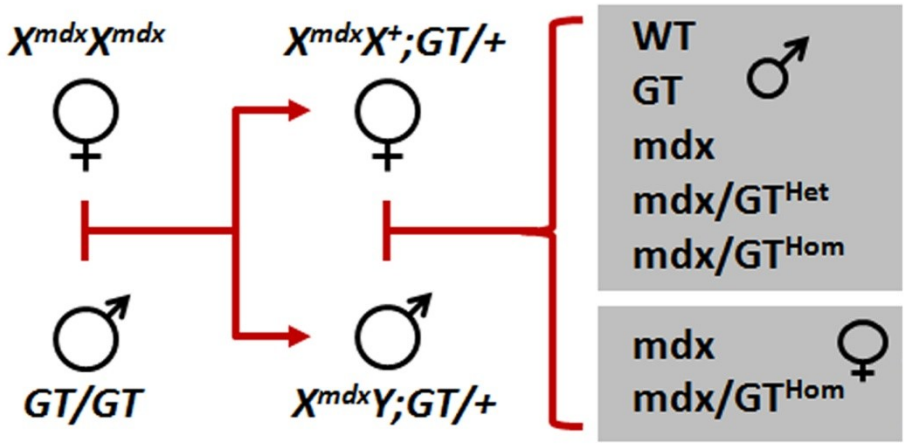
$X^{mdx}X^{mdx}$
$X^{mdx}X^{+};GT/+$
WT
GT
mdx
mdx/GT$^{Het}$
mdx/GT$^{Hom}$
GT/GT
$X^{mdx}Y;GT/+$
mdx
mdx/GT$^{Hom}$

**Figure 3.6: Mouse breeding scheme for genetic-based model of muscle injury.**

Genotypes of experimental mice are denoted in gray boxes. WT=wildtype; GT=GRAF1$^{gt/gt}$ (GRAF1-deficent); mdx=*mdx* (dystrophin-deficient); mdx/GT$^{Het}$=*mdx*/GRAF1$^{+/gt}$ (dystrophin-deficent/GRAF1 haploinsufficient); mdx/GT$^{Hom}$=*mdx*GRAF1$^{gt/gt}$ (dystrophin/GRAF1 double-deficent).

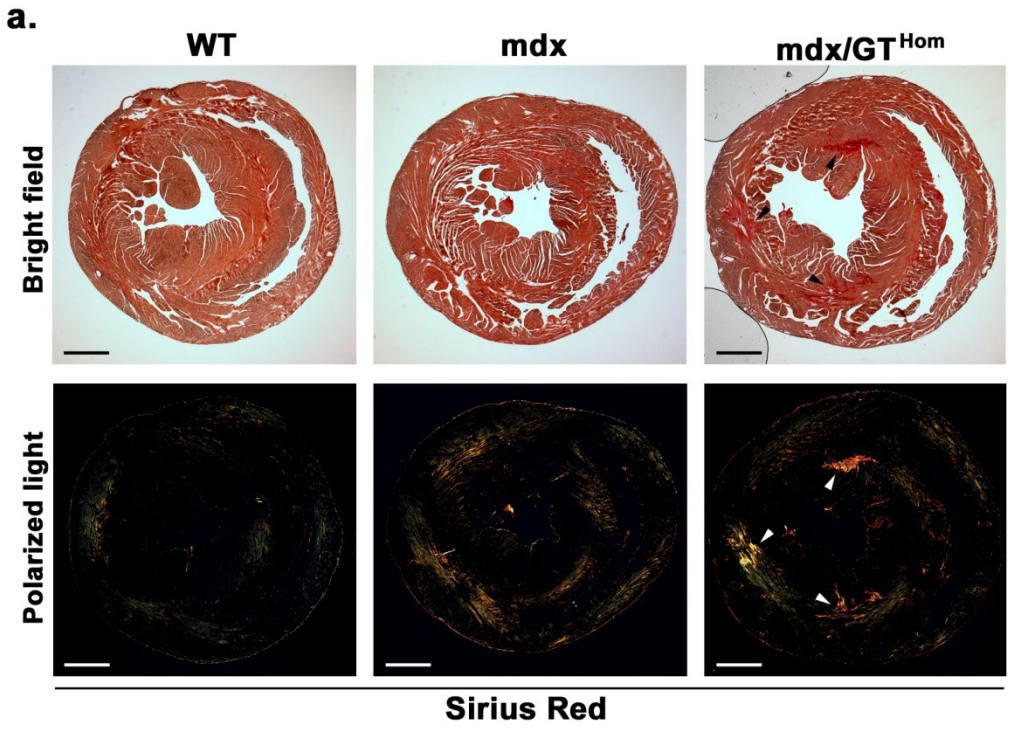
a.
WT
mdx
mdx/GT Hom
Bright field
Polarized light
Sirius Red

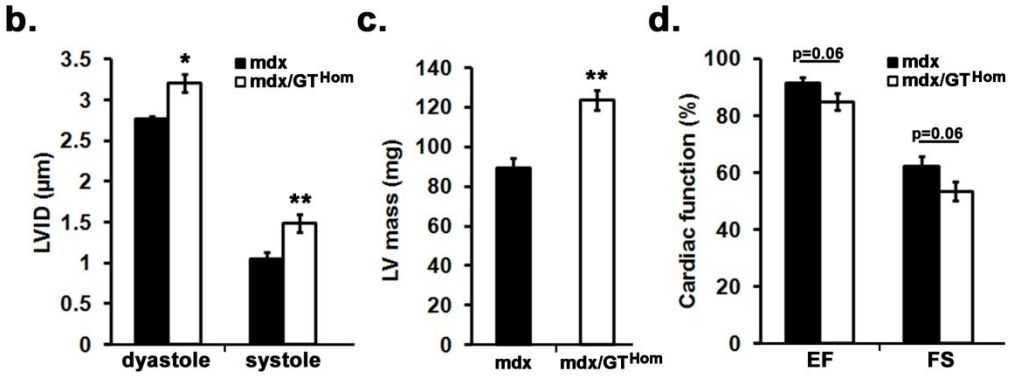
b.
LVID (µm)
mdx
mdx/GT Hom
dyastole
systole
c.
LV mass (mg)
mdx
mdx/GT Hom
d.
Cardiac function (%)
p=0.06
p=0.06
EF
FS

**Figure 3.7: GRAF1 depletion exacerbates cardiac fibrosis and reduces cardiac output in *mdx* mice. (a)** Heart cross sections from 6 month old male mice with indicated genotypes stained with Sirius red and visualized using bright field microscopy (*upper panels*) or under polarized light (*bottom panels*). Note fibrotic patches in the mdx/GT$^{Hom}$ heart (*arrowheads*). **(b)** and **(c)** Conscious echocardiographic analysis of left ventricular internal diameter (LVID) and LV mass, respectively, in 7 month old female mice. **(d)** Evaluation of cardiac output by calculated left ventricular ejection fraction (EF) and fractional shortening (FS). (*$p$<0.005, **$p$<0.01; $N$=4-5 mice per genotype). Data are represented as ± s.e.m. Scale bars=1.0 mm.

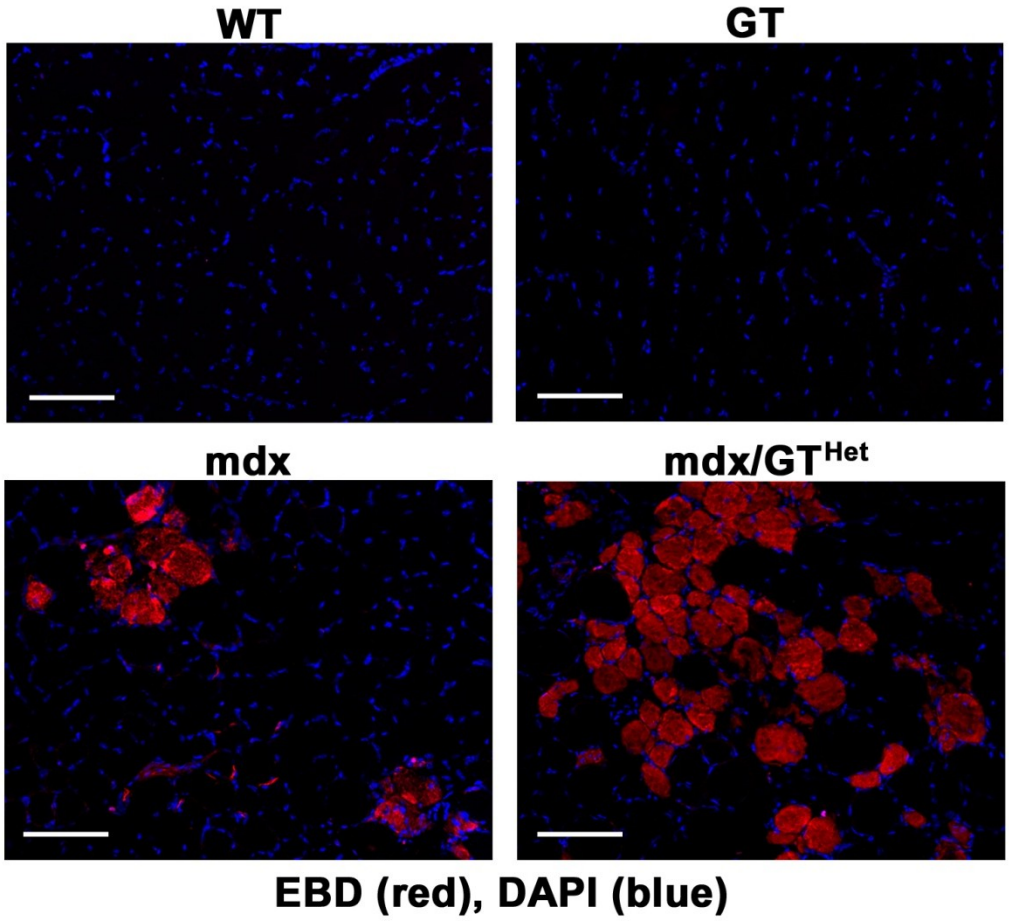
WT
GT
mdx
mdx/GT^Het
EBD (red), DAPI (blue)

**Figure 3.8: GRAF1 depletion increases Evans blue dye accumulation in young *mdx* muscle.** Representative images of EBD (red) accumulation in tibialis anterior muscle of 3 week old littermates with indicated genotypes. Mice were injected with EBD 24 hr prior to tissue harvest. Nuclei are counterstained with DAPI (blue). Scale bars=100 μm.

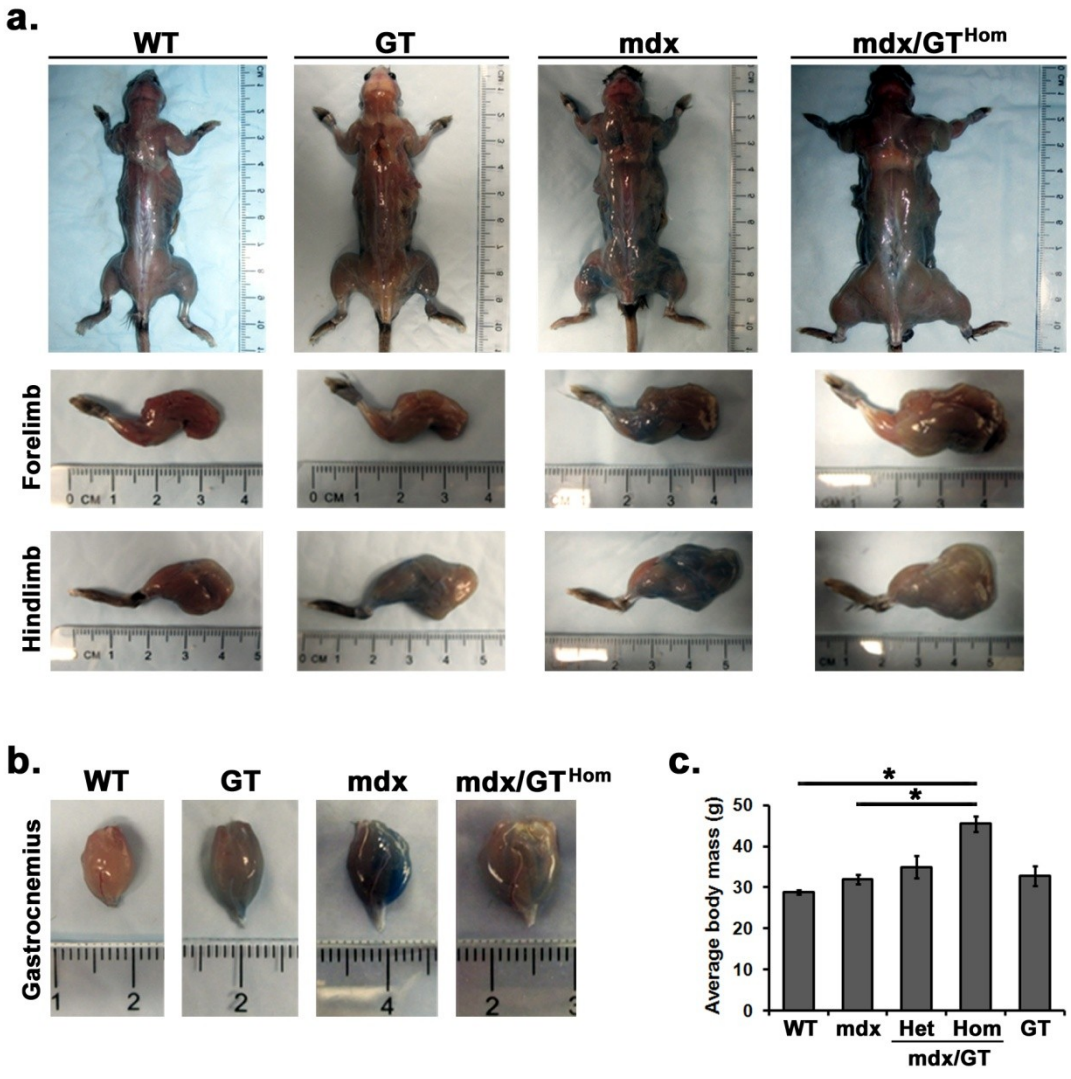
a.
WT
GT
mdx
mdx/GTHom
Forelimb
Hindlimb
b.
WT
GT
mdx
mdx/GTHom
Gastrocnemius
c.
Average body mass (g)
0
10
20
30
40
50
*
*
WT
mdx
Het
Hom
GT
mdx/GT

**Figure 3.9: GRAF1-depleted *mdx* mice exhibit increased muscle growth. (a)** Whole body images of 6 month old male mice with indicated genotypes. Note pronounced size increase of the whole body (*top panels*), forelimbs (*middle panels*), and hindlimbs (*bottom panels*) of mdx/$GT^{Hom}$, compared to age-matched controls. **(b)** Comparison of gastrocnemius muscles isolated from mice in (a) demonstrate marked muscle growth in mdx/$GT^{Hom}$ mice. **(c)** Average body mass of 6 month old male mice. (**p*<$5X10^{-4}$; *N*=5 mice per genotype). Data are represented as ± s.e.m.

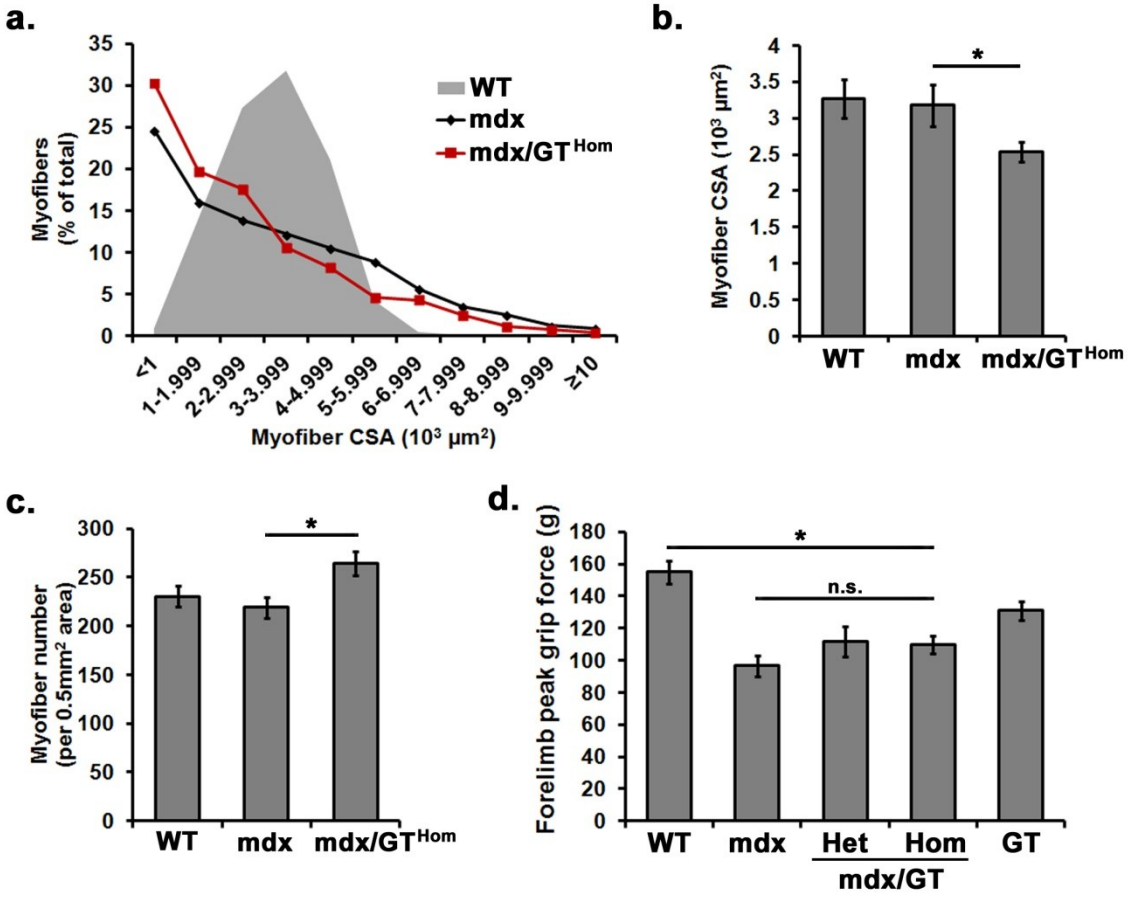
a.
Myofibers (% of total)
35
30
25
20
15
10
5
0
WT
mdx
mdx/GT Hom
<1
1-1.999
2-2.999
3-3.999
4-4.999
5-5.999
6-6.999
7-7.999
8-8.999
9-9.999
≥10
Myofiber CSA (10³ µm²)
b.
Myofiber CSA (10³ µm²)
4
3.5
3
2.5
2
1.5
1
0.5
0
*
WT
mdx
mdx/GT Hom
c.
Myofiber number (per 0.5mm² area)
300
250
200
150
100
50
0
*
WT
mdx
mdx/GT Hom
d.
Forelimb peak grip force (g)
180
160
140
120
100
80
60
40
20
0
*
n.s.
WT
mdx
Het
Hom
mdx/GT
GT

**Figure 3.10: mdx/GT$^{Hom}$ mice exhibit reduced myofiber size and grip strength. (a)** Frequency histogram demonstrating myofiber distribution by cross-sectional area (CSA) of tibialis anterior muscle from 6 month old male mice with indicated genotypes. **(b)** Average myofiber CSA of tibialis anterior muscle. (*$p$<0.001; $n$=350 myofibers per mouse; $N$=5 mice per genotype). **(c)** Average myofiber number per 0.5 mm$^2$ in cross sections of tibialis anterior muscle. (*$p$<0.05; $N$=5 mice per genotype). **(d)** To assess muscle strength, forelimb peak grip force was measured in 6 month old male mice. (*$p$<0.01, n.s.=no significance; $N$=5 mice per genotype). Data are represented as ± s.e.m.

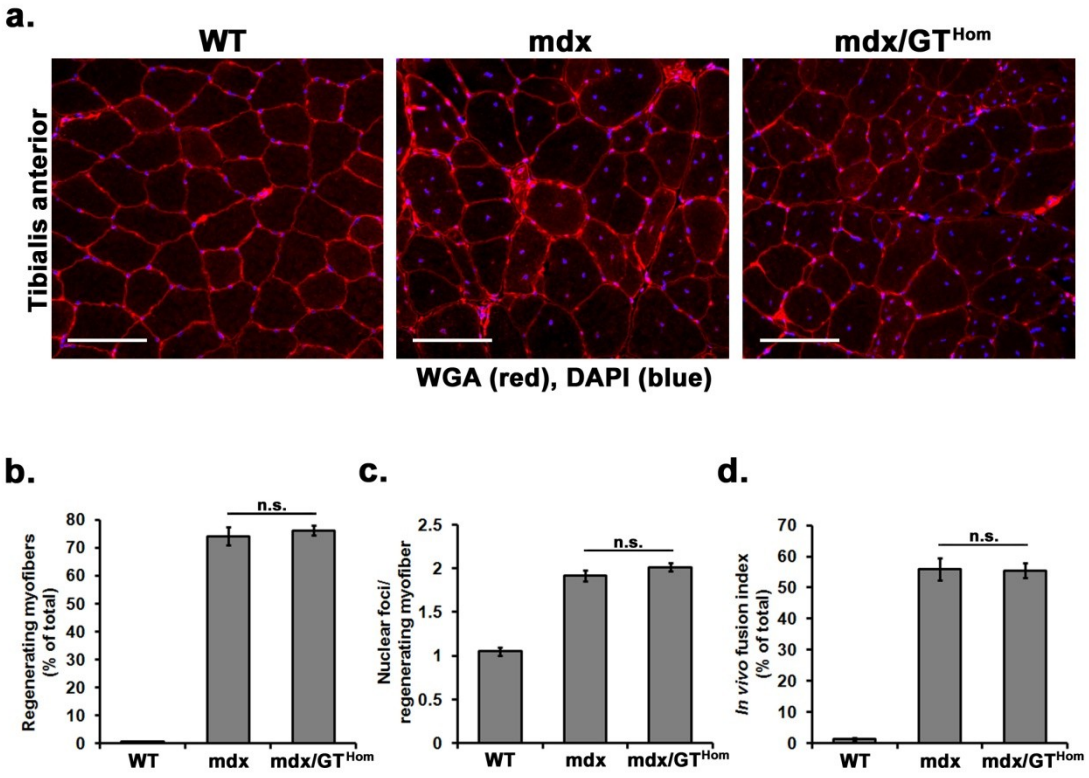
a.
WT
mdx
mdx/GT^Hom
Tibialis anterior
WGA (red), DAPI (blue)
b.
Regenerating myofibers (% of total)
n.s.
WT
mdx
mdx/GT^Hom
c.
Nuclear foci/ regenerating myofiber
n.s.
WT
mdx
mdx/GT^Hom
d.
In vivo fusion index (% of total)
n.s.
WT
mdx
mdx/GT^Hom

**Figure 3.11: GRAF1 depletion does not alter the regenerative capacity of tibialis anterior muscle in adult *mdx* mice.** **(a)** Representative cross-sectional images of tibialis anterior muscle from 6 month male mice with indicated genotypes. Note extensive nuclear foci in mdx and mdx/$GT^{Hom}$ muscle. Wheat germ agglutinin (WGA) (red) demarks myofiber boundaries. Nuclei are counterstained with DAPI (blue). **(b)** Graphical representation of the percentage of regenerating myofibers in the muscle. **(c)** Average nuclear foci per regenerating myofiber. **(d)** *In vivo* fusion index for regenerating myofibers. (n.s.=no significance*;* *n*=300 myofibers per mouse; *N*=5 mice per genotype). Data are represented as ± s.e.m. Scale bars=100 μm.

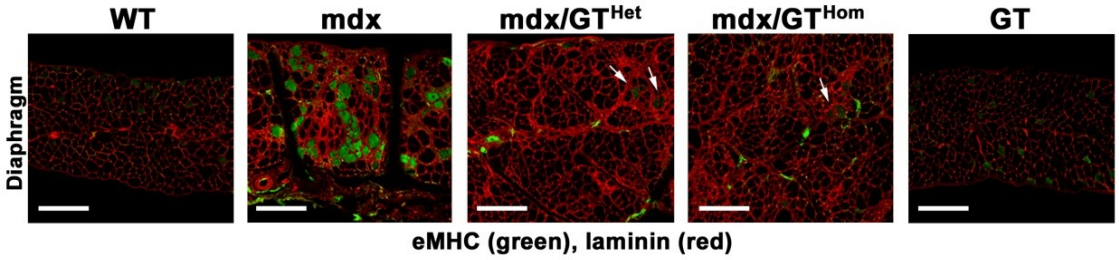
WT
mdx
mdx/GT^Het
mdx/GT^Hom
GT
Diaphragm
eMHC (green), laminin (red)

**Figure 3.12: GRAF1 depleted *mdx* diaphragms exhibit fewer regenerative fibers.** **(a)** Diaphragm cross sections from 6 month old male mice with indicated genotypes immunostained with eMHC (green) to demark regenerative fibers. Laminin (red) demarks myofiber boundaries. Note marked reduction in regenerating fibers in mdx/GT mice (*arrows*). Scale bars=20 μm.

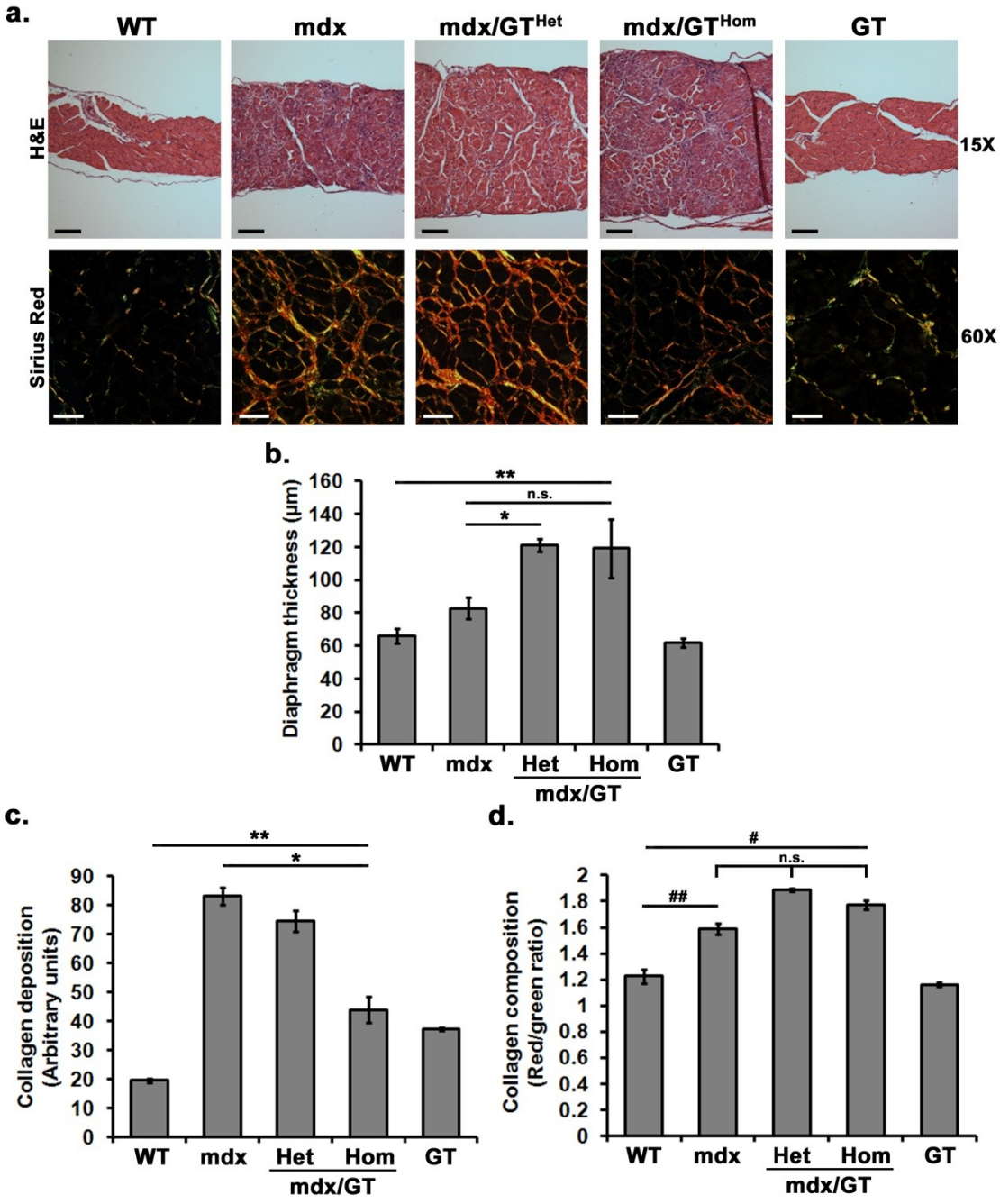
a.
WT
mdx
mdx/GTHet
mdx/GTHom
GT
H&E
15X
Sirius Red
60X
b.
Diaphragm thickness (µm)
**
n.s.
*
WT
mdx
Het
Hom
GT
mdx/GT
c.
Collagen deposition (Arbitrary units)
**
*
d.
Collagen composition (Red/green ratio)
#
n.s.
##

**Figure 3.13: GRAF1 depletion reduces diaphragm fibrosis but does not alter collagen composition in adult *mdx* mice.** **(a)** Diaphragm cross sections from 6 month old male mice with indicated genotypes stained with haematoxylin and eosin (H&E) (*top panels*) or Sirius red and imaged under polarized light to visualize fibrosis (*bottom panels*). **(b)** Quantification of average diaphragm thickness. Note significant increase mdx/GT mice. Data are represented as average±s.e.m. (**p*<0.005, ***p*<0.05, n.s.=no significance; *N*=5 mice per genotype). **(c)** and **(d)** Graphical representations of collagen deposition and composition, respectively, of diaphragms from 6 month old male mice (refer to methods for quantification details). (**p*<1X10$^{-4}$, ***p*<0.001, $^{\#}$*p*<0.005, $^{\#}$*p*<0.05, n.s.=no significance; *N*=5 mice per genotype). Black scale bars=25 μm; White scale bars=100 μm.

# CHAPTER 4

## CONCLUSIONS, PERSPECTIVES AND FUTURE DIRECTIONS

The data presented in this thesis supports a role for GRAF proteins in muscle maturation and repair. However, there are no documented instances of muscle disorders resulting solely from altered GRAF expression in either the skeletal or cardiac musculature of humans. However, we have shown that GRAF1 and GRAF2 are robustly expressed in regenerative skeletal myofibers in an adult patient with mixed myopathy (Figure 4.1).[3] Therefore, although GRAF may not be the main player of disease, based on our mechanistic studies, it may act as a genetic modifier of various monogenic or multi-factorial muscular disorders. Indeed, the pace and pattern of muscle weakness, along with onset of cardiomyopathy, is highly variable even when associated with the same identical mutation. Therefore, despite advancements in our understanding of the pathological mechanisms which lead to muscle disease (i.e. defects in the structural maintenance and repair of the plasma membrane), further work is required to identify other components which may explain the variation in disease severity. Such components will serve as candidate genes for the muscle diseases of unknown etiology as well as open up new avenues for therapeutic intervention.

Although the role of GRAF family members as genetic modifiers is yet to be determined, gene expression profiling of patients with Duchenne or Limb-girdle muscular dystrophies have demonstrated alterations in GRAF1 gene expression levels (NCBI GEO

Profiles). Furthermore, it would be interesting to assess whether GRAF1 levels actually correlate with disease onset or severity. Moreover, given that GRAF1 is a moderately large catalytic protein containing phosphorylation sites within its regulatory/protein-interacting domains, it is plausible that various single nucleotide polymorphisms (SNPs) may significantly alter the activity of this protein which could also influence muscle pathology. The fact that GRAF1 maintains the ability to auto-inhibit its catalytic activity as well as self-dimerize through it's BAR domain, strengthens this notion. Moreover, GRAF proteins make good targets for therapeutic intervention, as their catalytic activity may be relatively easily manipulated with pharmaceutical drugs. This is a simpler alternative to current, complicated therapeutic strategies for muscular dystrophies, such as DMD, which includes viral delivery of 'mini-dystrophins' and *in vivo* exon-skipping.

The GRAF1 gene trap mouse has been a wonderful model to study muscle biology, owing to the fact that GRAF1 is expressed and functions predominantly in muscle tissues. Moreover, the residual expression of GRAF1 in the brains of these mice may in fact be beneficial as altered GRAF1 regulation has been implicated in cases of mental retardation [130] and cerebellar ataxia [131-133]. However, it is important to bear in mind that this mouse is globally deficient for GRAF1, and therefore off target affects may influence skeletal muscle regulation in a non-cell autonomous fashion. For instance, GRAF1 has been extensively described as a putative tumor suppressor gene in cases of acute myeloid leukemia [134-140]. Indeed, GRAF1 gene trap mice may exhibit alterations in blood cell biology, although that remains to be determined. Nonetheless, alterations in blood cell dynamics could certainly affect muscle function, particularly in our dystrophin/GRAF1 double-deficient mouse model, as vascularization and inflammation are key determinants of disease

progression and severity in muscular dystrophies. Therefore, alternative models which present with skeletal muscle-specific alterations in GRAF1 may be warranted. Our lab has generated mice that can be induced to express recombinant GRAF1 or a dominant-negative variant (GAPm) that inhibits function of all GRAF family members in a Cre-dependent fashion. By crossing these mice with various skeletal muscle-specific gene promoter-driven Cre mouse lines, we can control GRAF1 expression, both upregulation or downregulation, in a temporal fashion during various stages of muscle development.

Moreover, this Cre-driven GRAF1 transgene could be bred into GRAF1-deficient or dystrophin/GRAF1 double-deficient mice to determine if we can restore proper muscle physiology or recapitulate the dystrophic phenotype, respectively. Alternatively, rescue experiments could be performed more easily, albeit with less specificity, by injection of AAV-GRAF1 into GRAF1-deficient mice. What's more, it would be interesting to see if treatment with the pharmacological RhoA/ROCK pathway inhibitor Y27632 could rescue normal muscle function and physiology in GRAF1-deficient mice, thereby demonstrating whether loss of GRAF1-dependent RhoA regulation is causal for the muscular defects seen in these mice.

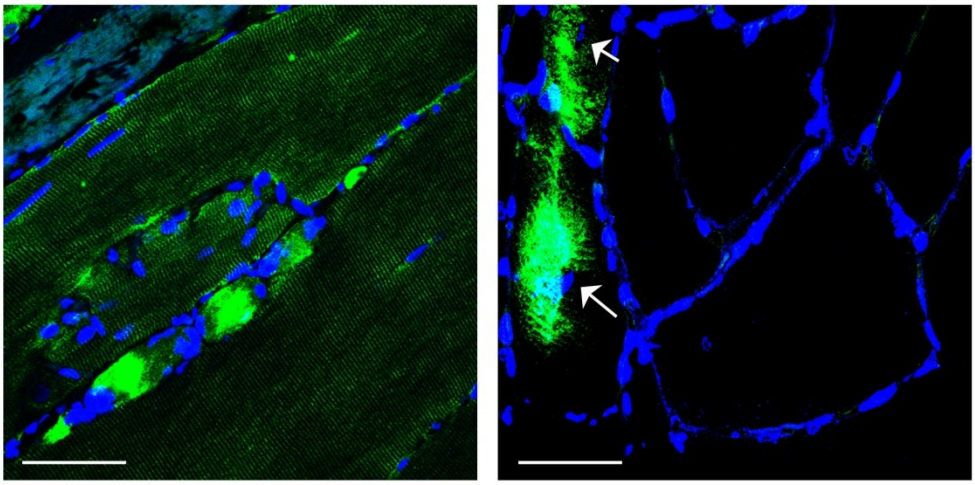

GRAF1 (green) DAPI (blue)  GRAF2 (green) DAPI (blue)

**Figure 4.1: GRAF1 and GRAF2 are up-regulated in diseased human muscle.**

Immunohistochemistry for GRAF1 and GRAF2 was performed on paraffin-embedded sections of muscle sections from a 40 year old patient with mixed myopathy. Both proteins were strongly expressed in regenerating fibers demarcated by centrally located nuclei (DAPI, blue, *arrows*). Data are representative of biopsies from 4 separate patients.

Scale bars=50 μm.

## ENDNOTES

[1] This chapter consists of material from a manuscript submitted to *Dev. Biol.* for peer review on March 12, 2014 and is co-authored by Kaitlin C. Lenhart, Abigail Becherer, Jianbin Li, Xiao Xiao, Elizabeth M. McNally, Christopher P. Mack, and Joan M. Taylor. Figures 2.7, 2.11b, 2.12a and 2.13b were collected by Joan M. Taylor, figures 2.8a, 2.9 and 2.10 were collected by Abigail Becherer, and grip force measurements were collected by Jianbin Li and printed in this chapter with their permission.

[2] Figures 3.1, 3.2, 3.3, 3.4 and 3.5 and corresponding data were collected and analyzed by Joan M. Taylor and Thomas J. O'Neill and printed in this chapter with their permission.

[3] Figure 4.1 was collected by Joan M. Taylor and printed with her permission.

## REFERENCES


1. Davies KE, Nowak KJ: **Molecular mechanisms of muscular dystrophies: old and new players.** *Nat Rev Mol Cell Biol* 2006, **7:**762-773.

2. Rahimov F, Kunkel LM: **The cell biology of disease: cellular and molecular mechanisms underlying muscular dystrophy.** *J Cell Biol* 2013, **201:**499-510.

3. Petrof BJ, Shrager JB, Stedman HH, Kelly AM, Sweeney HL: **Dystrophin protects the sarcolemma from stresses developed during muscle contraction.** *Proc Natl Acad Sci U S A* 1993, **90:**3710-3714.

4. Ervasti JM, Ohlendieck K, Kahl SD, Gaver MG, Campbell KP: **Deficiency of a glycoprotein component of the dystrophin complex in dystrophic muscle.** *Nature* 1990, **345:**315-319.

5. Liu J, Aoki M, Illa I, Wu C, Fardeau M, Angelini C, Serrano C, Urtizberea JA, Hentati F, Hamida MB, et al: **Dysferlin, a novel skeletal muscle gene, is mutated in Miyoshi myopathy and limb girdle muscular dystrophy.** *Nat Genet* 1998, **20:**31-36.

6. Bashir R, Britton S, Strachan T, Keers S, Vafiadaki E, Lako M, Richard I, Marchand S, Bourg N, Argov Z, et al: **A gene related to Caenorhabditis elegans spermatogenesis factor fer-1 is mutated in limb-girdle muscular dystrophy type 2B.** *Nat Genet* 1998, **20:**37-42.

7. Bansal D, Miyake K, Vogel SS, Groh S, Chen CC, Williamson R, McNeil PL, Campbell KP: **Defective membrane repair in dysferlin-deficient muscular dystrophy.** *Nature* 2003, **423:**168-172.

8. Christ B, Ordahl CP: **Early stages of chick somite development.** *Anat Embryol (Berl)* 1995, **191:**381-396.

9. Tremblay P, Dietrich S, Mericskay M, Schubert FR, Li Z, Paulin D: **A crucial role for Pax3 in the development of the hypaxial musculature and the long-range migration of muscle precursors.** *Dev Biol* 1998, **203:**49-61.

10. Rudnicki MA, Schnegelsberg PN, Stead RH, Braun T, Arnold HH, Jaenisch R: **MyoD or Myf-5 is required for the formation of skeletal muscle.** *Cell* 1993, **75:**1351-1359.

11. Tajbakhsh S, Rocancourt D, Cossu G, Buckingham M: **Redefining the genetic hierarchies controlling skeletal myogenesis: Pax-3 and Myf-5 act upstream of MyoD.** *Cell* 1997, **89:**127-138.

12. Hasty P, Bradley A, Morris JH, Edmondson DG, Venuti JM, Olson EN, Klein WH: **Muscle deficiency and neonatal death in mice with a targeted mutation in the myogenin gene.** *Nature* 1993, **364:**501-506.

13. Nabeshima Y, Hanaoka K, Hayasaka M, Esumi E, Li S, Nonaka I: **Myogenin gene disruption results in perinatal lethality because of severe muscle defect.** *Nature* 1993, **364:**532-535.

14. Rhodes SJ, Konieczny SF: **Identification of MRF4: a new member of the muscle regulatory factor gene family.** *Genes Dev* 1989, **3:**2050-2061.

15. Patapoutian A, Yoon JK, Miner JH, Wang S, Stark K, Wold B: **Disruption of the mouse MRF4 gene identifies multiple waves of myogenesis in the myotome.** *Development* 1995, **121:**3347-3358.

16. Mauro A: **Satellite cell of skeletal muscle fibers.** *J Biophys Biochem Cytol* 1961, **9:**493-495.

17. Relaix F, Zammit PS: **Satellite cells are essential for skeletal muscle regeneration: the cell on the edge returns centre stage.** *Development* 2012, **139:**2845-2856.

18. Kuang S, Kuroda K, Le Grand F, Rudnicki MA: **Asymmetric self-renewal and commitment of satellite stem cells in muscle.** *Cell* 2007, **129:**999-1010.

19. Luz MA, Marques MJ, Santo Neto H: **Impaired regeneration of dystrophin-deficient muscle fibers is caused by exhaustion of myogenic cells.** *Braz J Med Biol Res* 2002, **35:**691-695.

20. Sacco A, Mourkioti F, Tran R, Choi J, Llewellyn M, Kraft P, Shkreli M, Delp S, Pomerantz JH, Artandi SE, Blau HM: **Short telomeres and stem cell exhaustion model Duchenne muscular dystrophy in mdx/mTR mice.** *Cell* 2010, **143:**1059-1071.

21. Ridley AJ, Paterson HF, Johnston CL, Diekmann D, Hall A: **The small GTP-binding protein rac regulates growth factor-induced membrane ruffling.** *Cell* 1992, **70:**401-410.

22. Kozma R, Ahmed S, Best A, Lim L: **The Ras-related protein Cdc42Hs and bradykinin promote formation of peripheral actin microspikes and filopodia in Swiss 3T3 fibroblasts.** *Mol Cell Biol* 1995, **15:**1942-1952.

23. Ridley AJ, Hall A: **The small GTP-binding protein rho regulates the assembly of focal adhesions and actin stress fibers in response to growth factors.** *Cell* 1992, **70:**389-399.

24. Burridge K, Wennerberg K: **Rho and Rac take center stage.** *Cell* 2004, **116:**167-179.

25. Etienne-Manneville S, Hall A: **Rho GTPases in cell biology.** *Nature* 2002, **420:**629-635.

26. Fukata M, Nakagawa M, Kaibuchi K: **Roles of Rho-family GTPases in cell polarisation and directional migration.** *Curr Opin Cell Biol* 2003, **15:**590-597.

27. Raftopoulou M, Hall A: **Cell migration: Rho GTPases lead the way.** *Dev Biol* 2004, **265:**23-32.

28. Ridley AJ: **Rho: theme and variations.** *Curr Biol* 1996, **6:**1256-1264.

29. Meriane M, Roux P, Primig M, Fort P, Gauthier-Rouviere C: **Critical activities of Rac1 and Cdc42Hs in skeletal myogenesis: antagonistic effects of JNK and p38 pathways.** *Mol Biol Cell* 2000, **11:**2513-2528.

30. Meriane M, Charrasse S, Comunale F, Mery A, Fort P, Roux P, Gauthier-Rouviere C: **Participation of small GTPases Rac1 and Cdc42Hs in myoblast transformation.** *Oncogene* 2002, **21:**2901-2907.

31. Hill CS, Wynne J, Treisman R: **The Rho family GTPases RhoA, Rac1, and CDC42Hs regulate transcriptional activation by SRF.** *Cell* 1995, **81:**1159-1170.

32. Wei L, Zhou W, Croissant JD, Johansen FE, Prywes R, Balasubramanyam A, Schwartz RJ: **RhoA signaling via serum response factor plays an obligatory role in myogenic differentiation.** *J Biol Chem* 1998, **273:**30287-30294.

33. Carnac G, Primig M, Kitzmann M, Chafey P, Tuil D, Lamb N, Fernandez A: **RhoA GTPase and serum response factor control selectively the expression of MyoD without affecting Myf5 in mouse myoblasts.** *Mol Biol Cell* 1998, **9:**1891-1902.

34. Castellani L, Salvati E, Alema S, Falcone G: **Fine regulation of RhoA and Rock is required for skeletal muscle differentiation.** *J Biol Chem* 2006, **281:**15249-15257.

35. Charrasse S, Comunale F, Grumbach Y, Poulat F, Blangy A, Gauthier-Rouviere C: **RhoA GTPase regulates M-cadherin activity and myoblast fusion.** *Mol Biol Cell* 2006, **17:**749-759.

36. Nishiyama T, Kii I, Kudo A: **Inactivation of Rho/ROCK signaling is crucial for the nuclear accumulation of FKHR and myoblast fusion.** *J Biol Chem* 2004, **279:**47311-47319.

37. Iwasaki K, Hayashi K, Fujioka T, Sobue K: **Rho/Rho-associated kinase signal regulates myogenic differentiation via myocardin-related transcription factor-**

**A/Smad-dependent transcription of the Id3 gene.** *J Biol Chem* 2008, **283:**21230-21241.

38. Benezra R, Davis RL, Lockshon D, Turner DL, Weintraub H: **The protein Id: a negative regulator of helix-loop-helix DNA binding proteins.** *Cell* 1990, **61:**49-59.

39. Richardson BE, Beckett K, Nowak SJ, Baylies MK: **SCAR/WAVE and Arp2/3 are crucial for cytoskeletal remodeling at the site of myoblast fusion.** *Development* 2007, **134:**4357-4367.

40. Nowak SJ, Nahirney PC, Hadjantonakis AK, Baylies MK: **Nap1-mediated actin remodeling is essential for mammalian myoblast fusion.** *J Cell Sci* 2009, **122:**3282-3293.

41. Richard JP, Leikina E, Chernomordik LV: **Cytoskeleton reorganization in influenza hemagglutinin-initiated syncytium formation.** *Biochim Biophys Acta* 2009, **1788:**450-457.

42. Chen A, Leikina E, Melikov K, Podbilewicz B, Kozlov MM, Chernomordik LV: **Fusion-pore expansion during syncytium formation is restricted by an actin network.** *J Cell Sci* 2008, **121:**3619-3628.

43. Zachary I, Rozengurt E: **Focal adhesion kinase (p125FAK): a point of convergence in the action of neuropeptides, integrins, and oncogenes.** *Cell* 1992, **71:**891-894.

44. Schaller MD, Parsons JT: **Focal adhesion kinase and associated proteins.** *Curr Opin Cell Biol* 1994, **6:**705-710.

45. Vasyutina E, Martarelli B, Brakebusch C, Wende H, Birchmeier C: **The small G-proteins Rac1 and Cdc42 are essential for myoblast fusion in the mouse.** *Proc Natl Acad Sci U S A* 2009, **106:**8935-8940.

46. Hakeda-Suzuki S, Ng J, Tzu J, Dietzl G, Sun Y, Harms M, Nardine T, Luo L, Dickson BJ: **Rac function and regulation during Drosophila development.** *Nature* 2002, **416:**438-442.

47. Srinivas BP, Woo J, Leong WY, Roy S: **A conserved molecular pathway mediates myoblast fusion in insects and vertebrates.** *Nat Genet* 2007, **39:**781-786.

48. Sander EE, ten Klooster JP, van Delft S, van der Kammen RA, Collard JG: **Rac downregulates Rho activity: reciprocal balance between both GTPases determines cellular morphology and migratory behavior.** *J Cell Biol* 1999, **147:**1009-1022.

49. Charrasse S, Comunale F, Fortier M, Portales-Casamar E, Debant A, Gauthier-Rouviere C: **M-cadherin activates Rac1 GTPase through the Rho-GEF trio during myoblast fusion.** *Mol Biol Cell* 2007, **18:**1734-1743.

50. Haralalka S, Shelton C, Cartwright HN, Katzfey E, Janzen E, Abmayr SM: **Asymmetric Mbc, active Rac1 and F-actin foci in the fusion-competent myoblasts during myoblast fusion in Drosophila.** *Development* 2011, **138:**1551-1562.

51. Pajcini KV, Pomerantz JH, Alkan O, Doyonnas R, Blau HM: **Myoblasts and macrophages share molecular components that contribute to cell-cell fusion.** *J Cell Biol* 2008, **180:**1005-1019.

52. Doherty JT, Lenhart KC, Cameron MV, Mack CP, Conlon FL, Taylor JM: **Skeletal muscle differentiation and fusion are regulated by the BAR-containing Rho-GTPase-activating protein (Rho-GAP), GRAF1.** *J Biol Chem* 2011, **286:**25903-25921.

53. Chernomordik LV, Kozlov MM: **Protein-lipid interplay in fusion and fission of biological membranes.** *Annu Rev Biochem* 2003, **72:**175-207.

54. Richard JP, Leikina E, Langen R, Henne WM, Popova M, Balla T, McMahon HT, Kozlov MM, Chernomordik LV: **Intracellular curvature-generating proteins in cell-to-cell fusion.** *Biochem J* 2011, **440:**185-193.

55. Schroter RH, Lier S, Holz A, Bogdan S, Klambt C, Beck L, Renkawitz-Pohl R: **kette and blown fuse interact genetically during the second fusion step of myogenesis in Drosophila.** *Development* 2004, **131:**4501-4509.

56. Demonbreun AR, Fahrenbach JP, Deveaux K, Earley JU, Pytel P, McNally EM: **Impaired muscle growth and response to insulin-like growth factor 1 in dysferlin-mediated muscular dystrophy.** *Hum Mol Genet* 2011, **20:**779-789.

57. Doherty KR, Cave A, Davis DB, Delmonte AJ, Posey A, Earley JU, Hadhazy M, McNally EM: **Normal myoblast fusion requires myoferlin.** *Development* 2005, **132:**5565-5575.

58. Posey AD, Jr., Pytel P, Gardikiotes K, Demonbreun AR, Rainey M, George M, Band H, McNally EM: **Endocytic recycling proteins EHD1 and EHD2 interact with fer-1-like-5 (Fer1L5) and mediate myoblast fusion.** *J Biol Chem* 2011, **286:**7379-7388.

59. Lennon NJ, Kho A, Bacskai BJ, Perlmutter SL, Hyman BT, Brown RH, Jr.: **Dysferlin interacts with annexins A1 and A2 and mediates sarcolemmal wound-healing.** *J Biol Chem* 2003, **278:**50466-50473.

60. Cenacchi G, Fanin M, De Giorgi LB, Angelini C: **Ultrastructural changes in dysferlinopathy support defective membrane repair mechanism.** *J Clin Pathol* 2005, **58:**190-195.

61. Anderson LV, Davison K, Moss JA, Young C, Cullen MJ, Walsh J, Johnson MA, Bashir R, Britton S, Keers S, et al: **Dysferlin is a plasma membrane protein and is expressed early in human development.** *Hum Mol Genet* 1999, **8:**855-861.

62. Hildebrand JD, Taylor JM, Parsons JT: **An SH3 domain-containing GTPase-activating protein for Rho and Cdc42 associates with focal adhesion kinase.** *Mol Cell Biol* 1996, **16:**3169-3178.

63. Taylor JM, Hildebrand JD, Mack CP, Cox ME, Parsons JT: **Characterization of graf, the GTPase-activating protein for rho associated with focal adhesion kinase. Phosphorylation and possible regulation by mitogen-activated protein kinase.** *J Biol Chem* 1998, **273:**8063-8070.

64. Taylor JM, Macklem MM, Parsons JT: **Cytoskeletal changes induced by GRAF, the GTPase regulator associated with focal adhesion kinase, are mediated by Rho.** *J Cell Sci* 1999, **112 ( Pt 2):**231-242.

65. Longenecker KL, Zhang B, Derewenda U, Sheffield PJ, Dauter Z, Parsons JT, Zheng Y, Derewenda ZS: **Structure of the BH domain from graf and its implications for Rho GTPase recognition.** *J Biol Chem* 2000, **275:**38605-38610.

66. Ren G, Vajjhala P, Lee JS, Winsor B, Munn AL: **The BAR domain proteins: molding membranes in fission, fusion, and phagy.** *Microbiol Mol Biol Rev* 2006, **70:**37-120.

67. Lundmark R, Doherty GJ, Howes MT, Cortese K, Vallis Y, Parton RG, McMahon HT: **The GTPase-activating protein GRAF1 regulates the CLIC/GEEC endocytic pathway.** *Curr Biol* 2008, **18:**1802-1808.

68. Eberth A, Lundmark R, Gremer L, Dvorsky R, Koessmeier KT, McMahon HT, Ahmadian MR: **A BAR domain-mediated autoinhibitory mechanism for RhoGAPs of the GRAF family.** *Biochem J* 2009, **417:**371-377.

69. Bulfield G, Siller WG, Wight PA, Moore KJ: **X chromosome-linked muscular dystrophy (mdx) in the mouse.** *Proc Natl Acad Sci U S A* 1984, **81:**1189-1192.

70. Ryder-Cook AS, Sicinski P, Thomas K, Davies KE, Worton RG, Barnard EA, Darlison MG, Barnard PJ: **Localization of the mdx mutation within the mouse dystrophin gene.** *Embo J* 1988, **7:**3017-3021.

71. DiMario JX, Uzman A, Strohman RC: **Fiber regeneration is not persistent in dystrophic (MDX) mouse skeletal muscle.** *Dev Biol* 1991, **148:**314-321.

72. Peckham M: **Engineering a multi-nucleated myotube, the role of the actin cytoskeleton.** *J Microsc* 2008, **231:**486-493.

73. Schafer G, Weber S, Holz A, Bogdan S, Schumacher S, Muller A, Renkawitz-Pohl R, Onel SF: **The Wiskott-Aldrich syndrome protein (WASP) is essential for myoblast fusion in Drosophila.** *Dev Biol* 2007, **304:**664-674.

74. Swailes NT, Knight PJ, Peckham M: **Actin filament organization in aligned prefusion myoblasts.** *J Anat* 2004, **205:**381-391.

75. Kalderon N, Gilula NB: **Membrane events involved in myoblast fusion.** *J Cell Biol* 1979, **81:**411-425.

76. Martens S, Kozlov MM, McMahon HT: **How synaptotagmin promotes membrane fusion.** *Science* 2007, **316:**1205-1208.

77. Han R, Campbell KP: **Dysferlin and muscle membrane repair.** *Curr Opin Cell Biol* 2007, **19:**409-416.

78. Posey AD, Jr., Pytel P, Gardikiotes K, Demonbreun AR, Rainey M, George M, Band H, McNally EM: **Endocytic Recycling Proteins EHD1 and EHD2 Interact with Fer-1-like-5 (Fer1L5) and Mediate Myoblast Fusion.** *J Biol Chem* 2011, **286:**7379-7388.

79. Doherty KR, Demonbreun AR, Wallace GQ, Cave A, Posey AD, Heretis K, Pytel P, McNally EM: **The endocytic recycling protein EHD2 interacts with myoferlin to regulate myoblast fusion.** *J Biol Chem* 2008, **283:**20252-20260.

80. Cai C, Masumiya H, Weisleder N, Pan Z, Nishi M, Komazaki S, Takeshima H, Ma J: **MG53 regulates membrane budding and exocytosis in muscle cells.** *J Biol Chem* 2009, **284:**3314-3322.

81. Evesson FJ, Peat RA, Lek A, Brilot F, Lo HP, Dale RC, Parton RG, North KN, Cooper ST: **Reduced plasma membrane expression of dysferlin mutants is attributed to accelerated endocytosis via a syntaxin-4-associated pathway.** *J Biol Chem* 2010, **285:**28529-28539.

82. Wallace GQ, McNally EM: **Mechanisms of muscle degeneration, regeneration, and repair in the muscular dystrophies.** *Annu Rev Physiol* 2009, **71:**37-57.

83. Matsuda C, Hayashi YK, Ogawa M, Aoki M, Murayama K, Nishino I, Nonaka I, Arahata K, Brown RH, Jr.: **The sarcolemmal proteins dysferlin and caveolin-3 interact in skeletal muscle.** *Hum Mol Genet* 2001, **10:**1761-1766.

84. Cai C, Weisleder N, Ko JK, Komazaki S, Sunada Y, Nishi M, Takeshima H, Ma J: **Membrane repair defects in muscular dystrophy are linked to altered**

**interaction between MG53, caveolin-3, and dysferlin.** *J Biol Chem* 2009, **284:**15894-15902.

85. Hildebrand JD, Taylor JM, Parsons JT: **An SH3 domain-containing GTPase-activating protein for Rho and Cdc42 associates with focal adhesion kinase.** *Mol Cell Biol* 1996, **16:**3169-3178.

86. Taylor JM, Macklem MM, Parsons JT: **Cytoskeletal changes induced by GRAF, the GTPase regulator associated with focal adhesion kinase, are mediated by Rho.** *J Cell Sci* 1999, **112 ( Pt 2):**231-242.

87. Taylor JM, Hildebrand JD, Mack CP, Cox ME, Parsons JT: **Characterization of graf, the GTPase-activating protein for rho associated with focal adhesion kinase. Phosphorylation and possible regulation by mitogen-activated protein kinase.** *J Biol Chem* 1998, **273:**8063-8070.

88. Doherty JT, Lenhart KC, Cameron MV, Mack CP, Conlon FL, Taylor JM: **Skeletal muscle differentiation and fusion are regulated by the BAR-containing Rho-GTPase-activating protein (Rho-GAP), GRAF1.** *J Biol Chem* 2011, **286:**25903-25921.

89. Braunschweig U, Gueroussov S, Plocik AM, Graveley BR, Blencowe BJ: **Dynamic integration of splicing within gene regulatory pathways.** *Cell* 2013, **152:**1252-1269.

90. Qiao C, Li J, Jiang J, Zhu X, Wang B, Li J, Xiao X: **Myostatin propeptide gene delivery by adeno-associated virus serotype 8 vectors enhances muscle growth and ameliorates dystrophic phenotypes in mdx mice.** *Hum Gene Ther* 2008, **19:**241-254.

91. Blau HM, Chiu CP, Pavlath GK, Webster C: **Muscle gene expression in heterokaryons.** *Adv Exp Med Biol* 1985, **182:**231-247.

92. Yaffe D: **Retention of differentiation potentialities during prolonged cultivation of myogenic cells.** *Proc Natl Acad Sci U S A* 1968, **61:**477-483.

93. Green SA, Kelly RB: **Low density lipoprotein receptor and cation-independent mannose 6-phosphate receptor are transported from the cell surface to the Golgi apparatus at equal rates in PC12 cells.** *J Cell Biol* 1992, **117:**47-55.

94. Cai B, Giridharan SS, Zhang J, Saxena S, Bahl K, Schmidt JA, Sorgen PL, Guo W, Naslavsky N, Caplan S: **Differential roles of C-terminal Eps15 homology domain proteins as vesiculators and tubulators of recycling endosomes.** *J Biol Chem* 2013, **288:**30172-30180.

95. Bai X, Lenhart KC, Bird KE, Suen AA, Rojas M, Kakoki M, Li F, Smithies O, Mack CP, Taylor JM: **The smooth muscle-selective RhoGAP GRAF3 is a critical regulator of vascular tone and hypertension.** *Nat Commun* 2013, **4:**2910.

96. Ren XR, Du QS, Huang YZ, Ao SZ, Mei L, Xiong WC: **Regulation of CDC42 GTPase by proline-rich tyrosine kinase 2 interacting with PSGAP, a novel pleckstrin homology and Src homology 3 domain containing rhoGAP protein.** *J Cell Biol* 2001, **152:**971-984.

97. Duan R, Gallagher PJ: **Dependence of myoblast fusion on a cortical actin wall and nonmuscle myosin IIA.** *Dev Biol* 2009, **325:**374-385.

98. Narumiya S, Ishizaki T, Watanabe N: **Rho effectors and reorganization of actin cytoskeleton.** *FEBS Lett* 1997, **410:**68-72.

99. Yamana N, Arakawa Y, Nishino T, Kurokawa K, Tanji M, Itoh RE, Monypenny J, Ishizaki T, Bito H, Nozaki K, et al: **The Rho-mDia1 pathway regulates cell polarity and focal adhesion turnover in migrating cells through mobilizing Apc and c-Src.** *Mol Cell Biol* 2006, **26:**6844-6858.

100. Posey AD, Jr., Demonbreun A, McNally EM: **Ferlin proteins in myoblast fusion and muscle growth.** *Curr Top Dev Biol* 2011, **96:**203-230.

101. Suetsugu S: **The proposed functions of membrane curvatures mediated by the BAR domain superfamily proteins.** *J Biochem* 2010, **148:**1-12.

102. Marrink SJ, Mark AE: **The mechanism of vesicle fusion as revealed by molecular dynamics simulations.** *J Am Chem Soc* 2003, **125:**11144-11145.

103. Chanturiya A, Scaria P, Kuksenok O, Woodle MC: **Probing the mechanism of fusion in a two-dimensional computer simulation.** *Biophys J* 2002, **82:**3072-3080.

104. Simionescu A, Pavlath GK: **Molecular mechanisms of myoblast fusion across species.** *Adv Exp Med Biol* 2011, **713:**113-135.

105. Henne WM, Kent HM, Ford MG, Hegde BG, Daumke O, Butler PJ, Mittal R, Langen R, Evans PR, McMahon HT: **Structure and analysis of FCHo2 F-BAR domain: a dimerizing and membrane recruitment module that effects membrane curvature.** *Structure* 2007, **15:**839-852.

106. Eberth A, Lundmark R, Gremer L, Dvorsky R, Koessmeier KT, McMahon HT, Ahmadian MR: **A BAR domain-mediated autoinhibitory mechanism for RhoGAPs of the GRAF family.** *Biochem J* 2009, **417:**371-377.

107. Lundmark R, Doherty GJ, Howes MT, Cortese K, Vallis Y, Parton RG, McMahon HT: **The GTPase-activating protein GRAF1 regulates the CLIC/GEEC endocytic pathway.** *Curr Biol* 2008, **18:**1802-1808.

108. Richard JP, Leikina E, Langen R, Henne WM, Popova M, Balla T, McMahon HT, Kozlov MM, Chernomordik LV: **Intracellular curvature-generating proteins in cell-to-cell fusion.** *Biochem J* 2011, **440:**185-193.

109. Ren XR, Du QS, Huang YZ, Ao SZ, Mei L, Xiong WC: **Regulation of CDC42 GTPase by proline-rich tyrosine kinase 2 interacting with PSGAP, a novel pleckstrin homology and Src homology 3 domain containing rhoGAP protein.** *J Cell Biol* 2001, **152:**971-984.

110. Fernando P, Sandoz JS, Ding W, de Repentigny Y, Brunette S, Kelly JF, Kothary R, Megeney LA: **Bin1 SRC homology 3 domain acts as a scaffold for myofiber sarcomere assembly.** *J Biol Chem* 2009, **284:**27674-27686.

111. Wechsler-Reya RJ, Elliott KJ, Prendergast GC: **A role for the putative tumor suppressor Bin1 in muscle cell differentiation.** *Mol Cell Biol* 1998, **18:**566-575.

112. Simionescu-Bankston A, Leoni G, Wang Y, Pham PP, Ramalingam A, DuHadaway JB, Faundez V, Nusrat A, Prendergast GC, Pavlath GK: **The N-BAR domain protein, Bin3, regulates Rac1- and Cdc42-dependent processes in myogenesis.** *Dev Biol* 2013, **382:**160-171.

113. DiMichele LA, Hakim ZS, Sayers RL, Rojas M, Schwartz RJ, Mack CP, Taylor JM: **Transient expression of FRNK reveals stage-specific requirement for focal adhesion kinase activity in cardiac growth.** *Circ Res* 2009, **104:**1201-1208.

114. Koeppel MA, McCarthy CC, Moertl E, Jakobi R: **Identification and characterization of PS-GAP as a novel regulator of caspase-activated PAK-2.** *J Biol Chem* 2004, **279:**53653-53664.

115. Jansen KM, Pavlath GK: **Molecular control of mammalian myoblast fusion.** *Methods Mol Biol* 2008, **475:**115-133.

116. Hochreiter-Hufford AE, Lee CS, Kinchen JM, Sokolowski JD, Arandjelovic S, Call JA, Klibanov AL, Yan Z, Mandell JW, Ravichandran KS: **Phosphatidylserine receptor BAI1 and apoptotic cells as new promoters of myoblast fusion.** *Nature* 2013, **497:**263-267.

117. Rybakova IN, Patel JR, Ervasti JM: **The dystrophin complex forms a mechanically strong link between the sarcolemma and costameric actin.** *J Cell Biol* 2000, **150:**1209-1214.

118. Jung D, Yang B, Meyer J, Chamberlain JS, Campbell KP: **Identification and characterization of the dystrophin anchoring site on beta-dystroglycan.** *J Biol Chem* 1995, **270:**27305-27310.

119. Koenig M, Monaco AP, Kunkel LM: **The complete sequence of dystrophin predicts a rod-shaped cytoskeletal protein.** *Cell* 1988, **53:**219-228.

120. Reddy A, Caler EV, Andrews NW: **Plasma membrane repair is mediated by Ca(2+)-regulated exocytosis of lysosomes.** *Cell* 2001, **106:**157-169.

121. Wenzel K, Geier C, Qadri F, Hubner N, Schulz H, Erdmann B, Gross V, Bauer D, Dechend R, Dietz R, et al: **Dysfunction of dysferlin-deficient hearts.** *J Mol Med (Berl)* 2007, **85:**1203-1214.

122. Han R, Bansal D, Miyake K, Muniz VP, Weiss RM, McNeil PL, Campbell KP: **Dysferlin-mediated membrane repair protects the heart from stress-induced left ventricular injury.** *J Clin Invest* 2007, **117:**1805-1813.

123. Han R, Rader EP, Levy JR, Bansal D, Campbell KP: **Dystrophin deficiency exacerbates skeletal muscle pathology in dysferlin-null mice.** *Skelet Muscle* 2011, **1:**35.

124. Straub V, Rafael JA, Chamberlain JS, Campbell KP: **Animal models for muscular dystrophy show different patterns of sarcolemmal disruption.** *J Cell Biol* 1997, **139:**375-385.

125. Wenzel K, Geier C, Qadri F, Hubner N, Schulz H, Erdmann B, Gross V, Bauer D, Dechend R, Dietz R, et al: **Dysfunction of dysferlin-deficient hearts.** *Journal of molecular medicine* 2007, **85:**1203-1214.

126. Shin JH, Hakim CH, Zhang K, Duan D: **Genotyping mdx, mdx3cv, and mdx4cv mice by primer competition polymerase chain reaction.** *Muscle Nerve* 2011, **43:**283-286.

127. Cheng Z, Dimichele LA, Rojas M, Vaziri C, Mack CP, Taylor JM: **Focal adhesion kinase antagonizes doxorubicin cardiotoxicity via p21(Cip1.).** *J Mol Cell Cardiol* 2014, **67:**1-11.

128. Qiao C, Li J, Jiang J, Zhu X, Wang B, Xiao X: **Myostatin propeptide gene delivery by adeno-associated virus serotype 8 vectors enhances muscle growth and ameliorates dystrophic phenotypes in mdx mice.** *Human gene therapy* 2008, **19:**241-254.

129. Louch WE, Sheehan KA, Wolska BM: **Methods in cardiomyocyte isolation, culture, and gene transfer.** *J Mol Cell Cardiol* 2011, **51:**288-298.

130. Barresi V, Ragusa A, Fichera M, Musso N, Castiglia L, Rappazzo G, Travali S, Mattina T, Romano C, Cocchi G, Condorelli DF: **Decreased expression of GRAF1/OPHN-1-L in the X-linked alpha thalassemia mental retardation syndrome.** *BMC Med Genomics* 2010, **3:**28.

131. Doss S, Numann A, Ziegler A, Siebert E, Borowski K, Stocker W, Pruss H, Wildemann B, Endres M, Jarius S: **Anti-Ca/anti-ARHGAP26 antibodies associated with cerebellar atrophy and cognitive decline.** *J Neuroimmunol* 2014, **267:**102-104.

132. Jarius S, Martinez-Garcia P, Hernandez AL, Brase JC, Borowski K, Regula JU, Meinck HM, Stocker W, Wildemann B, Wandinger KP: **Two new cases of anti-Ca (anti-ARHGAP26/GRAF) autoantibody-associated cerebellar ataxia.** *J Neuroinflammation* 2013, **10:**7.

133. Jarius S, Wandinger KP, Horn S, Heuer H, Wildemann B: **A new Purkinje cell antibody (anti-Ca) associated with subacute cerebellar ataxia: immunological characterization.** *J Neuroinflammation* 2010, **7:**21.

134. Qian J, Qian Z, Lin J, Yao DM, Chen Q, Li Y, Ji RB, Yang J, Xiao GF, Wang YL: **Abnormal methylation of GRAF promoter Chinese patients with acute myeloid leukemia.** *Leuk Res* 2011, **35:**783-786.

135. Qian Z, Qian J, Lin J, Yao DM, Chen Q, Ji RB, Li Y, Xiao GF, Li JY: **GTPase regulator associated with the focal adhesion kinase (GRAF) transcript was down-regulated in patients with myeloid malignancies.** *J Exp Clin Cancer Res* 2010, **29:**111.

136. Qian Z, Lin J, Qian J, Yao DM, Wang YL, Han LX, Zhu ZH, Xiao GF: **[Quantification of GRAF gene expression in patients with acute myeloid leukemia using EvaGreen real time quantitative PCR].** *Zhonghua Yi Xue Yi Chuan Xue Za Zhi* 2010, **27:**290-293.

137. Bojesen SE, Ammerpohl O, Weinhausl A, Haas OA, Mettal H, Bohle RM, Borkhardt A, Fuchs U: **Characterisation of the GRAF gene promoter and its methylation in patients with acute myeloid leukaemia and myelodysplastic syndrome.** *Br J Cancer* 2006, **94:**323-332.

138. Wilda M, Perez AV, Bruch J, Woessmann W, Metzler M, Fuchs U, Borkhardt A: **Use of MLL/GRAF fusion mRNA for measurement of minimal residual disease during chemotherapy in an infant with acute monoblastic leukemia (AML-M5).** *Genes Chromosomes Cancer* 2005, **43:**424-426.

139. Panagopoulos I, Kitagawa A, Isaksson M, Morse H, Mitelman F, Johansson B: **MLL/GRAF fusion in an infant acute monocytic leukemia (AML M5b) with a**

**cytogenetically cryptic ins(5;11)(q31;q23q23).** *Genes Chromosomes Cancer* 2004, **41:**400-404.

140. Borkhardt A, Bojesen S, Haas OA, Fuchs U, Bartelheimer D, Loncarevic IF, Bohle RM, Harbott J, Repp R, Jaeger U, et al: **The human GRAF gene is fused to MLL in a unique t(5;11)(q31;q23) and both alleles are disrupted in three cases of myelodysplastic syndrome/acute myeloid leukemia with a deletion 5q.** *Proc Natl Acad Sci U S A* 2000, **97:**9168-9173.